NASA TECHNICAL MEMORANDUM

NASA TM X-2774

NASA TM X-2774

CASE FILE COPY

EFFECT OF FIN PLANFORM ON THE AERODYNAMIC CHARACTERISTICS OF A WINGLESS MISSILE WITH AFT CRUCIFORM CONTROLS AT MACH 1.60, 2.36, AND 2.86

by Charles D. Trescot, Jr., Gerald V. Foster, and C. Donald Babb

Langley Research Center
Hampton, Va. 23665

NATIONAL AERONAUTICS AND SPACE ADMINISTRATION • WASHINGTON, D. C. • JULY 1973

1. Report No.	2. Government Accession No.	3. Recipient's Catalog No.
NASA TM X-2774		

4. Title and Subtitle	5. Report Date
EFFECT OF FIN PLANFORM ON THE AERODYNAMIC CHARACTERISTICS OF A WINGLESS MISSILE WITH AFT CRUCIFORM CONTROLS AT MACH 1.60, 2.36, AND 2.86	July 1973
	6. Performing Organization Code
7. Author(s)	8. Performing Organization Report No.
Charles D. Trescot, Jr., Gerald V. Foster, and C. Donald Babb	L-8783
	10. Work Unit No.
9. Performing Organization Name and Address	501-17-01-12
NASA Langley Research Center Hampton, Va. 23665	11. Contract or Grant No.
	13. Type of Report and Period Covered
12. Sponsoring Agency Name and Address	Technical Memorandum
National Aeronautics and Space Administration Washington, D.C. 20546	14. Sponsoring Agency Code

15. Supplementary Notes

16. Abstract

An investigation has been made in the Langley Unitary Plan wind tunnel to determine the effects of fin planform on the static longitudinal aerodynamic characteristics of a wingless maneuvering missile configuration having cruciform, all-movable, aft control surfaces. The tests were made at Mach numbers of 1.60, 2.36, and 2.86 through an angle-of-attack range from about -4° to 22°, at an angle of sideslip of 0°, and at a Reynolds number of 8.2×10^{6} based on model length. The pitch-control data were obtained at model roll angles of 0° and 45°. Control-surface forces and moments were also measured. Four alternate fin planforms were investigated.

17. Key Words (Suggested by Author(s))	18. Distribution Statement
Aft missile controls Control loads	Unclassified – Unlimited

19. Security Classif. (of this report)	20. Security Classif. (of this page)	21. No. of Pages	22. Price*
Unclassified	Unclassified	99	$3.00

*For sale by the National Technical Information Service, Springfield, Virginia 22151

EFFECT OF FIN PLANFORM ON THE AERODYNAMIC CHARACTERISTICS OF A WINGLESS MISSILE WITH AFT CRUCIFORM CONTROLS AT MACH 1.60, 2.36, AND 2.86

By Charles D. Trescot, Jr., Gerald V. Foster,
and C. Donald Babb
Langley Research Center

SUMMARY

An investigation has been made in the Langley Unitary Plan wind tunnel to determine the effects of fin planform on the static longitudinal aerodynamic characteristics of a wingless maneuverable missile configuration having cruciform, all-movable, aft control surfaces. The tests were made at Mach numbers of 1.60, 2.36, and 2.86 through an angle-of-attack range from about -4° to 22°, at an angle of sideslip of 0°, and at a Reynolds number of 8.2×10^{6} based on model length.

The results of the test indicate that there are no large differences in the aerodynamic results due to fin taper ratio or trailing-edge sweep. An increase in aspect ratio, however, leads to an increase in stability level, lift-curve slope, and pitch-control effectiveness. The fin normal-force and bending-moment coefficients peak at an angle of attack of about 8° for the fin panel at a roll attitude of 45° (roll attitude of fin panel is 0° when fin is on top of model in vertical position) due to a body "shielding" effect at high angles of attack. For the fin panel at roll attitudes of 90° and 135°, these coefficients continually increase to the highest test angle of attack. The slopes of the normal-force and bending-moment curves are the greatest for the fin with the highest aspect ratio and indicate only small differences because of taper ratio or trailing-edge sweep. There was little effect of fin planform or Mach number on the fin hinge-moment coefficients.

INTRODUCTION

An investigation has been made by the National Aeronautics and Space Administration to determine the effect of fin planform on the static aerodynamic characteristics of a model of a wingless maneuverable missile configuration. The model had cruciform, all-movable, aft control surfaces. Four alternate fin planforms were investigated. Results of wind-tunnel tests on a similar configuration can be found in reference 1.

The investigation was made in the Langley Unitary Plan wind tunnel at Mach numbers of 1.60, 2.36, and 2.86 and at a Reynolds number of 8.2×10^6 based on model length. The angle of attack was varied from about -4° to 22° at a sideslip angle of 0°. The pitch control data were obtained at model roll angles of 0° and 45°. In addition to the complete force and moment data, control-surface forces and moments were also measured.

SYMBOLS

The longitudinal characteristics of the model are referred to the body axis system except for lift and drag which are referred to the stability axis system. Both body axis and stability axis systems are fixed in the vertical-horizontal planes regardless of the model roll angle. The moment reference was located at 52.08 percent of the body length.

A maximum cross-sectional area of body, 0.004560 meter^2

A_c control-surface reference area, 0.004309 meter^2

b reference span, control surface (see table I)

C_A axial-force coefficient, $\frac{\text{Axial force}}{qA}$

$C_{A,c}$ chamber axial-force coefficient, $\frac{\text{Chamber axial force}}{qA}$

C_{BM} coefficient of control-surface root bending moment, $\frac{\text{Bending moment}}{qA_c b}$

C_D drag coefficient, $\frac{\text{Drag}}{qA}$

$C_{D,c}$ chamber drag coefficient, $\frac{\text{Chamber drag}}{qA}$

$C_{D,o}$ drag coefficient at $\alpha = 0^\circ$

C_{HM} coefficient of control-surface hinge moment, $\frac{\text{Hinge moment}}{qA_c c}$

C_L lift coefficient, $\frac{\text{Lift}}{qA}$

C_{L_α} lift-curve slope at $\alpha = 0^\circ$, per degree

C_m pitching-moment coefficient, $\frac{\text{Pitching moment}}{qAd}$

C_{m_δ} pitch control effectiveness at zero angle of attack, per degree of deflection, $\frac{\Delta C_m}{\Delta \delta_H}$

C_N normal-force coefficient, $\frac{\text{Normal force}}{qA}$

C_{NF} coefficient of control-surface normal force, $\frac{\text{Normal force}}{qA_c}$

c reference chord, control surface (see table I)

d body diameter, 7.62 centimeters

M free-stream Mach number

q free-stream dynamic pressure

$\frac{x_{ac}}{l}$ aerodynamic-center location in body lengths (measured from nose)

α angle of attack, degrees

δ_H pitch control deflection of control surfaces (negative with leading edge down; two fins deflected for $\phi = 0^\circ$; four fins deflected for $\phi = 45^\circ$), degrees

ϕ model roll angle, positive clockwise when viewed from rear ($\phi = 0^\circ$ when fins are in horizontal and vertical positions), degrees

ϕ_f roll attitude of specific fin panel, positive clockwise when viewed from rear ($\phi_f = 0^\circ$ when fin is on top of model in vertical position), degrees

APPARATUS AND METHODS

Tunnel

The tests were made in the low Mach number test section of the Langley Unitary Plan wind tunnel, which is a variable-pressure continuous-flow facility. The test section is approximately 1.22 meters square and 2.13 meters long. The nozzle leading to the test section is of the asymmetric sliding-block type which provides a continuous variation in test-section Mach number from about 1.5 to 2.9.

Model

Details of the model are shown in figure 1. The body had a fineness ratio of 13.06 and consisted of a 3-caliber nose with an apex radius of 0.030 cm, a cylindrical center-body, and a 4° boattail afterbody. The model was wingless and was provided with four sets of cruciform, all movable aft control surfaces of varying planform. (See fig. 1(b).) Two external body fairings, 180° apart and interdigitated with the controls, extended from model station 38.81 cm to the model base. Details of the four fins tested are shown in figure 1(b) and table I. The fins, identified herein as T_9, T_{10}, T_{11}, and T_{12}, were designed to have the same exposed area. In addition, fins T_9, T_{10}, and T_{11} have a common span and aspect ratio. Fins T_9 and T_{10} differed in leading-edge sweep angle and planform taper ratio. Fins T_9 and T_{11} have the same planform taper ratio but differ in planform due to a change in trailing-edge sweep angle from zero with T_9 to a forward sweep angle with T_{11}. Fin T_{12} has a greater span and consequently a greater aspect ratio than the other fins.

Tests

For the present tests, the Mach numbers, stagnation pressures, and stagnation temperatures were as follows:

M	Stagnation pressure, kN/m^2	Stagnation temperature, K
1.60	68.28	339
2.36	94.56	339
2.86	123.05	339

The stagnation dewpoint was maintained sufficiently low (239 K) to assure negligible condensation effects. The tests were made through an angle-of-attack range from about -4° to 22° at a sideslip angle of 0° and at a Reynolds number of 8.2×10^6 based on model length. All configurations were tested at roll angles of 0° and 45°.

All tests were made with the boundary-layer transition point fixed by means of roughness strips. The leading edges of the 0.16-cm-wide transition strips were located 3.05 cm aft of the body nose and 1.02 cm streamwise behind the fin leading edges. All transition strips were composed of No. 50 sand grains having a nominal diameter of 0.033 cm.

Measurements

The aerodynamic forces and moments on the model were measured by means of a six-component, internal, strain-gage balance. Forces and moments on the fins were measured by means of three-component strain-gage balances built with the fins. For fins T_{10}, T_{11}, and T_{12}, fin loads were measured on two of the panels of each set of fins; these panels were located at the top and right side of the body when viewed from the rear at a model roll angle of zero. For fin T_9, fin loads were measured only on one panel; this panel was located at the right side of the body when viewed from the rear at a model roll angle of zero. The model was rolled in order to afford ϕ_f variation for fin loads. Balance chamber pressure was measured by means of a static-pressure orifice located within the balance cavity.

Corrections

The angles of attack have been corrected for sting and balance deflection due to aerodynamic loads and for tunnel airflow misalinement. The axial-force and drag data have been adjusted to a condition of free-stream static pressure acting at the model base and typical values of these corrections are shown in figure 2.

PRESENTATION OF RESULTS

DISCUSSION

The basic longitudinal aerodynamic characteristics of the configuration at $\phi = 0^o$ and 45^o with fins T_9, T_{10}, T_{11}, and T_{12} (figs. 3 to 10) indicate that over the Mach number range of this investigation, the pitching-moment and lift curves are nonlinear. A progressive decrease in stability occurs for each configuration as the Mach number is increased. Changes in fin taper ratio and trailing-edge sweep $(T_9$, T_{10}, and $T_{11})$ have no large effect on these basic characteristics. Increasing the aspect ratio (T_{12}), however, generally causes an increase in stability and lift-curve slope throughout the test Mach number range.

The summary of longitudinal characteristics (fig. 11) indicates an aerodynamic-center shift of about 10 percent of the body length over the Mach number range from 1.60 to 2.86 with the model at $\phi = 0^o$ and 45^o. The configuration with the highest aspect ratio fin (T_{12}) has the most rearward aerodynamic-center location. The pitch control effectiveness C_{m_δ} and lift-curve slope C_{L_α} decrease with an increase in Mach number for all fins with the model at $\phi = 0^o$ and 45^o. However, deflection of each fin configuration is effective in producing positive pitch control. The fin with the highest aspect ratio (T_{12})

generally has the highest values of C_{m_δ} and C_{L_α}. However, the T_{12} configuration also has slightly higher values of minimum drag coefficient because of the greater thickness ratio.

Results showing the variation of the fin load coefficients with angle of attack for fins T_9, T_{10}, T_{11}, and T_{12} are presented in figures 12 to 23. It should be noted that for each of these fins, the bending-moment data C_{BM} and hinge-moment data C_{HM} are based on the span and root chord, respectively, of each fin; the area of each fin planform is the same. There are no large differences in the data due to changes in taper ratio or trailing-edge sweep $(T_9, T_{10}, \text{and } T_{11})$ for the fin panel at $\phi_f = 45^o$. Increasing the aspect ratio (T_{12}) generally leads to noticeably greater values of maximum normal-force and bending-moment coefficients for the fin panel at $\phi_f = 45^o$. As would be expected, an increase in Mach number causes a slight decrease in C_{NF} and C_{BM} for all of the fin configurations tested. For the fin panel at $\phi_f = 45^o$, it should be noted that the normal-force and bending-moment coefficients peak at $\alpha \approx 8^o$; above this angle of attack, the C_{NF} and C_{BM} values generally decrease somewhat. These decreases are due to body "shielding" (low pressures generated on the leeward side of the body) at these angles of attack. For the fin panels at $\phi_f = 90^o$ and 135^o, the normal-force and bending-moment coefficients continually increase to the highest test angle of attack. For each of these ϕ_f variations, the slopes of the normal-force and bending-moment coefficients with α for fins T_{10} and T_{11} are about the same and are slightly greater than those for fin T_9. Fin T_{12} has the greatest slope of normal-force and bending-moment coefficients of all the fins tested because of the greater aspect ratio. There are no large differences in hinge-moment coefficient for any of the fins tested and there is little effect of Mach number on the hinge-moment coefficients.

CONCLUSIONS

Wind-tunnel tests of a wingless missile configuration with aft tail controls at Mach numbers from 1.60 to 2.86 to determine the effects of fin planform on the model aerodynamic characteristics and fin loads lead to the following conclusions:

1. There are no large differences in the aerodynamic results due to fin taper ratio or trailing-edge sweep. An increase in aspect ratio, however, leads to an increase in stability level, lift-curve slope, and pitch-control effectiveness.

2. The fin normal-force and bending-moment coefficients peak at angle of attack approximately equal to 8^o for the fin panel at roll attitude of 45^o due to a body shielding effect at high angles of attack. For the fin panel at roll attitudes of 90^o and 135^o, these coefficients continually increase to the highest test angle of attack.

3. The slopes of the normal-force and bending-moment curves are the greatest for the fin with the highest aspect ratio and indicate only small differences due to taper ratio or trailing-edge sweep.

4. There was little effect of fin planform or Mach number on the fin hinge-moment coefficients.

Langley Research Center,
National Aeronautics and Space Administration,
Hampton, Va., April 9, 1973.

REFERENCE

1. Fuller, Dennis E.; Richardson, Celia S.; and Spearman, M. Leroy: Aerodynamic Characteristics of a Wingless Missile With Aft Cruciform Controls at Mach Numbers From 2.30 to 4.63. NASA TM X-2488, 1972.

TABLE I.- FIN CHARACTERISTICS

	T_9	T_{10}	T_{11}	T_{12}
Exposed semispan (reference span), cm	4.244	4.244	4.244	5.715
Exposed root chord (reference chord), cm	14.303	12.695	14.303	10.620
Exposed area per panel, cm^2	43.097	43.097	43.097	43.097
Maximum thickness, cm	1.016	1.016	1.016	1.016
Exposed aspect ratio	0.418	0.418	0.418	0.758
Exposed taper ratio	0.42	0.60	0.42	0.42
Leading-edge sweep, deg	62.90	50.10	57.23	47.15

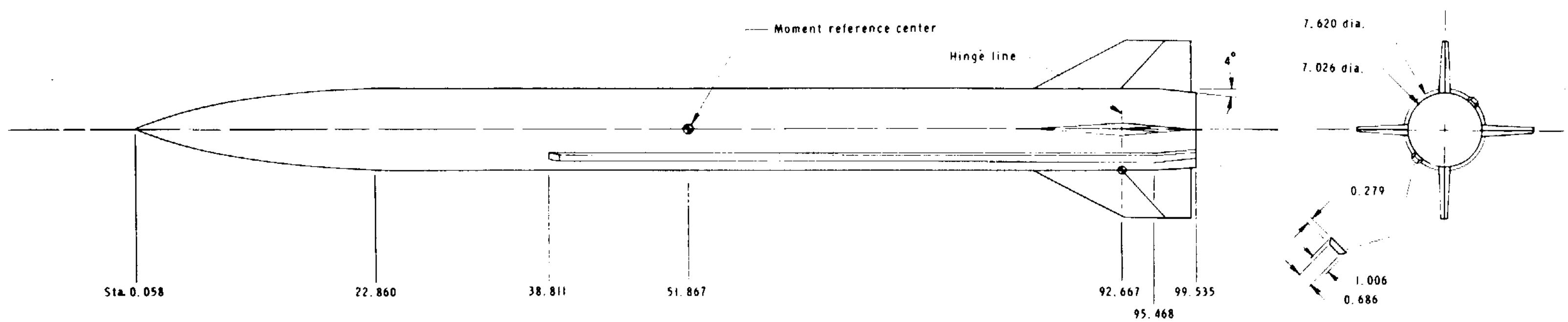

(a) Model details.

Figure 1.- Drawing of model. All dimensions are in centimeters unless otherwise noted.

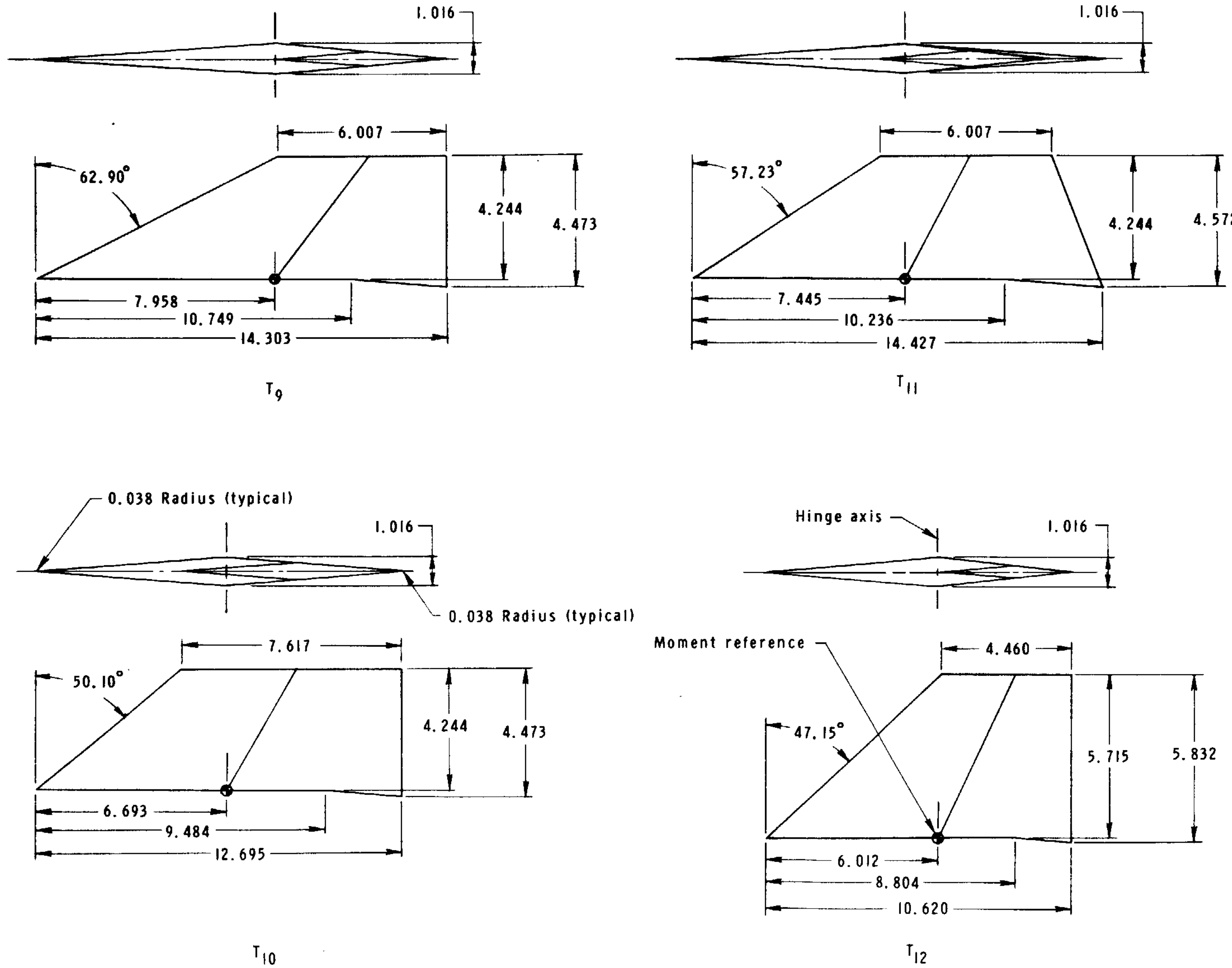

(b) Fin details.

Figure 1.- Concluded.

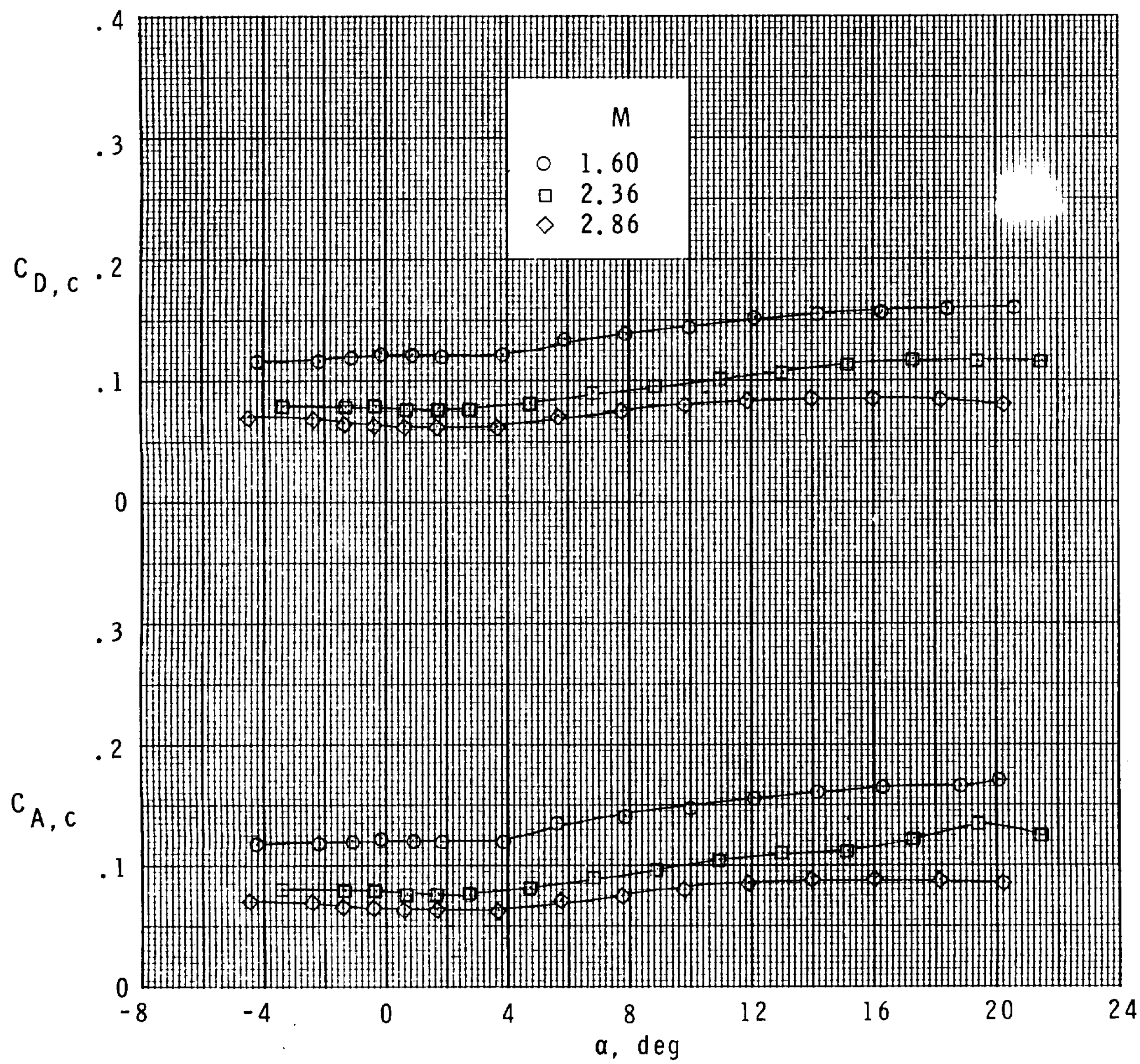

Figure 2.- Typical values of chamber axial-force and drag coefficients.

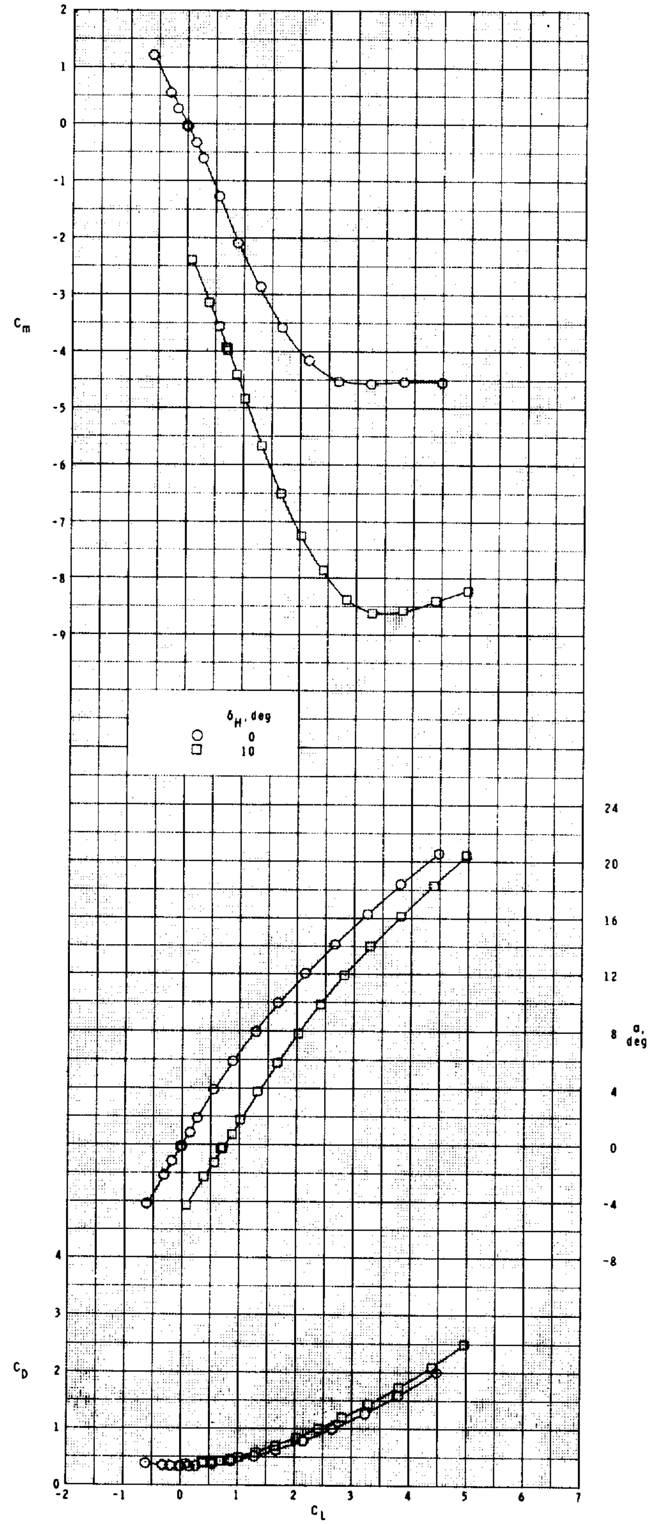

(a) M = 1.60.

Figure 3.- Longitudinal aerodynamic characteristics of the configuration with fin T_9 at $\phi = 0^o$.

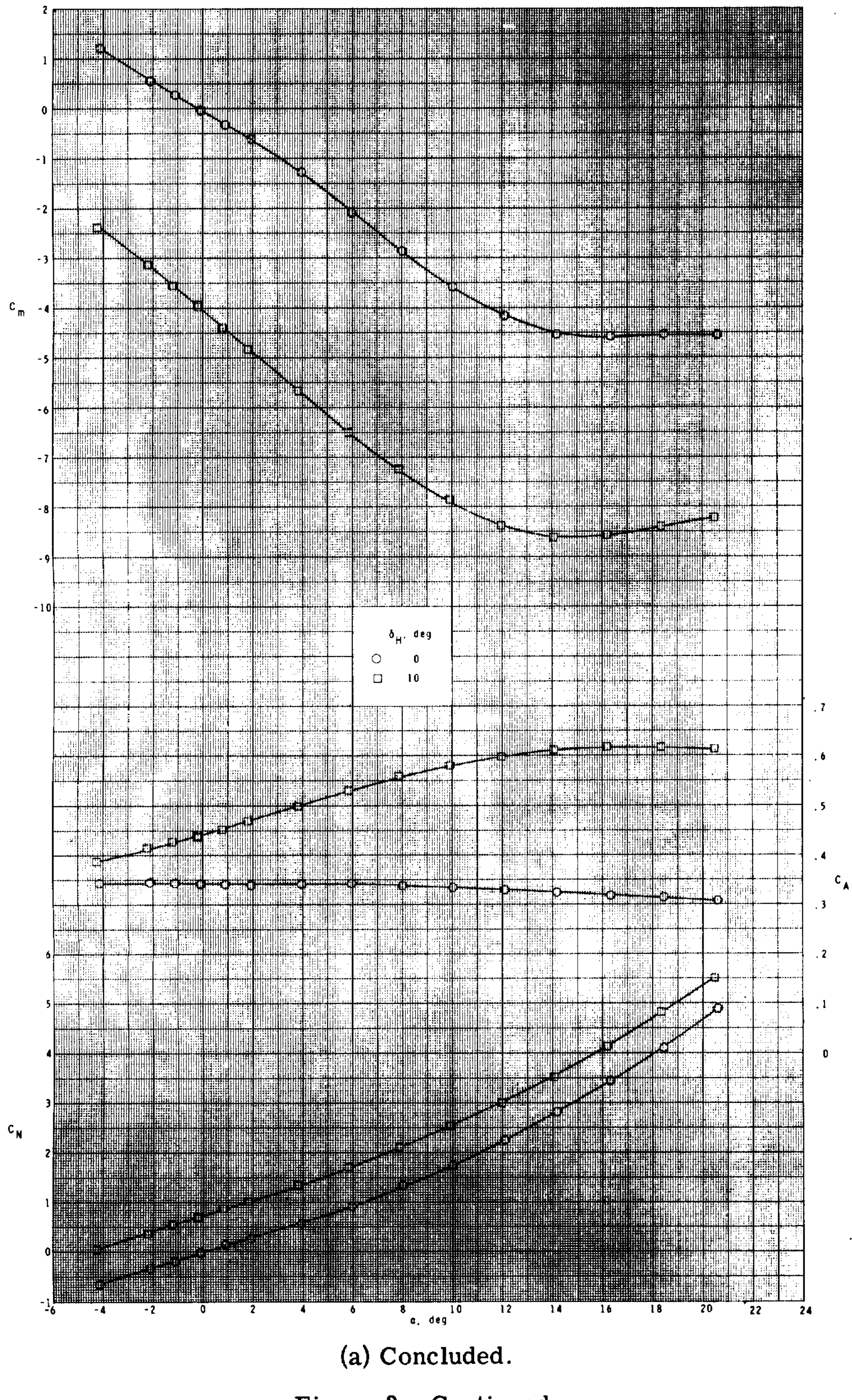

(a) Concluded.

Figure 3.- Continued.

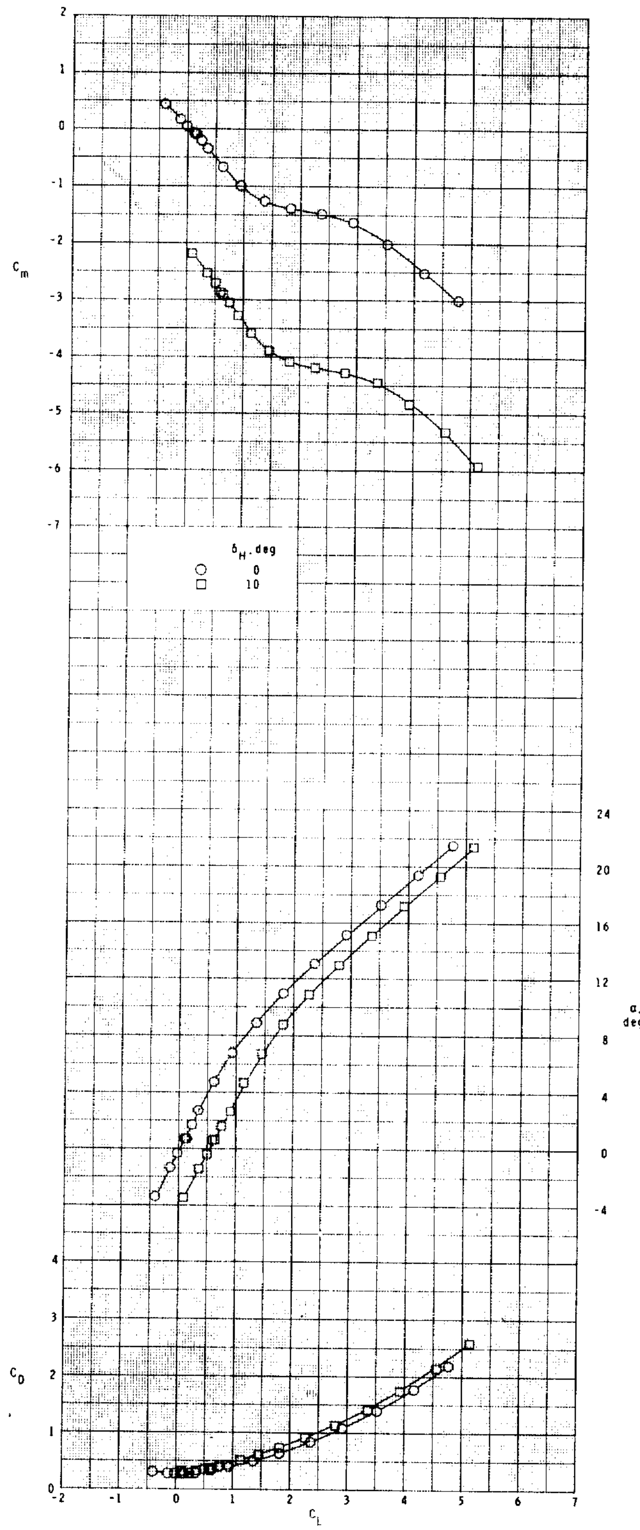

(b) M = 2.36.

Figure 3.- Continued.

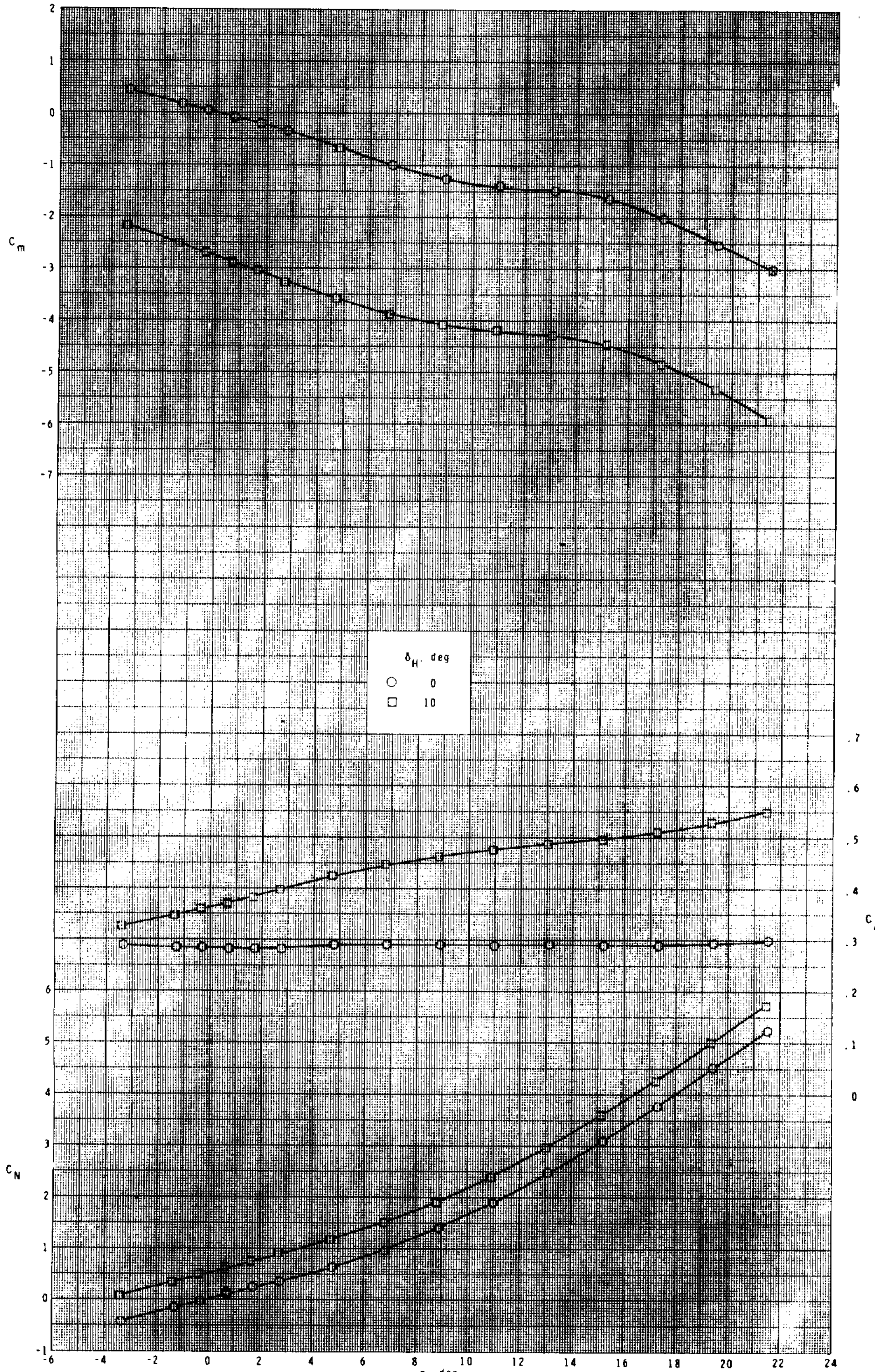

(b) Concluded.

Figure 3.- Continued.

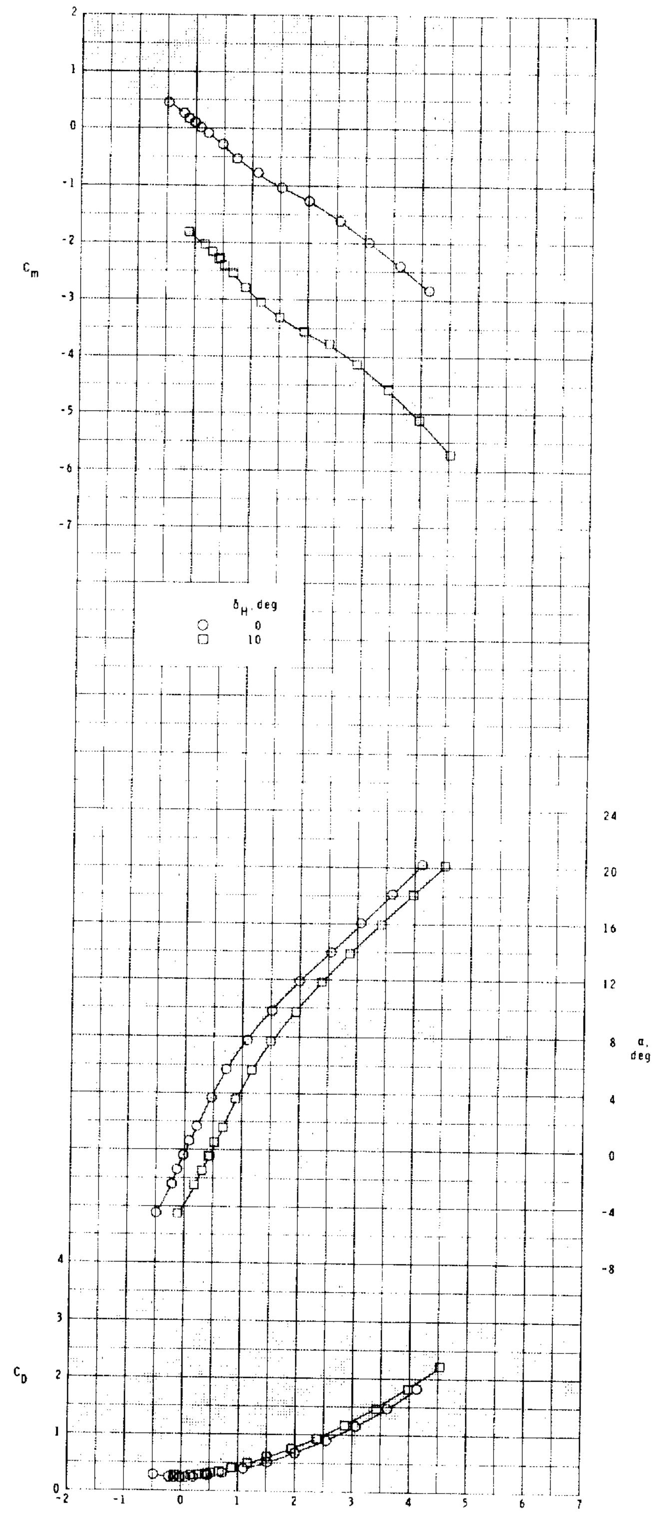

(c) M = 2.86.

Figure 3.- Continued.

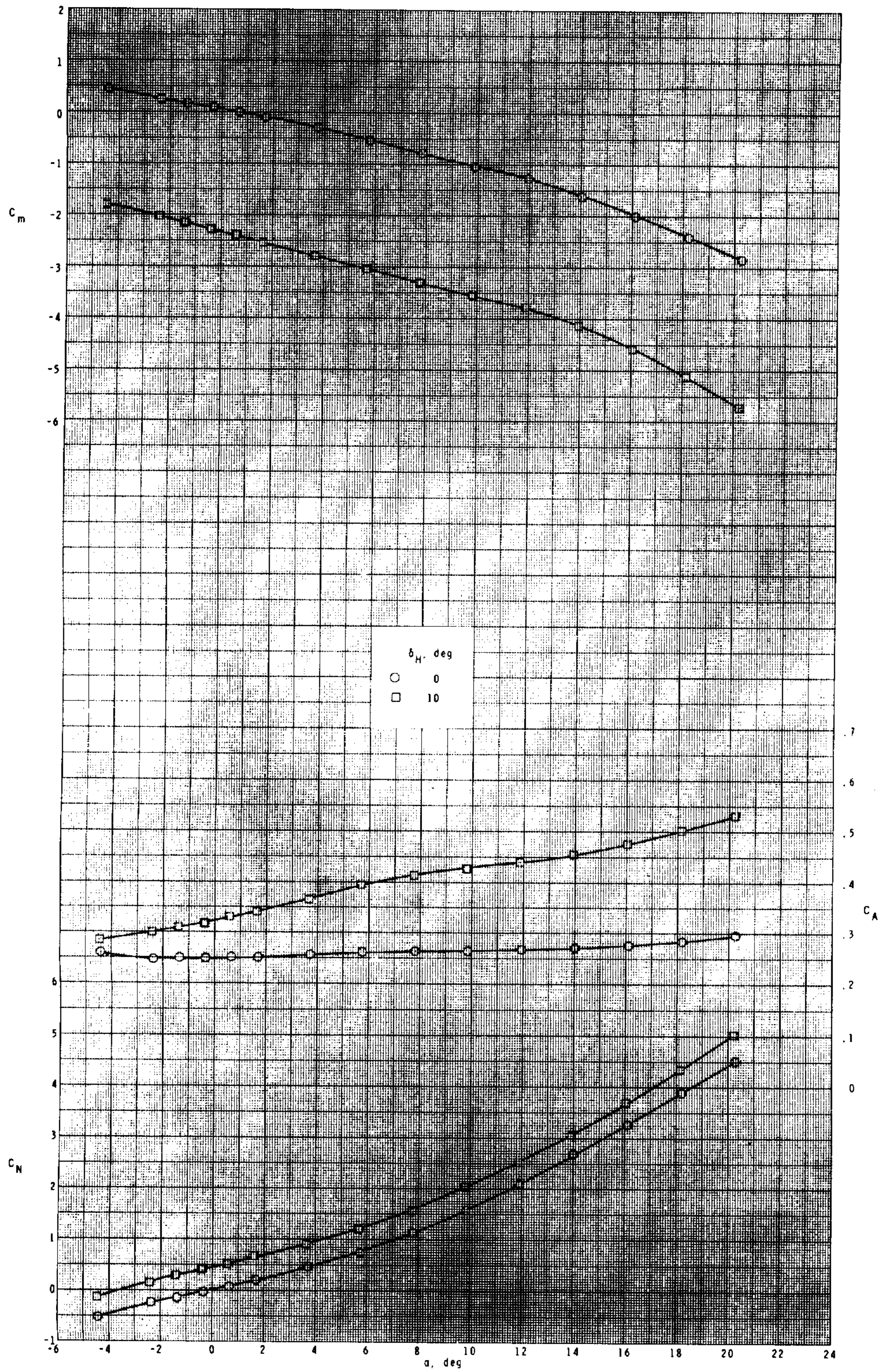

(c) Concluded.

Figure 3.- Concluded.

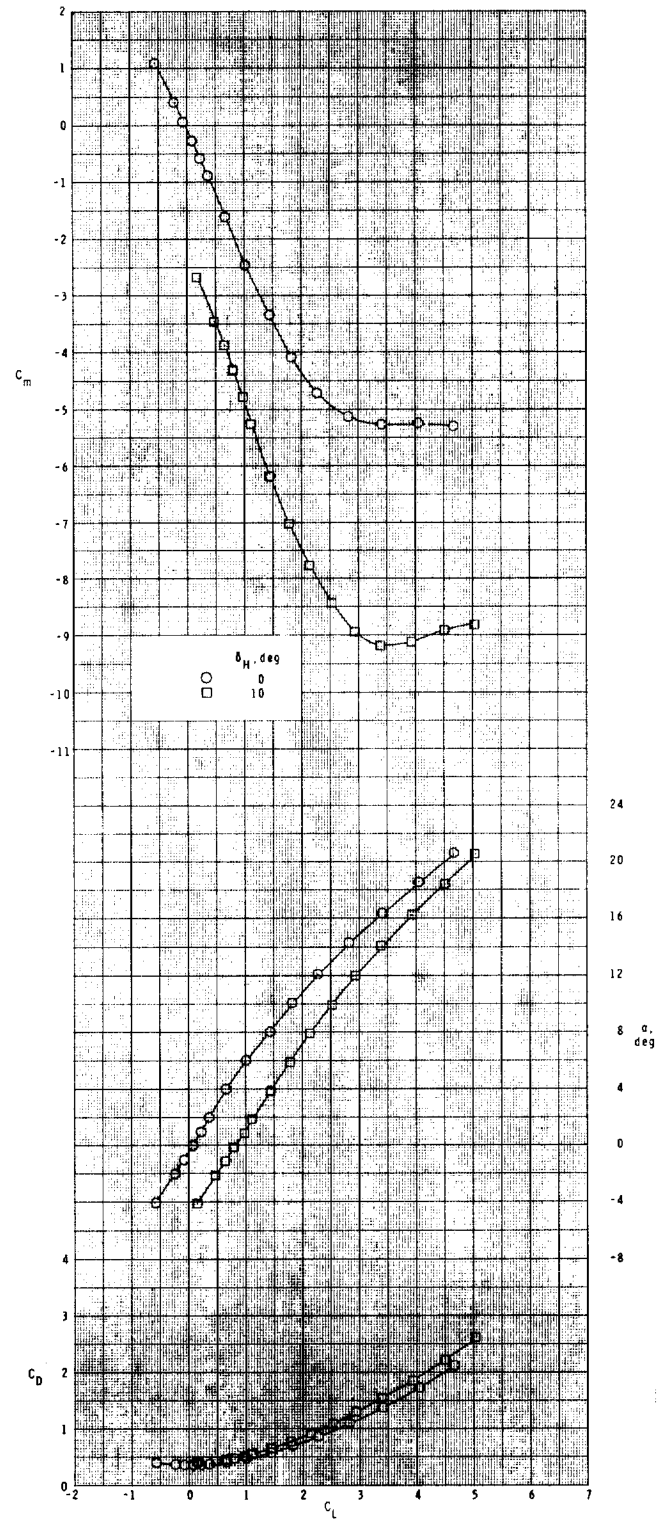

(a) M = 1.60.

Figure 4.- Longitudinal aerodynamic characteristics of the configuration with fin T_{10} at $\phi = 0^{\circ}$.

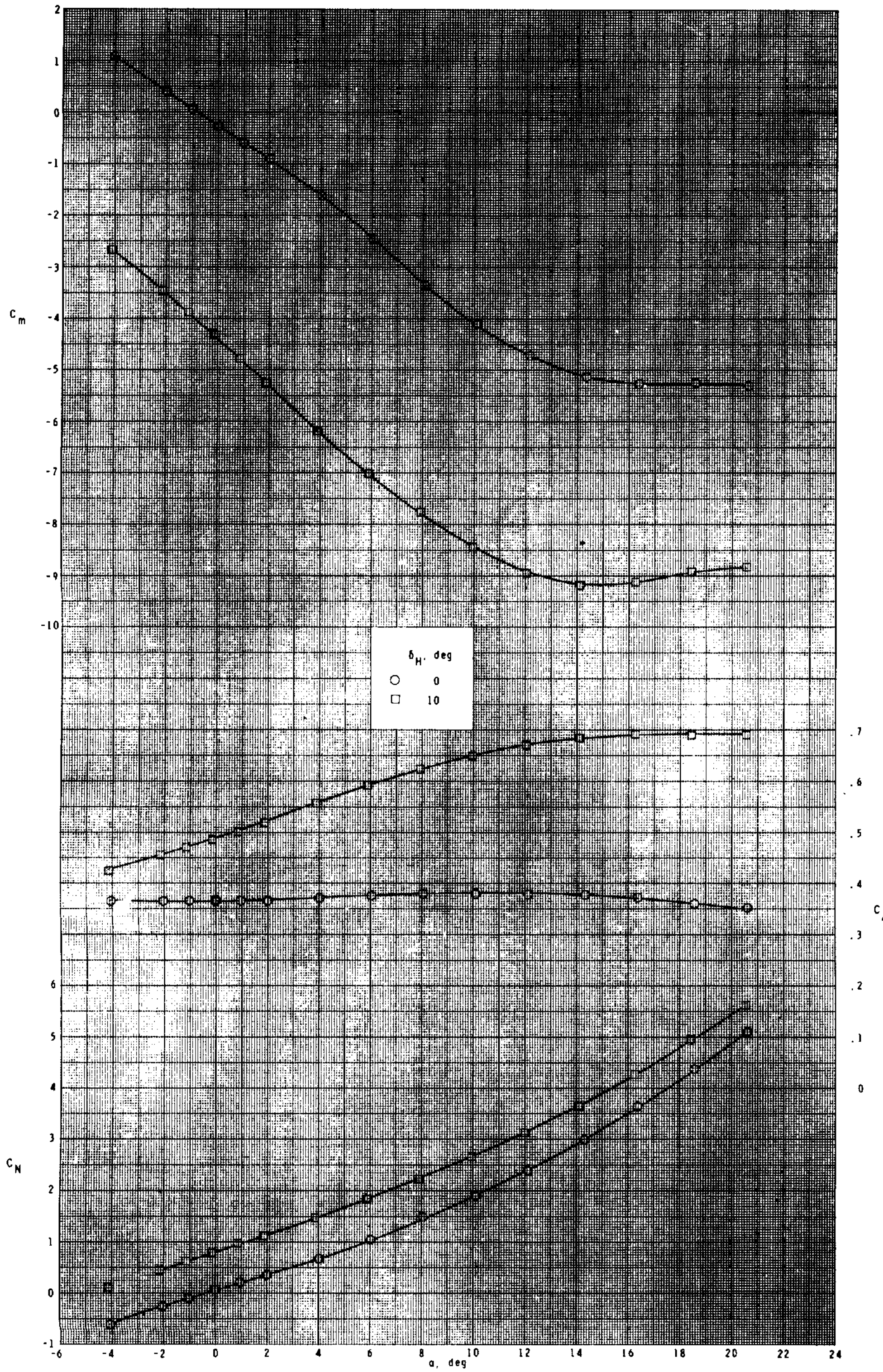

(a) Concluded.

Figure 4.- Continued.

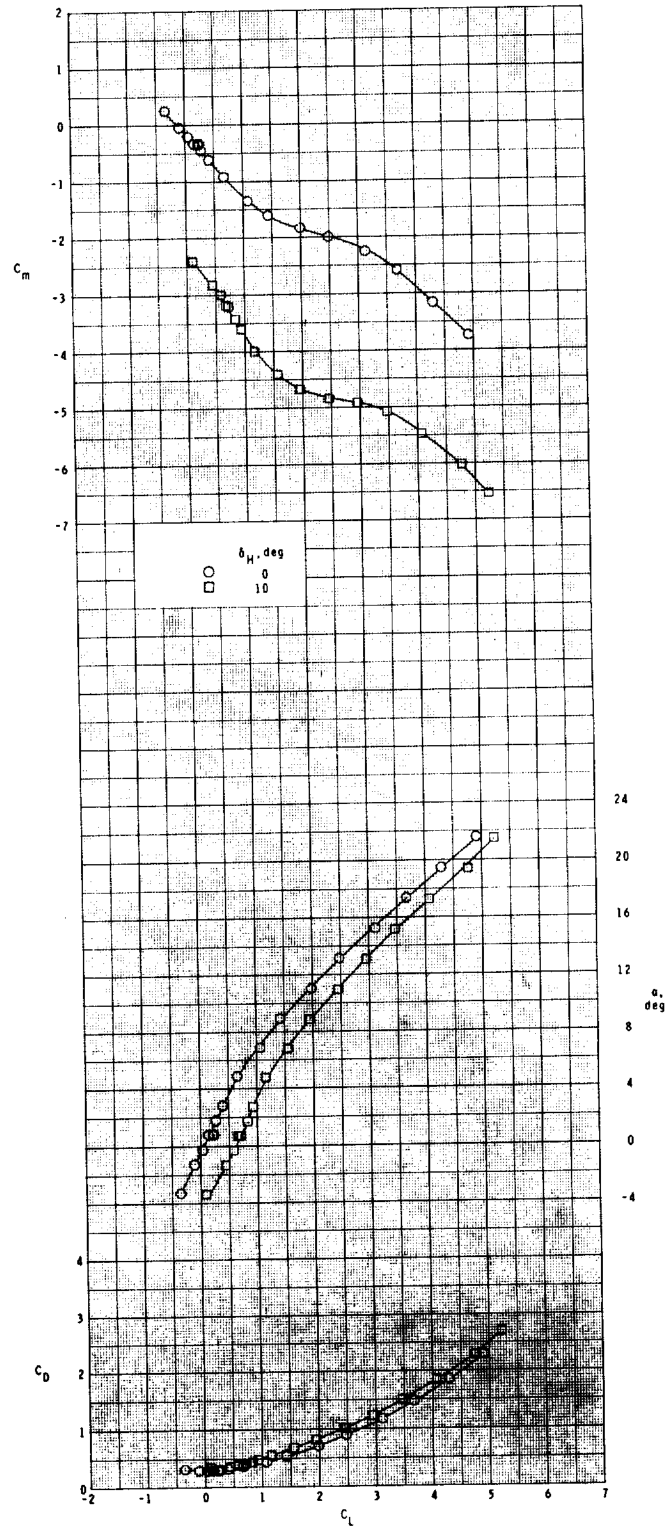

(b) M = 2.36.

Figure 4.- Continued.

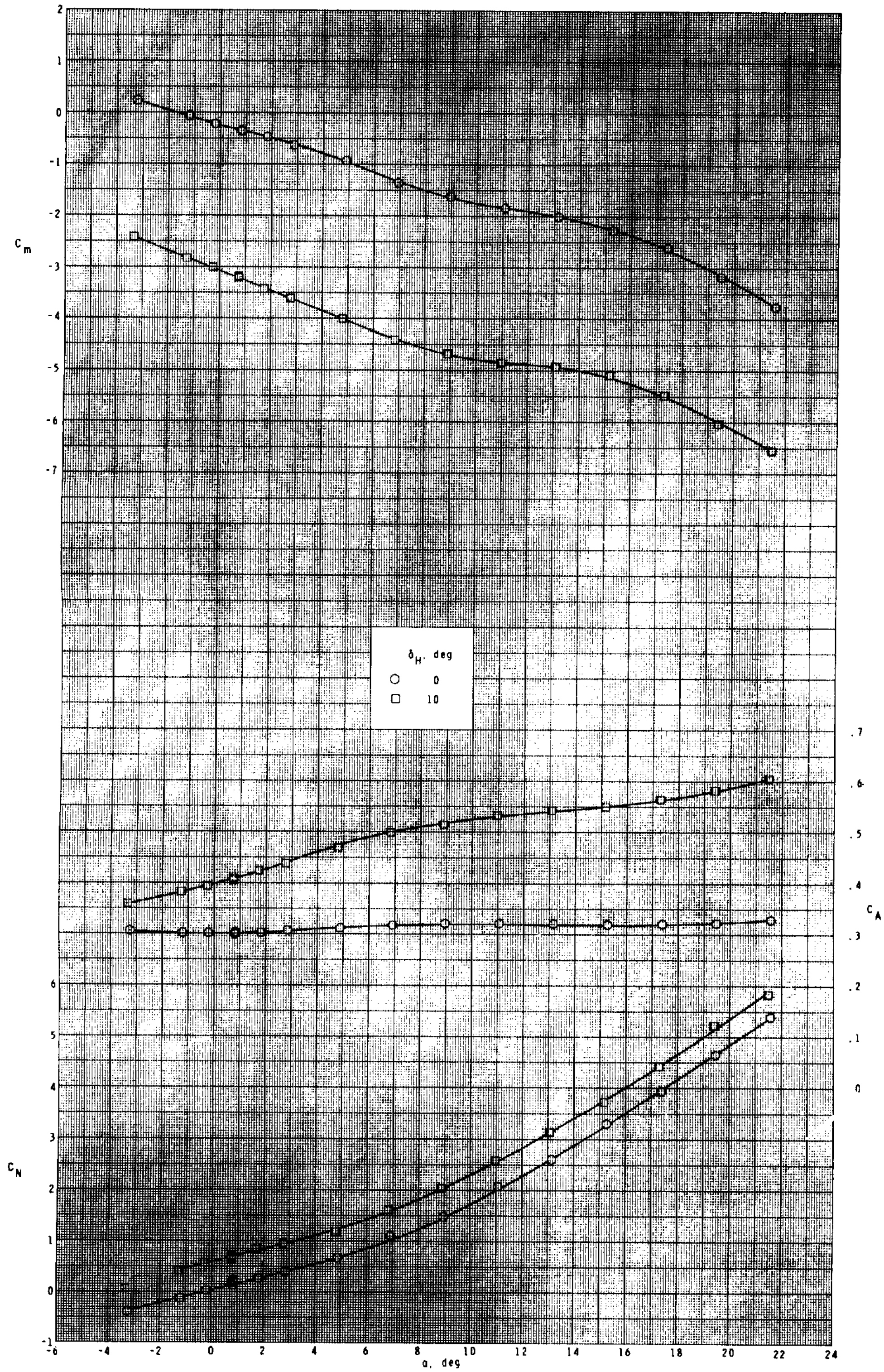

(b) Concluded.

Figure 4.- Continued.

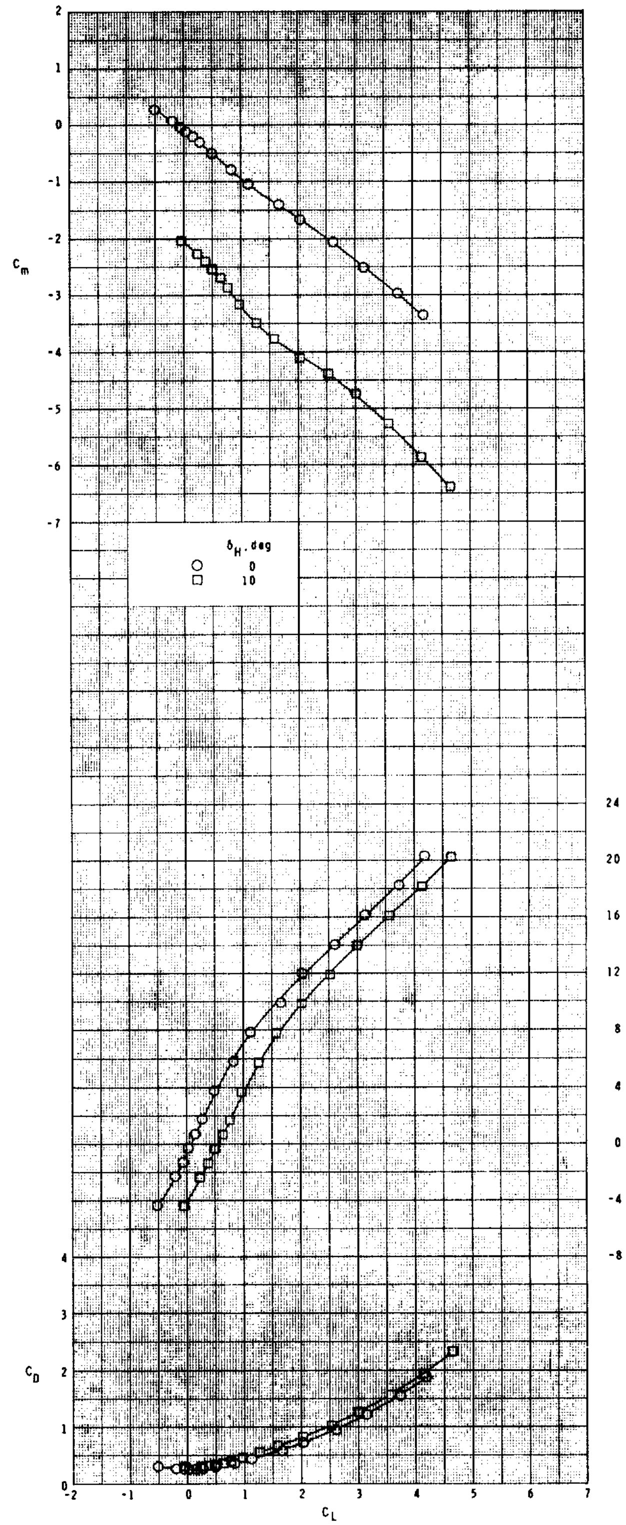

(c) M = 2.86.

Figure 4.- Continued.

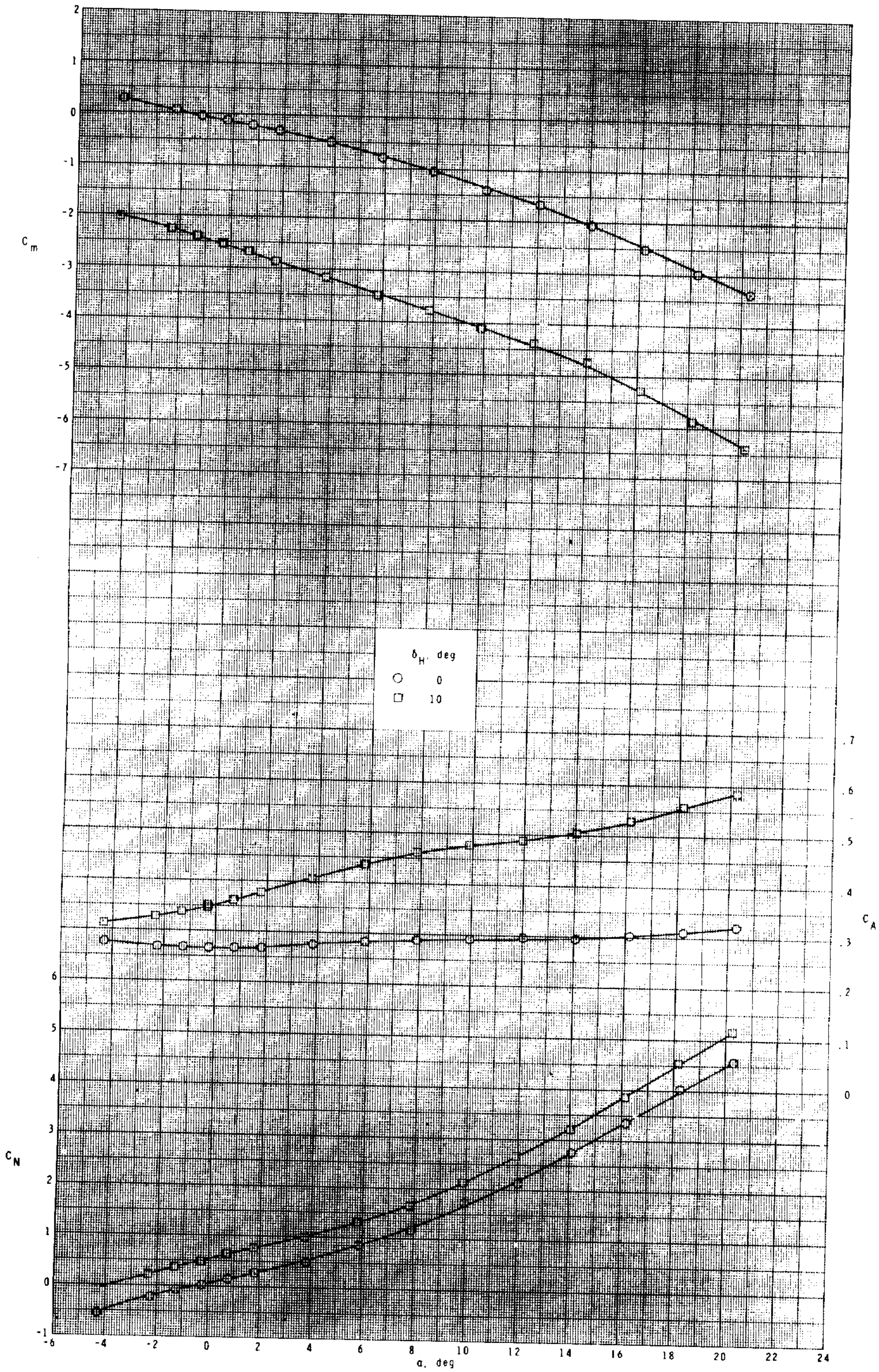

(c) Concluded.

Figure 4.- Concluded.

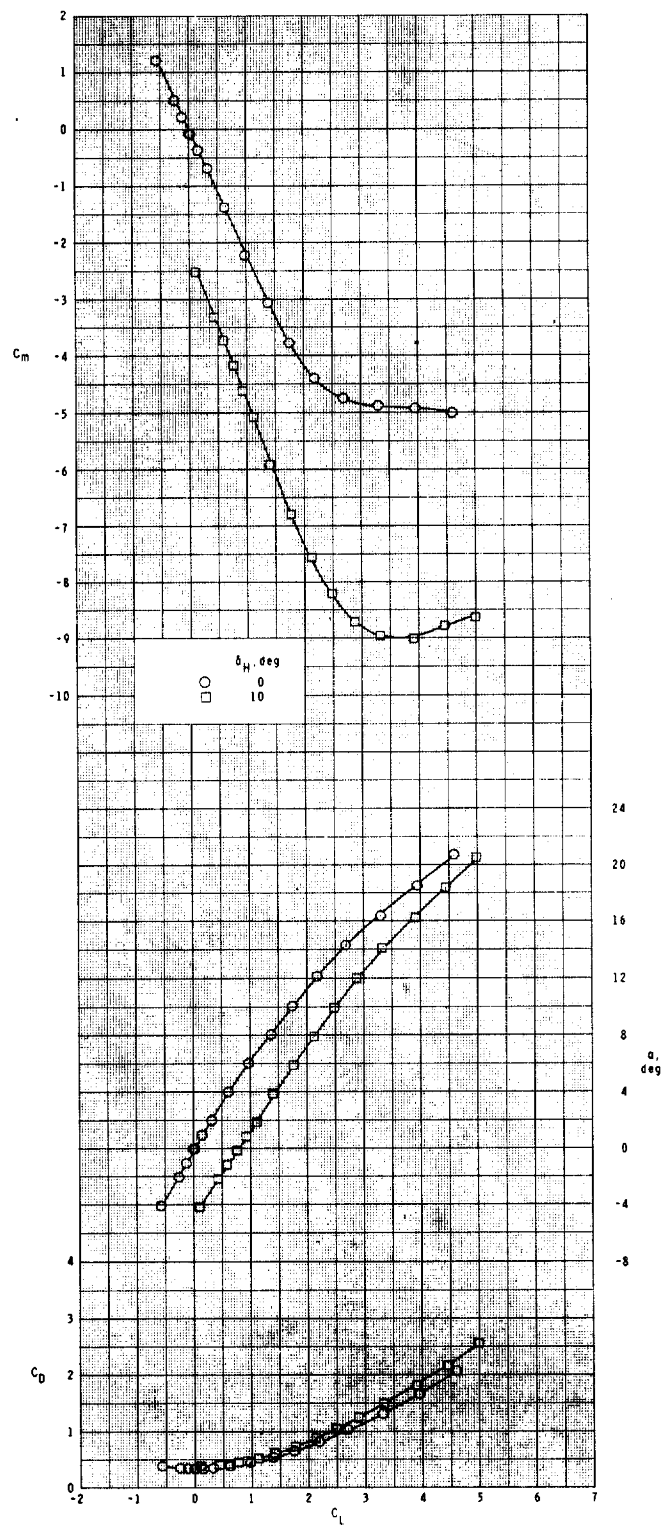

(a) M = 1.60.

Figure 5.- Longitudinal aerodynamic characteristics of the configuration with fin T_{11} at $\phi = 0^{\circ}$.

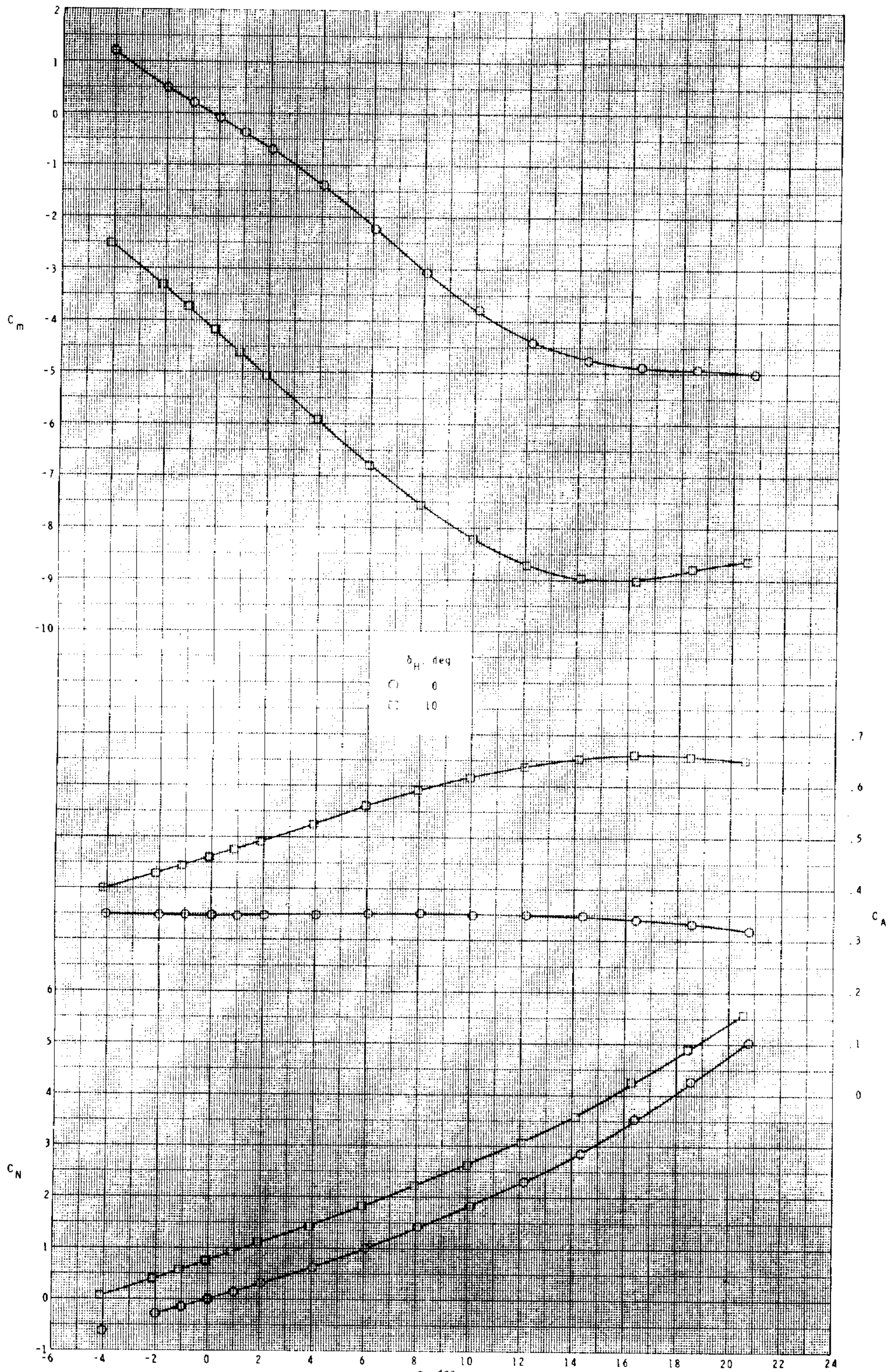

(a) Concluded.

Figure 5.- Continued.

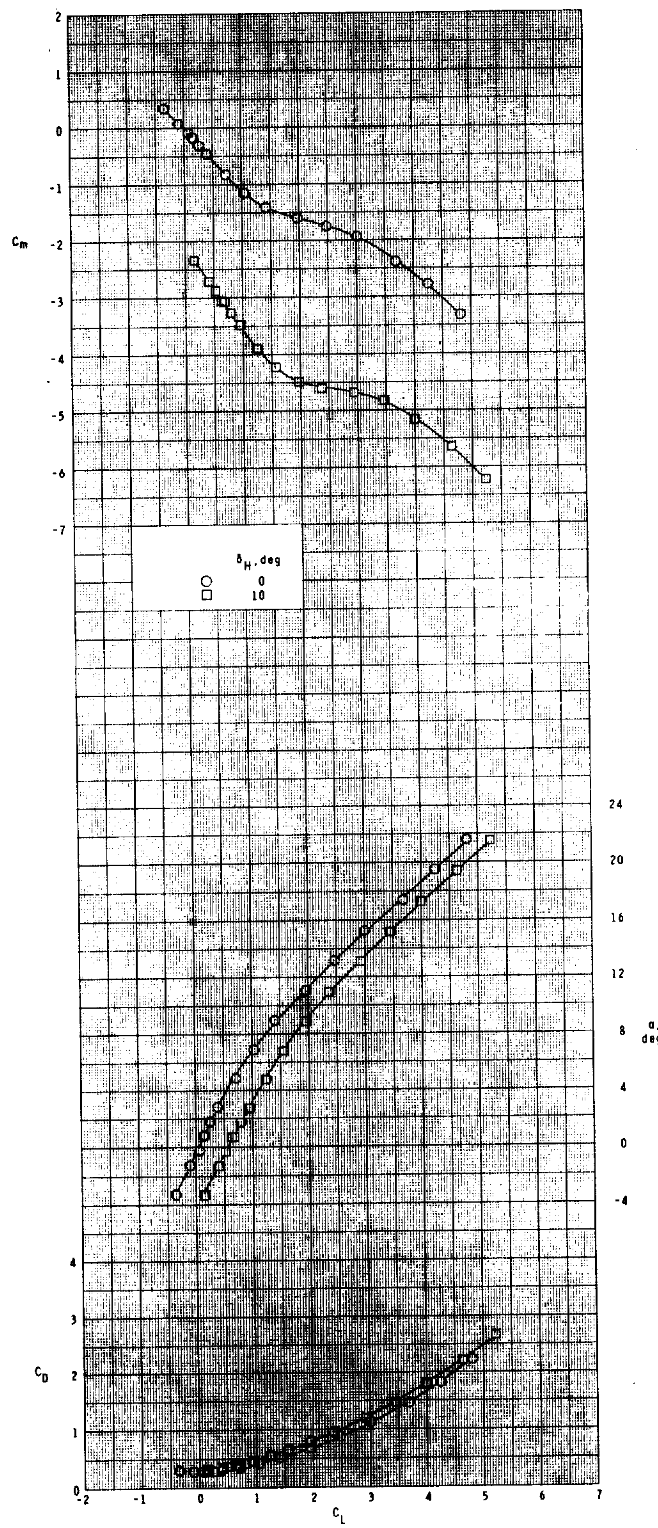

(b) M = 2.36.

Figure 5.- Continued.

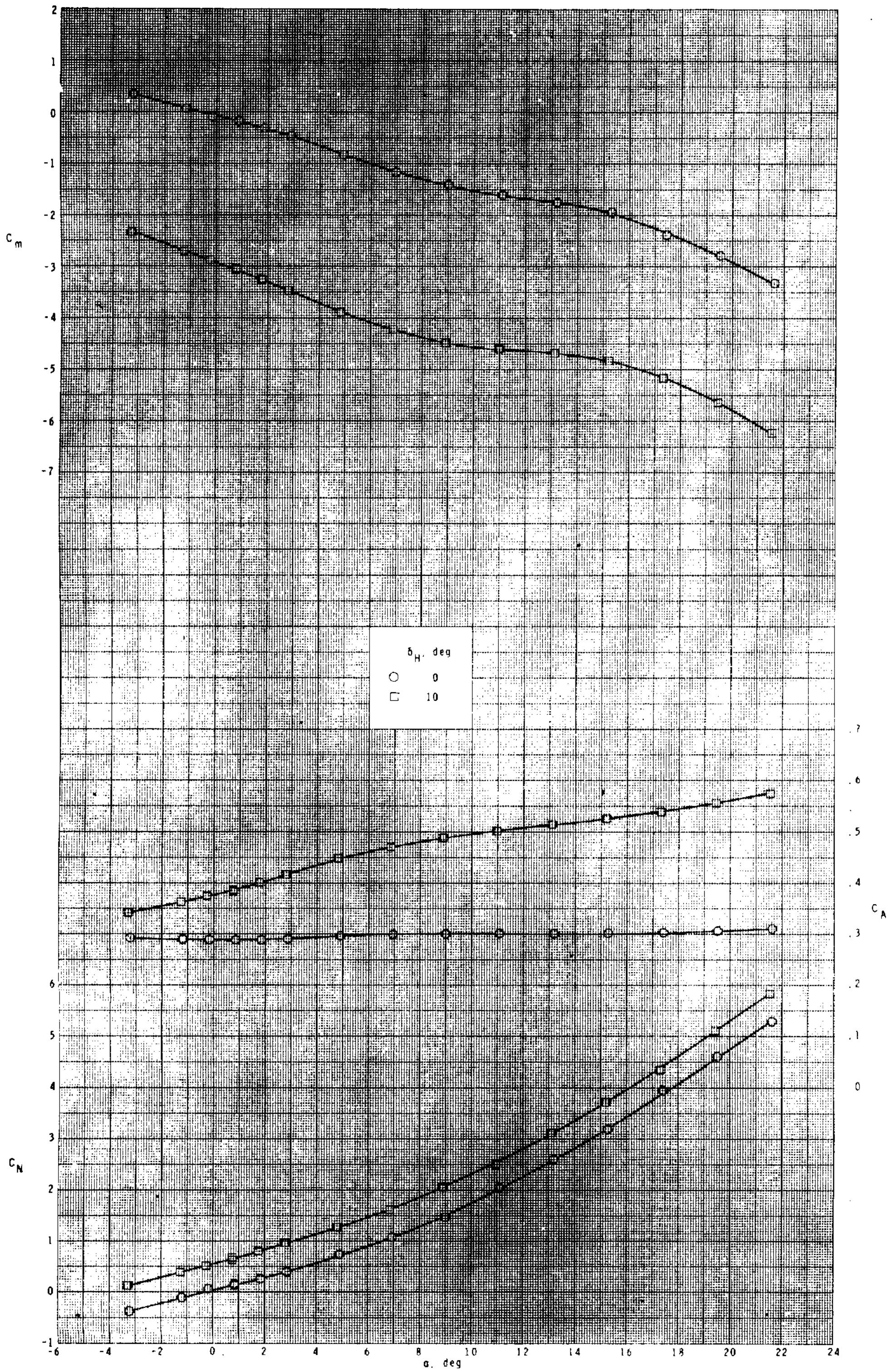

(b) Concluded.

Figure 5.- Continued.

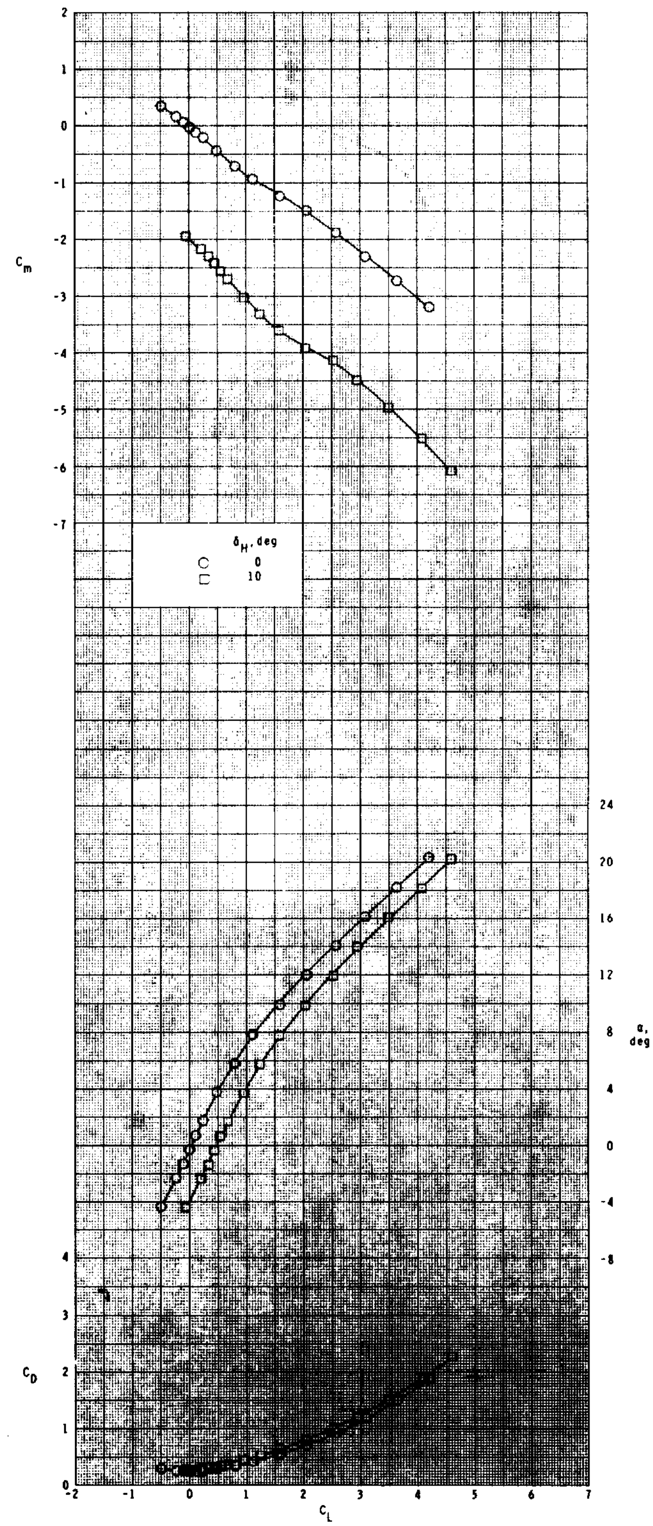

(c) M = 2.86.

Figure 5.- Continued.

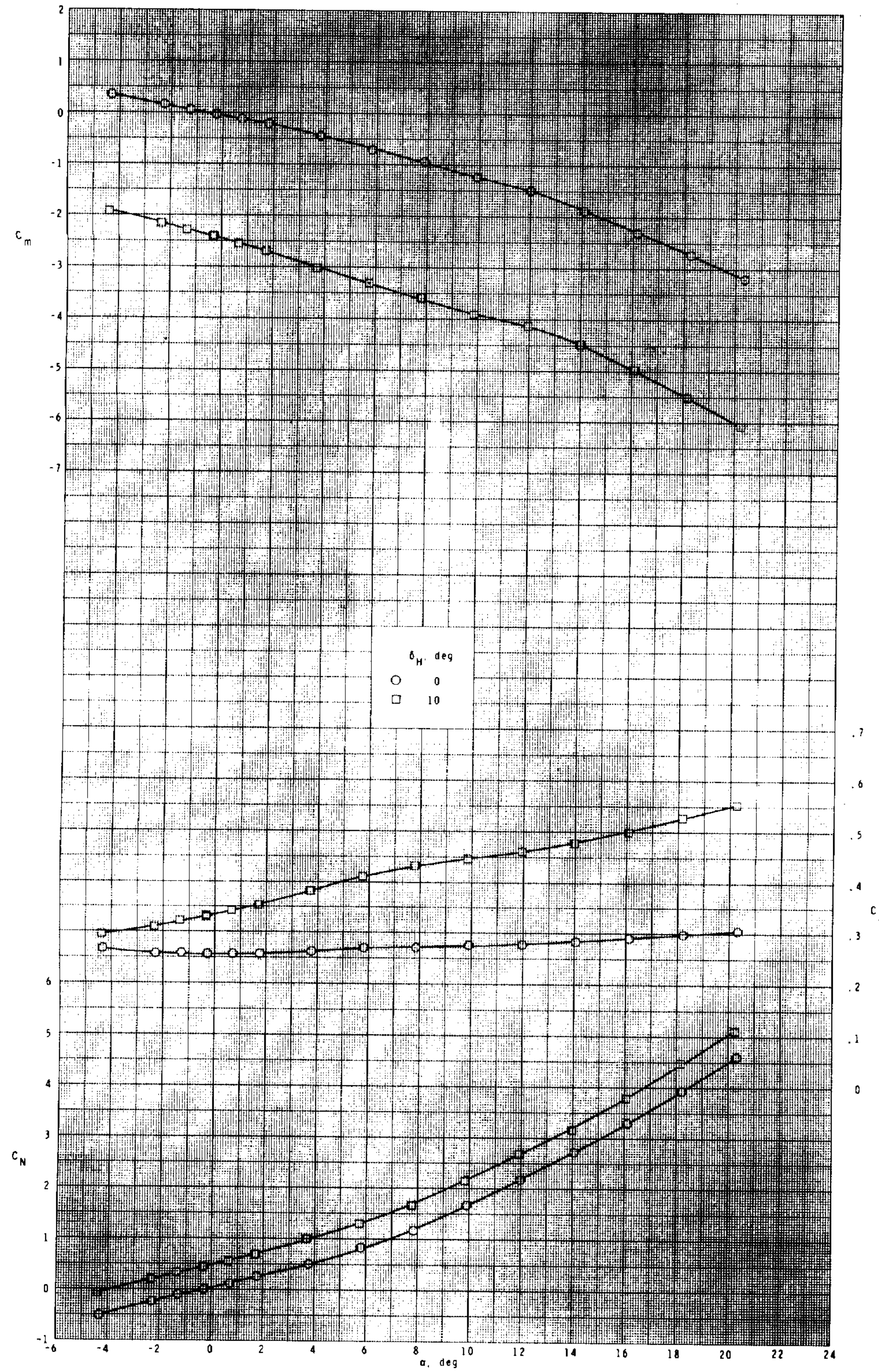

(c) Concluded.

Figure 5.- Concluded.

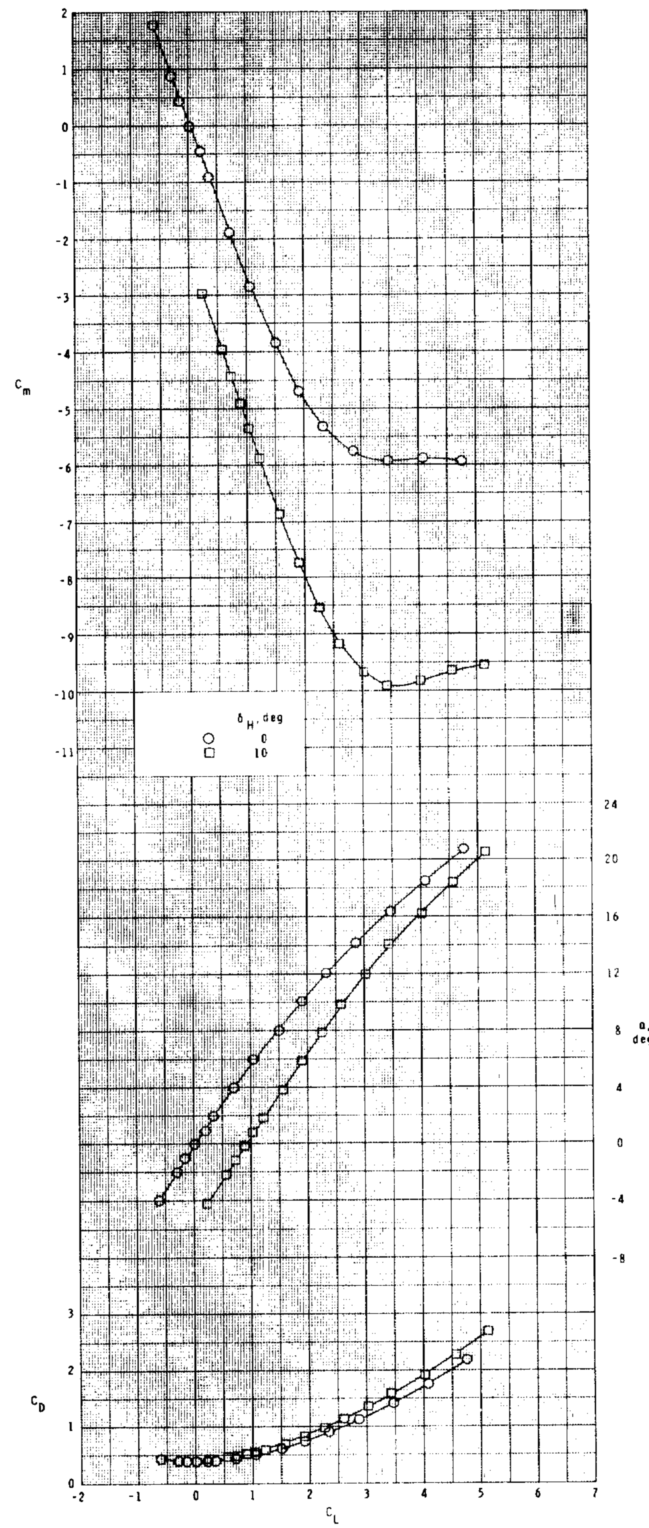

(a) M = 1.60.

Figure 6.- Longitudinal aerodynamic characteristics of the configuration with fin T_{12} at $\phi = 0^{\circ}$.

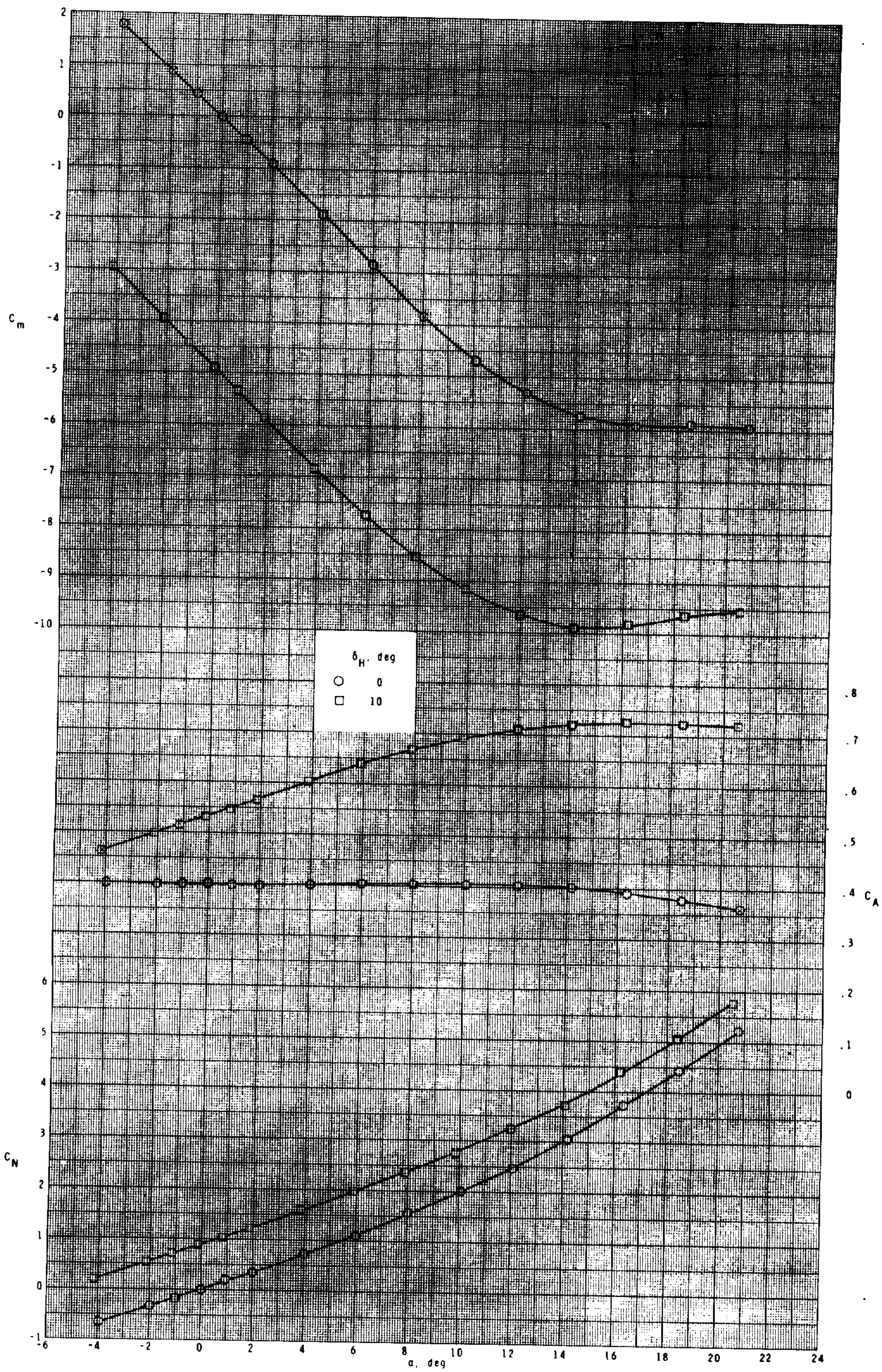

(a) Concluded.

Figure 6.- Continued.

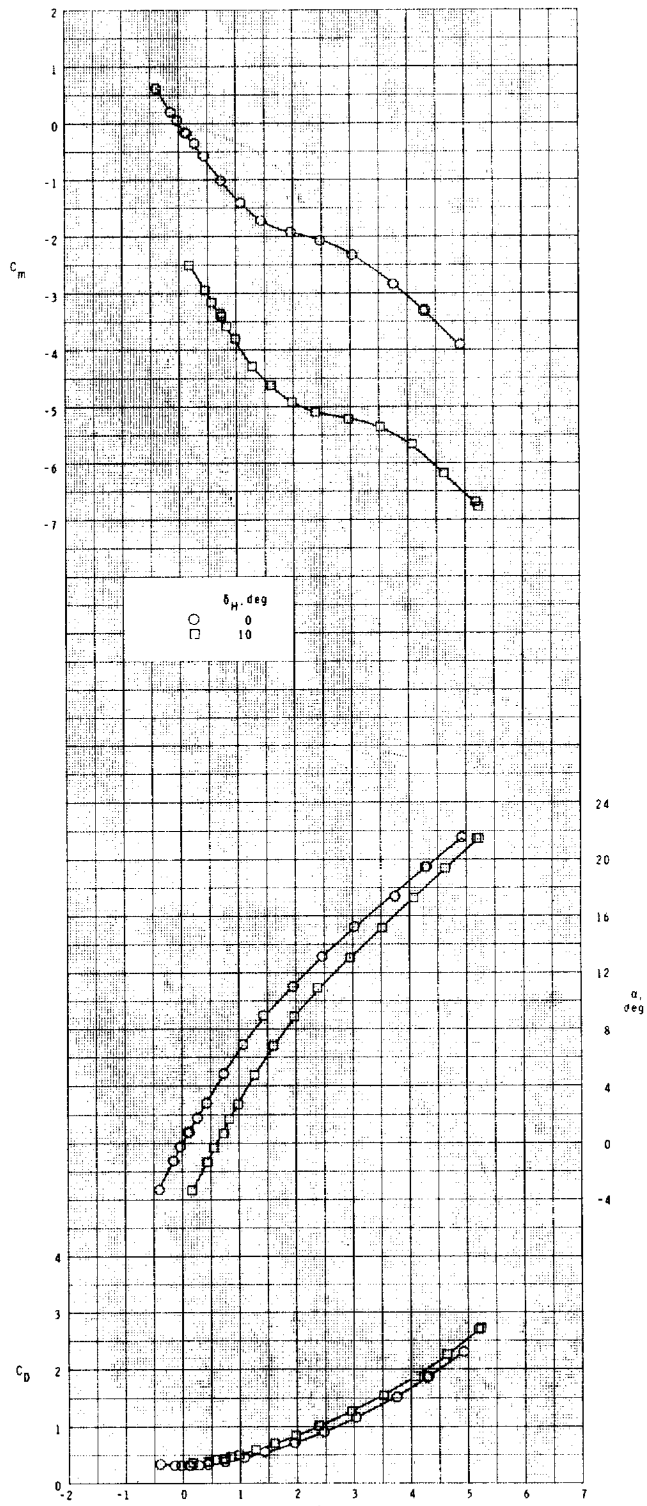

(b) M = 2.36.

Figure 6.- Continued.

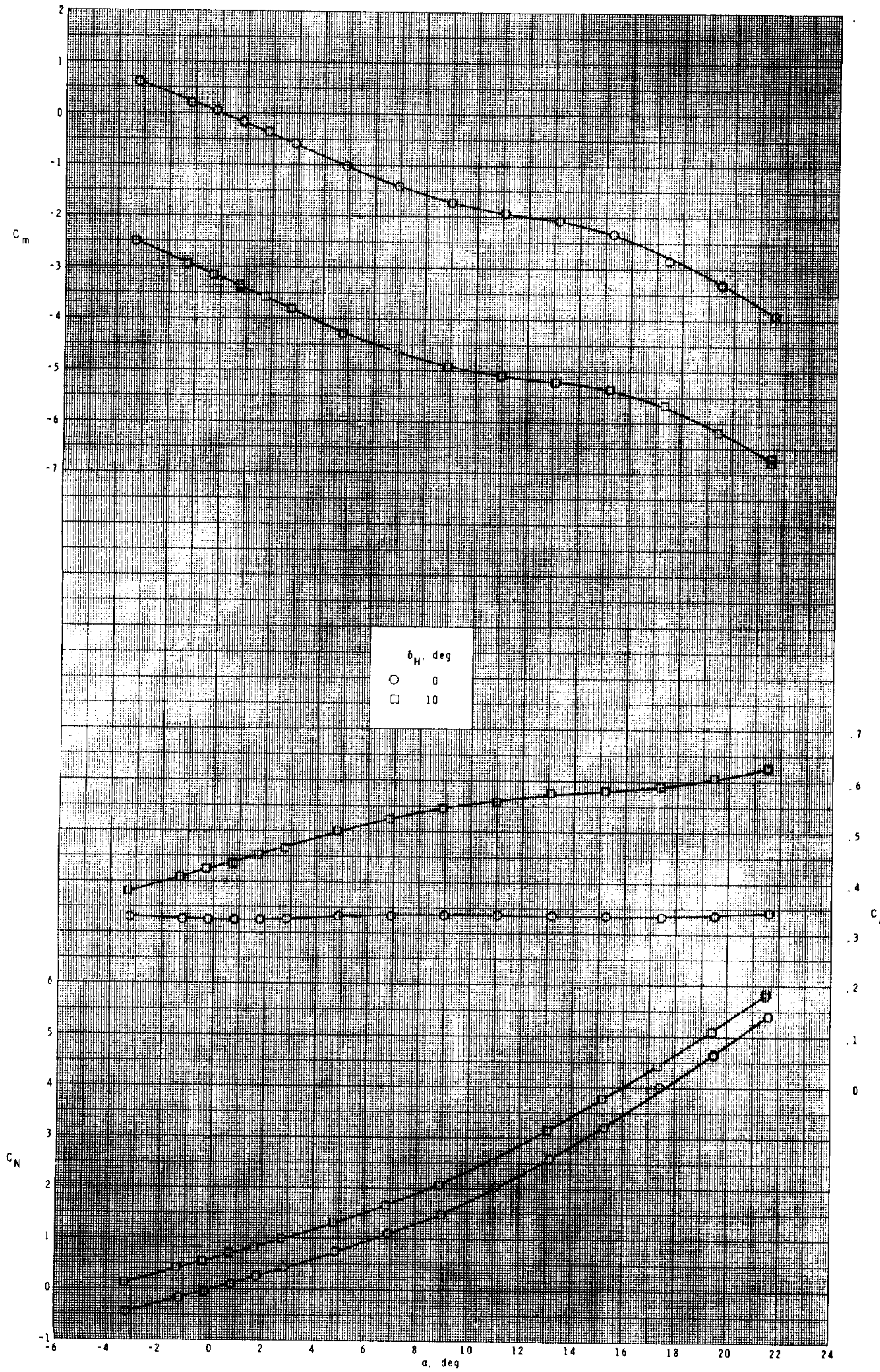

(b) Concluded.

Figure 6.- Continued.

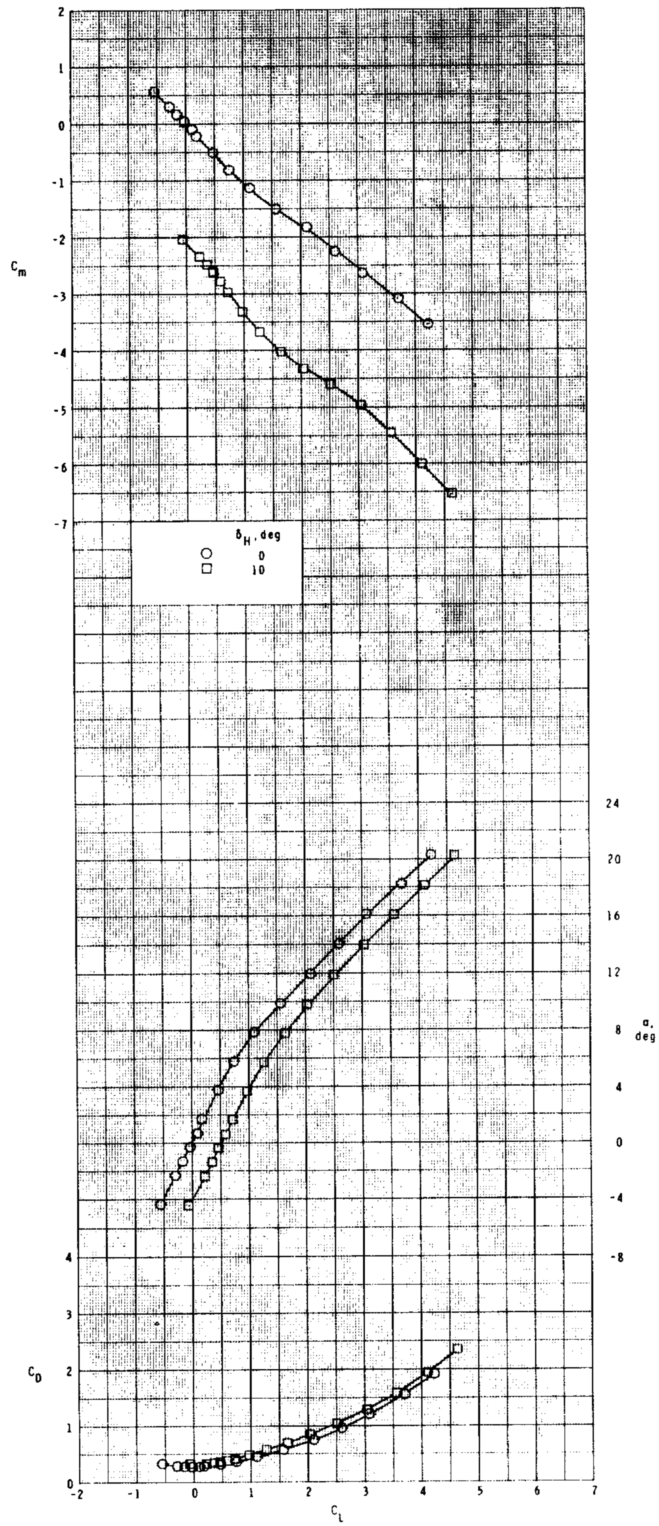

(c) M = 2.86.

Figure 6.- Continued.

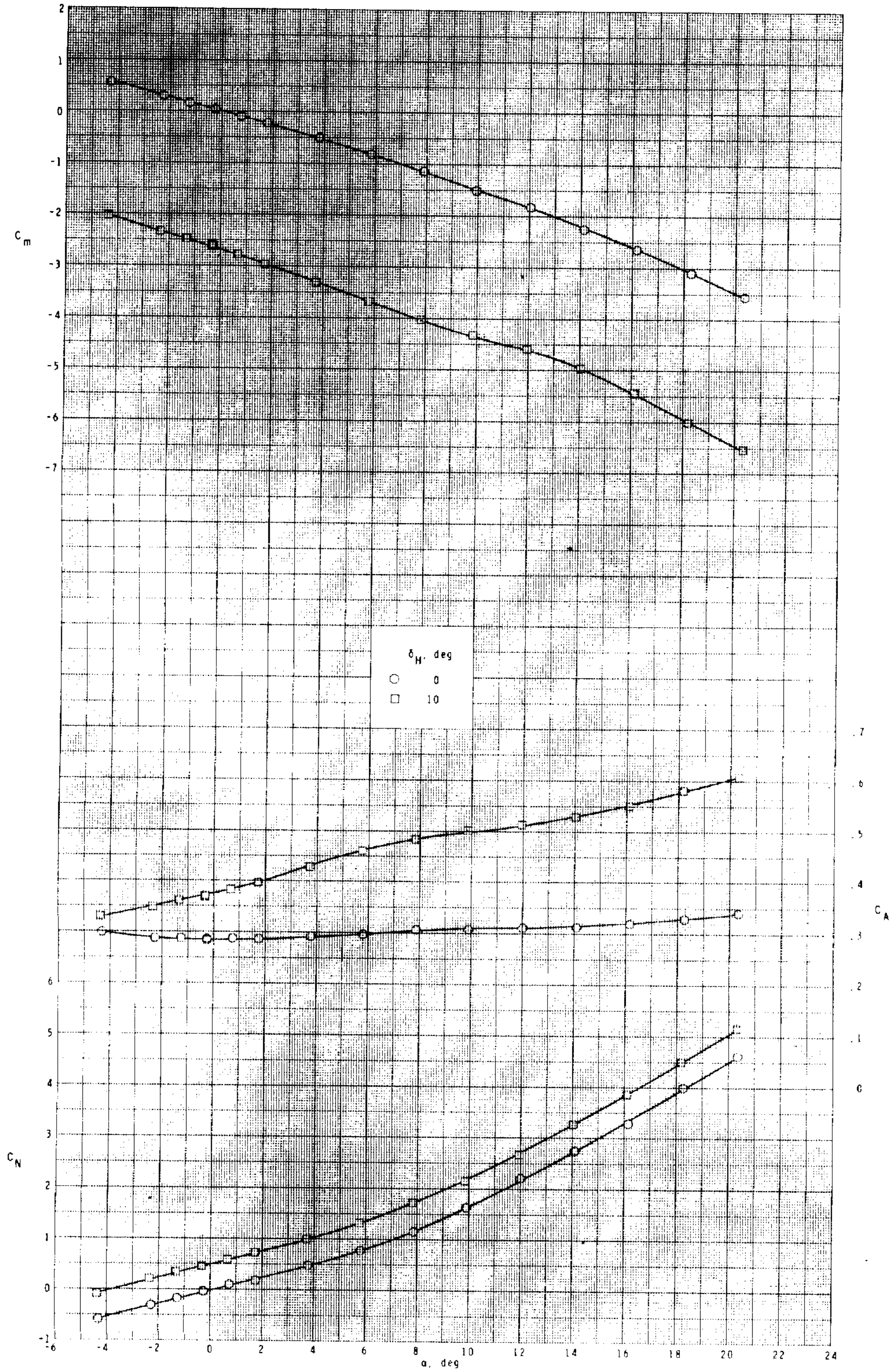

(c) Concluded.

Figure 6.- Concluded.

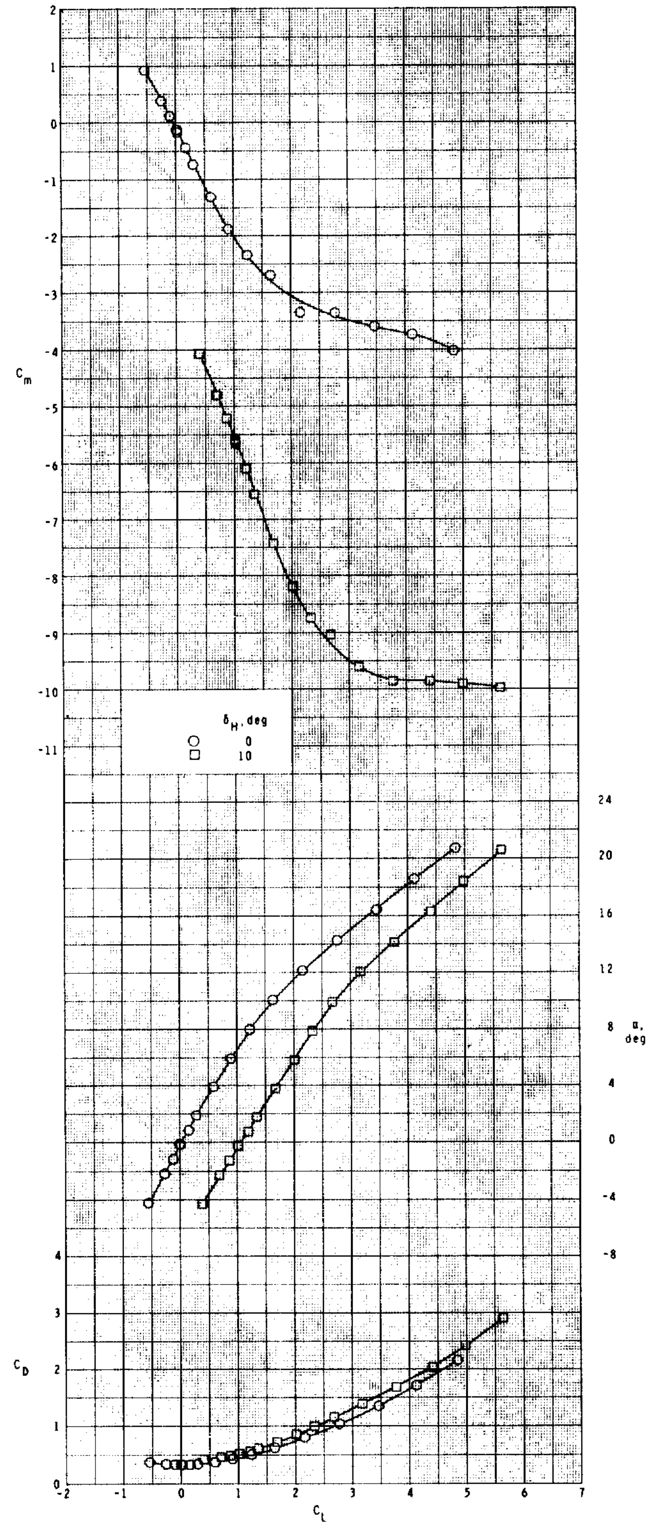

(a) M = 1.60.

Figure 7.- Longitudinal aerodynamic characteristics of the configuration with fin T_9 at $\phi = 45^{\circ}$.

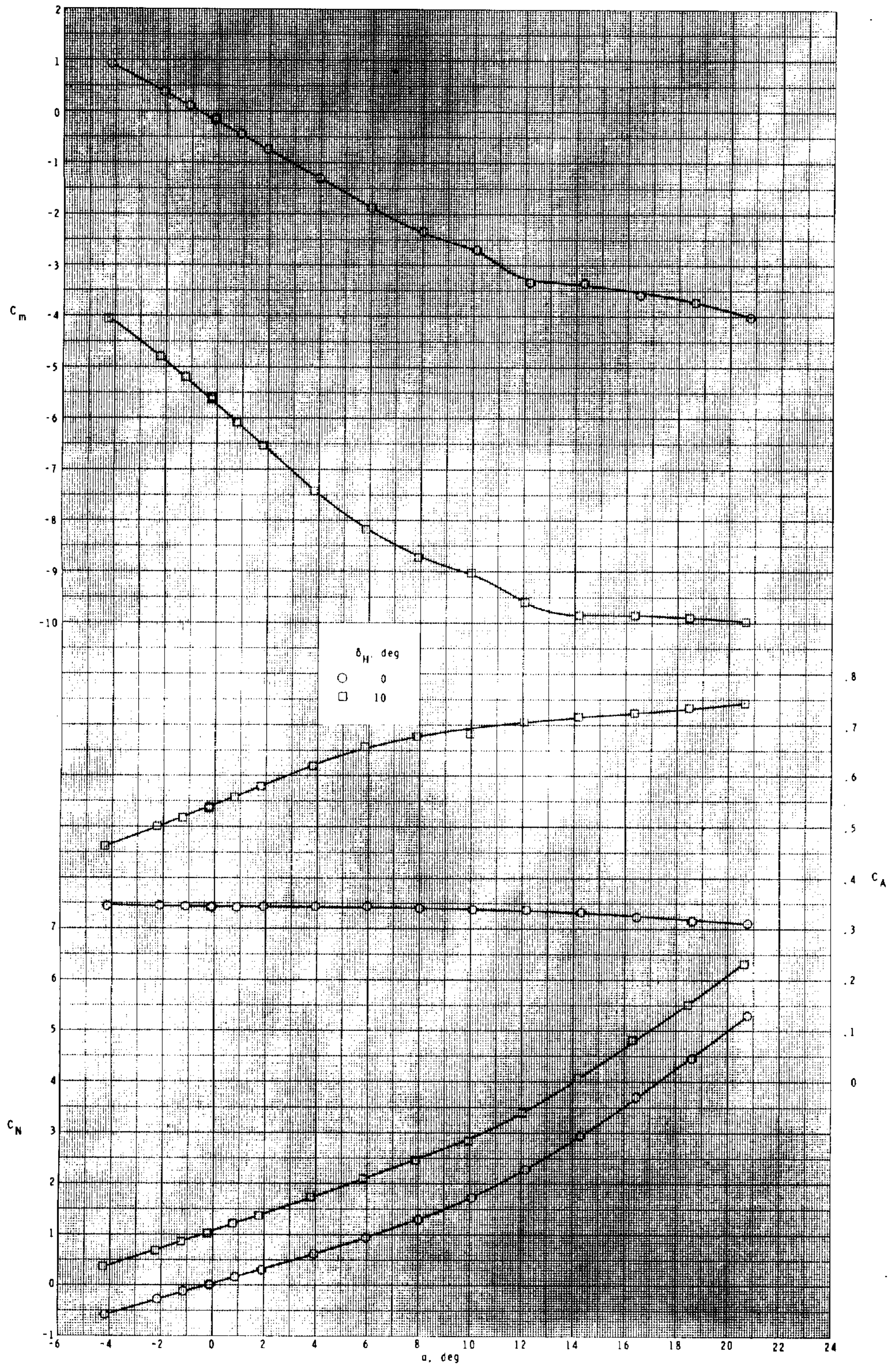

(a) Concluded.

Figure 7.- Continued.

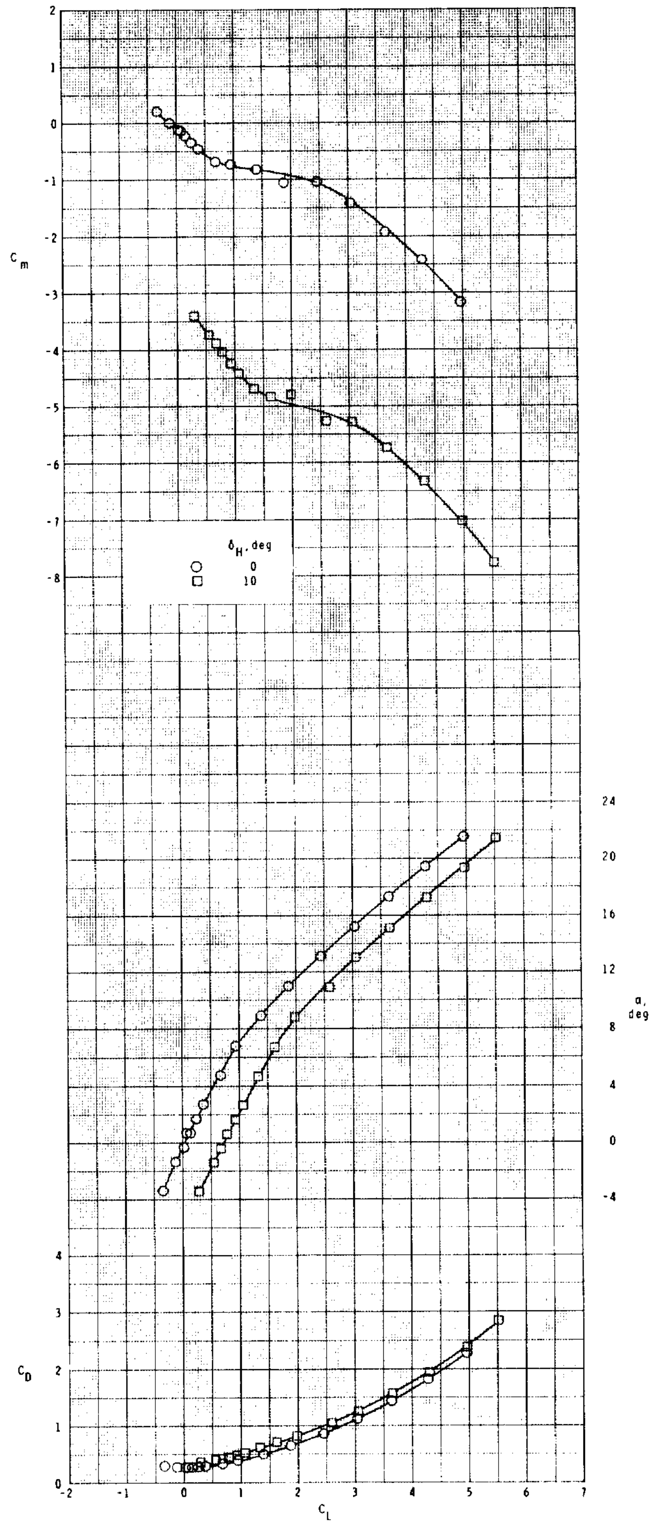

(b) M = 2.36.

Figure 7.- Continued.

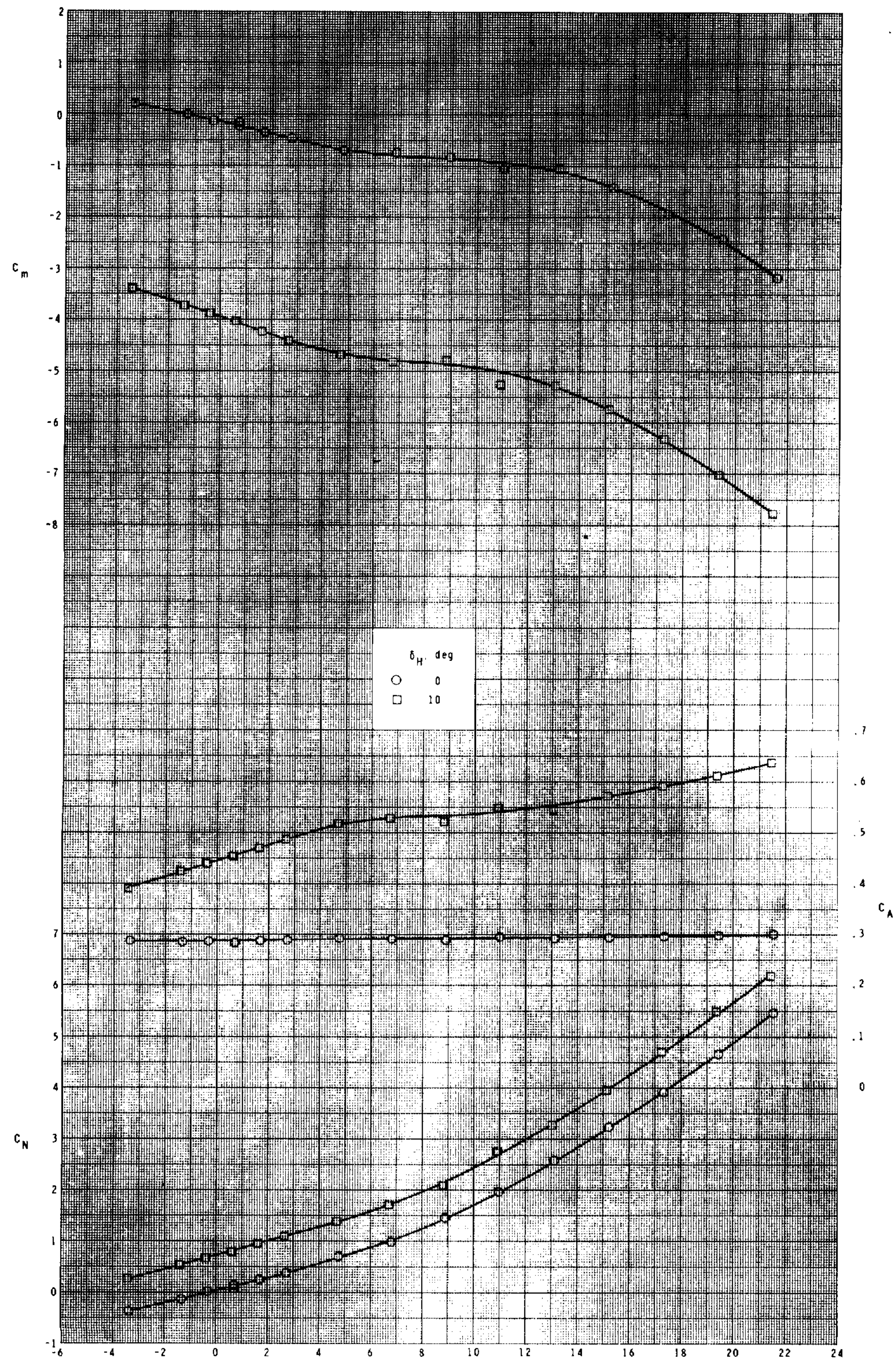

(b) Concluded.

Figure 7.- Continued.

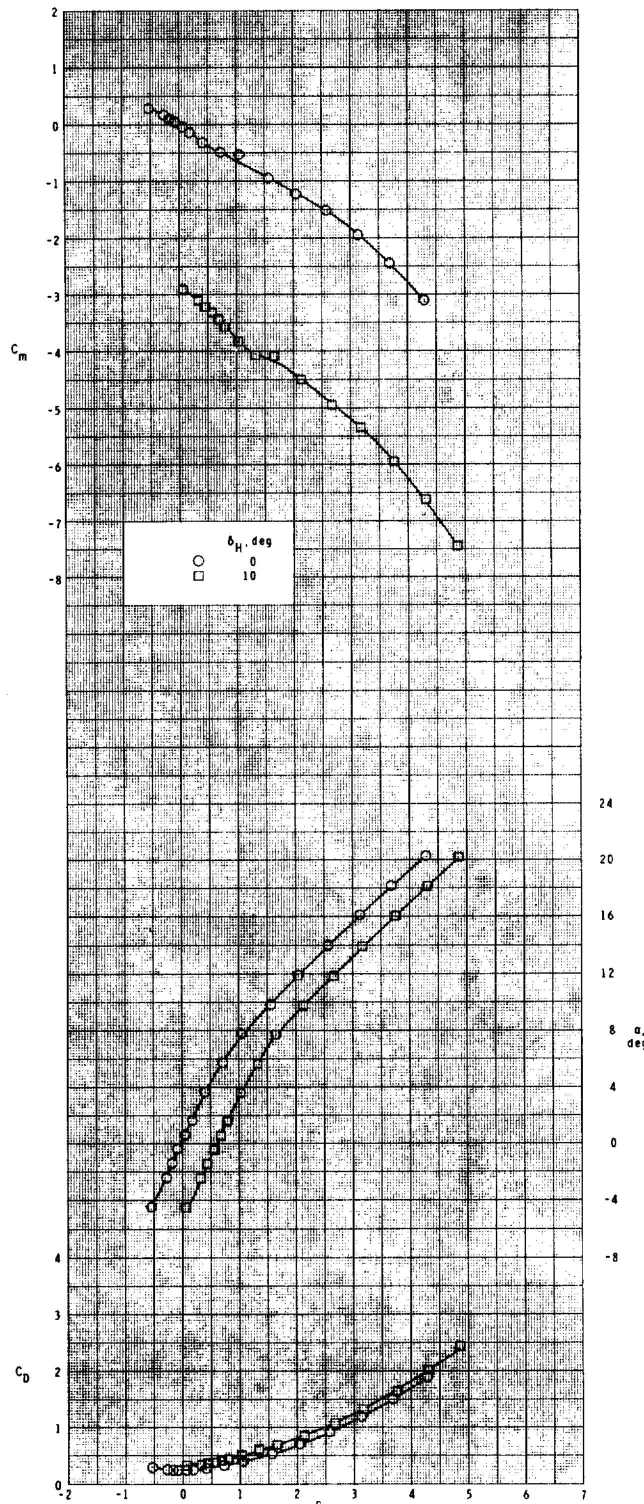

(c) M = 2.86.

Figure 7.- Continued.

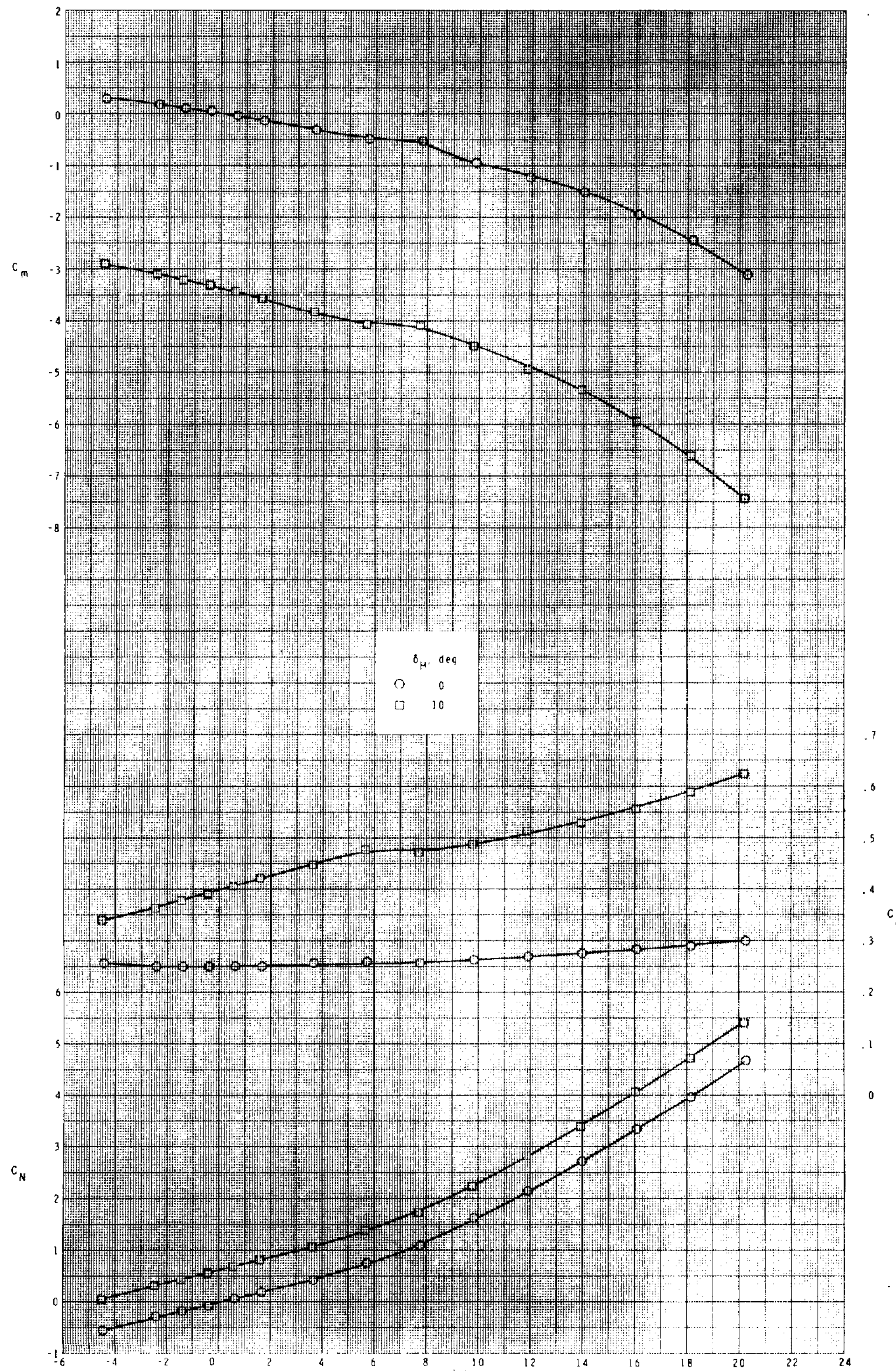

(c) Concluded.

Figure 7.- Concluded.

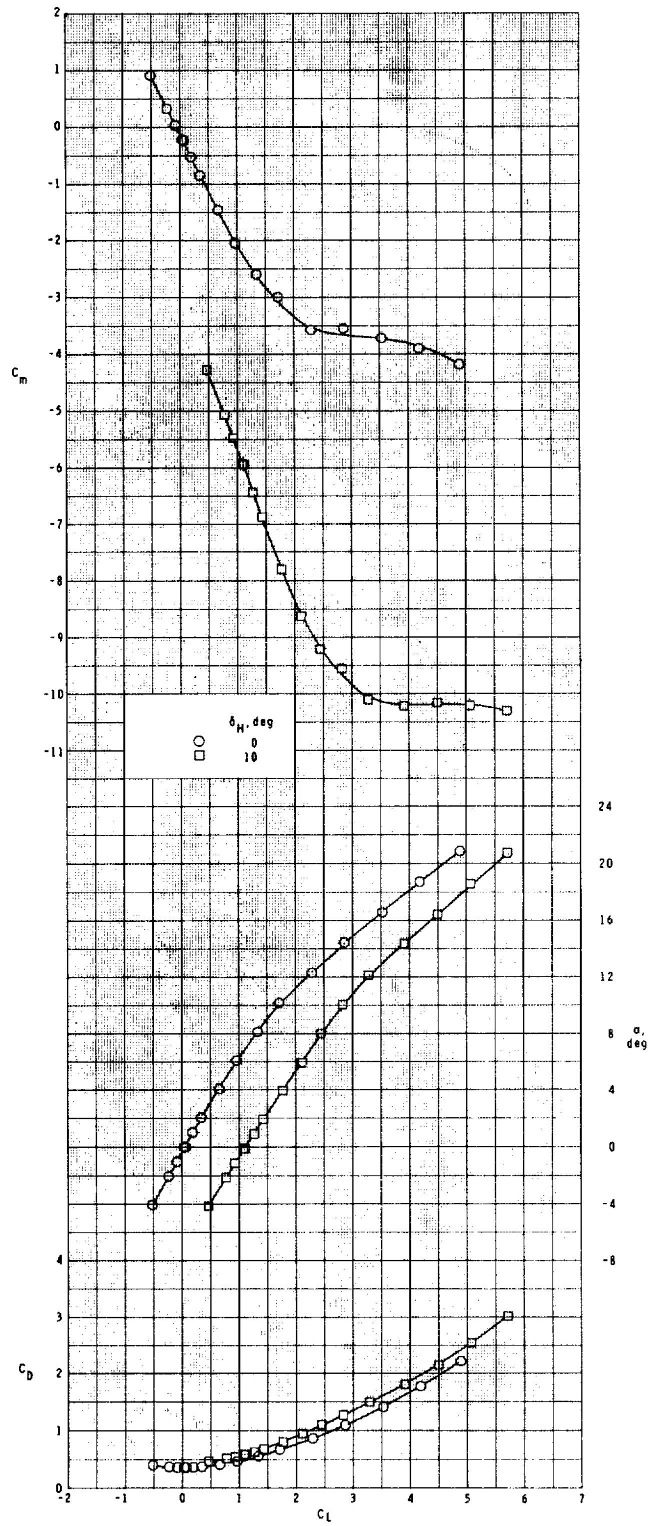

(a) M = 1.60.

Figure 8.- Longitudinal aerodynamic characteristics of the configuration with fin T_{10} at $\phi = 45^{\circ}$.

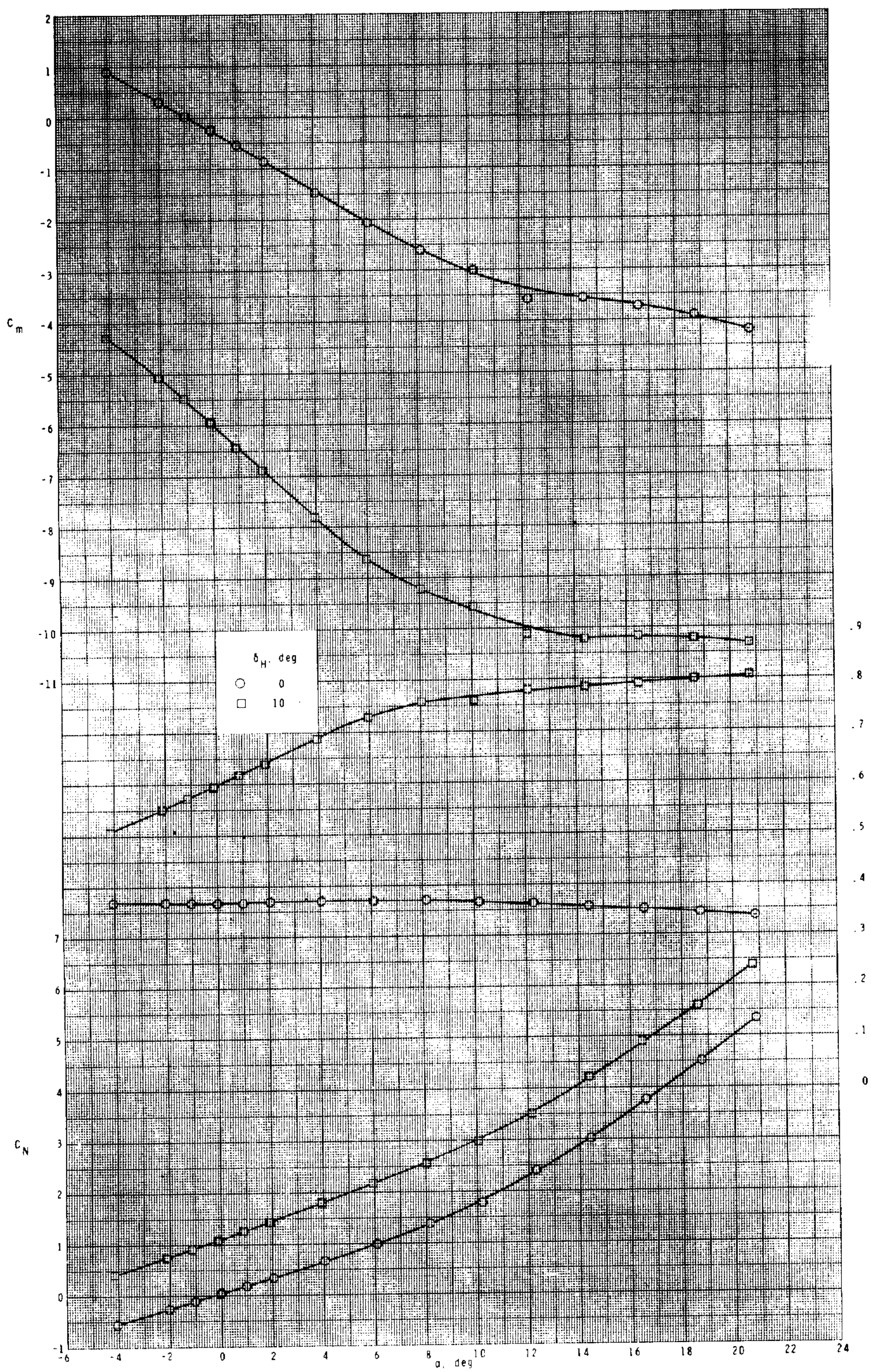

(a) Concluded.

Figure 8.- Continued.

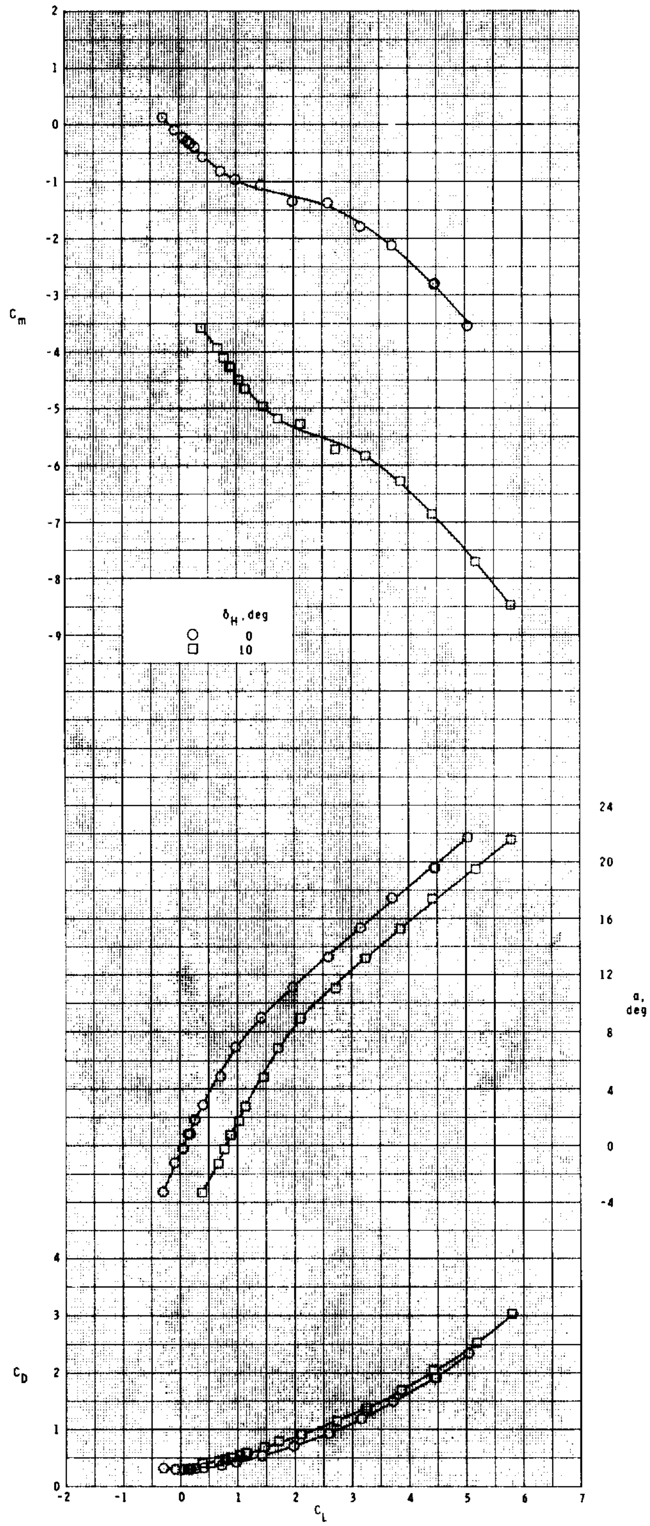

(b) M = 2.36.

Figure 8.- Continued.

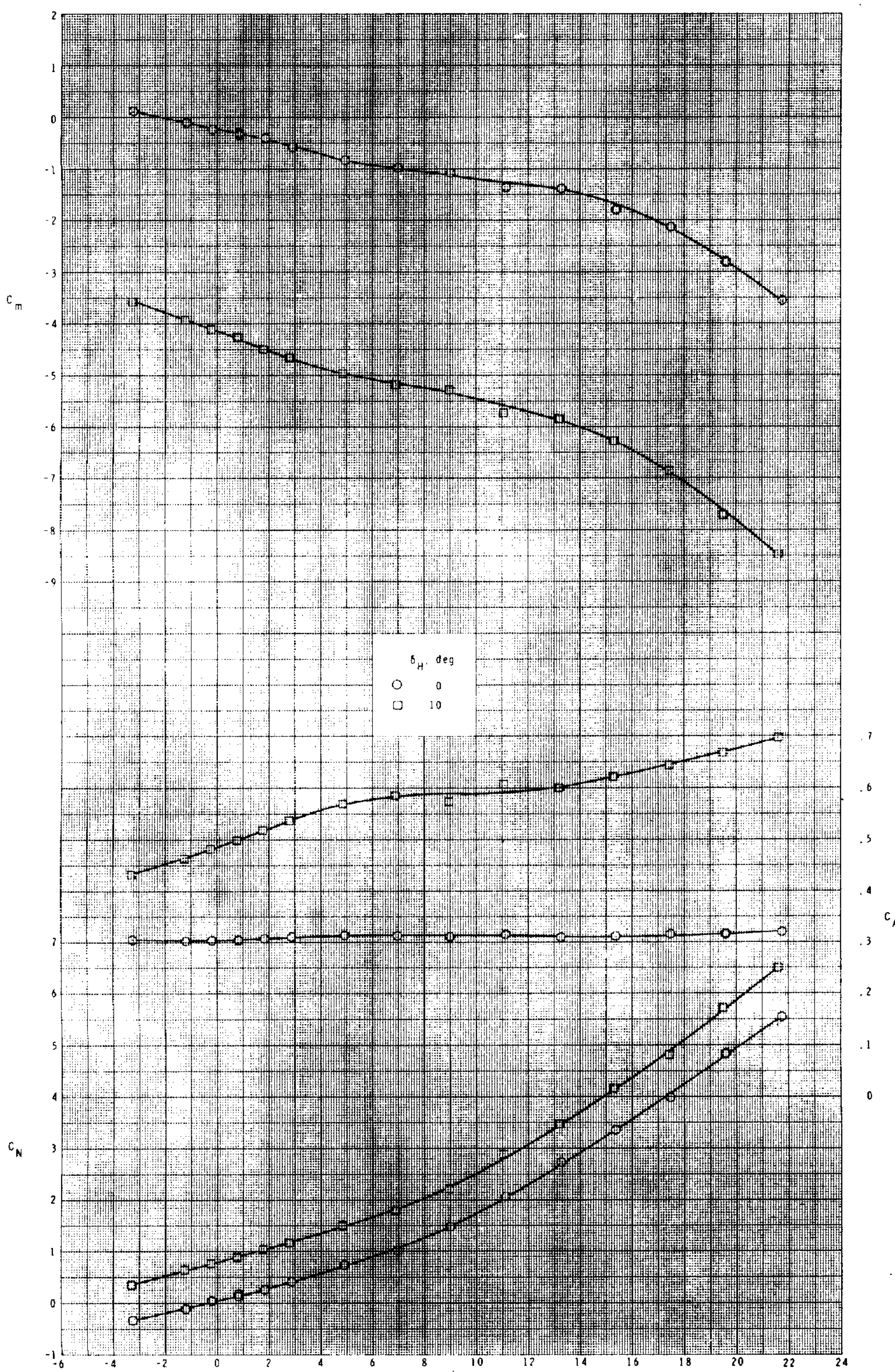

(b) Concluded.

Figure 8.- Continued.

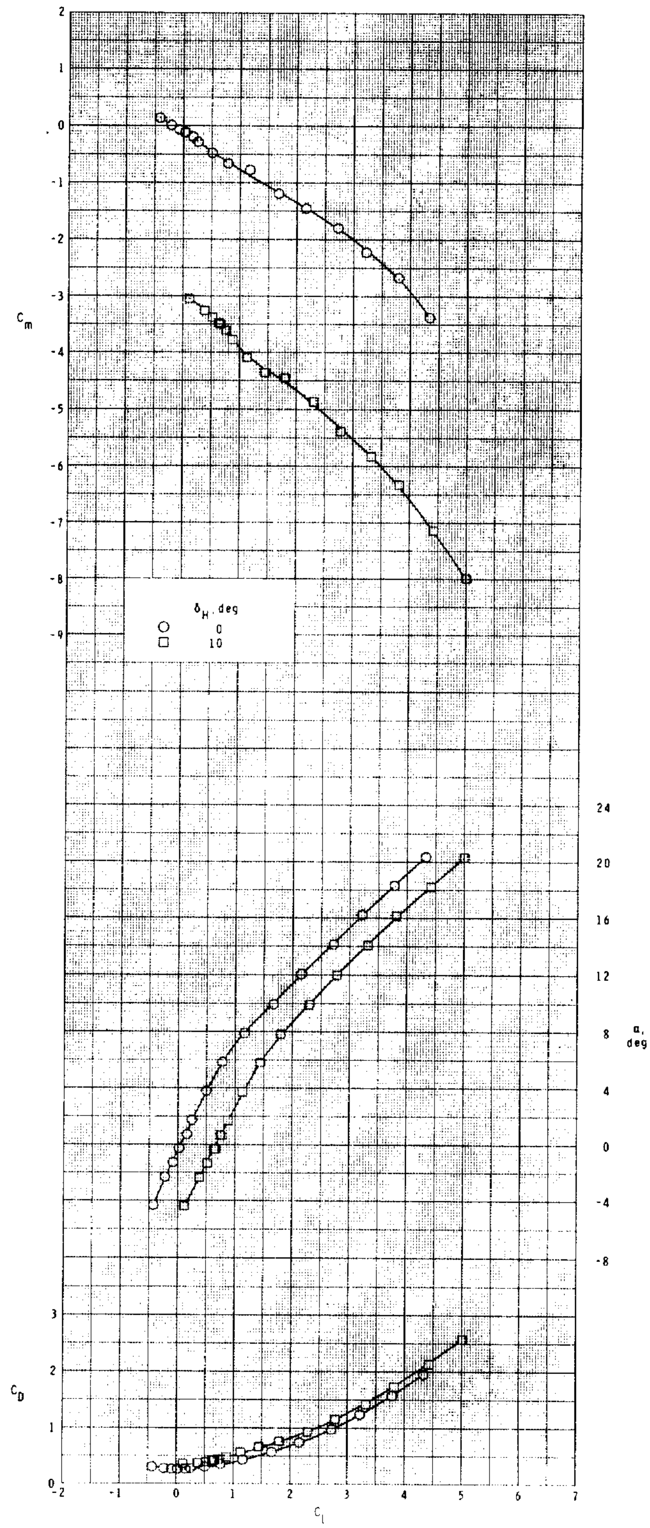

(c) M = 2.86.

Figure 8.- Continued.

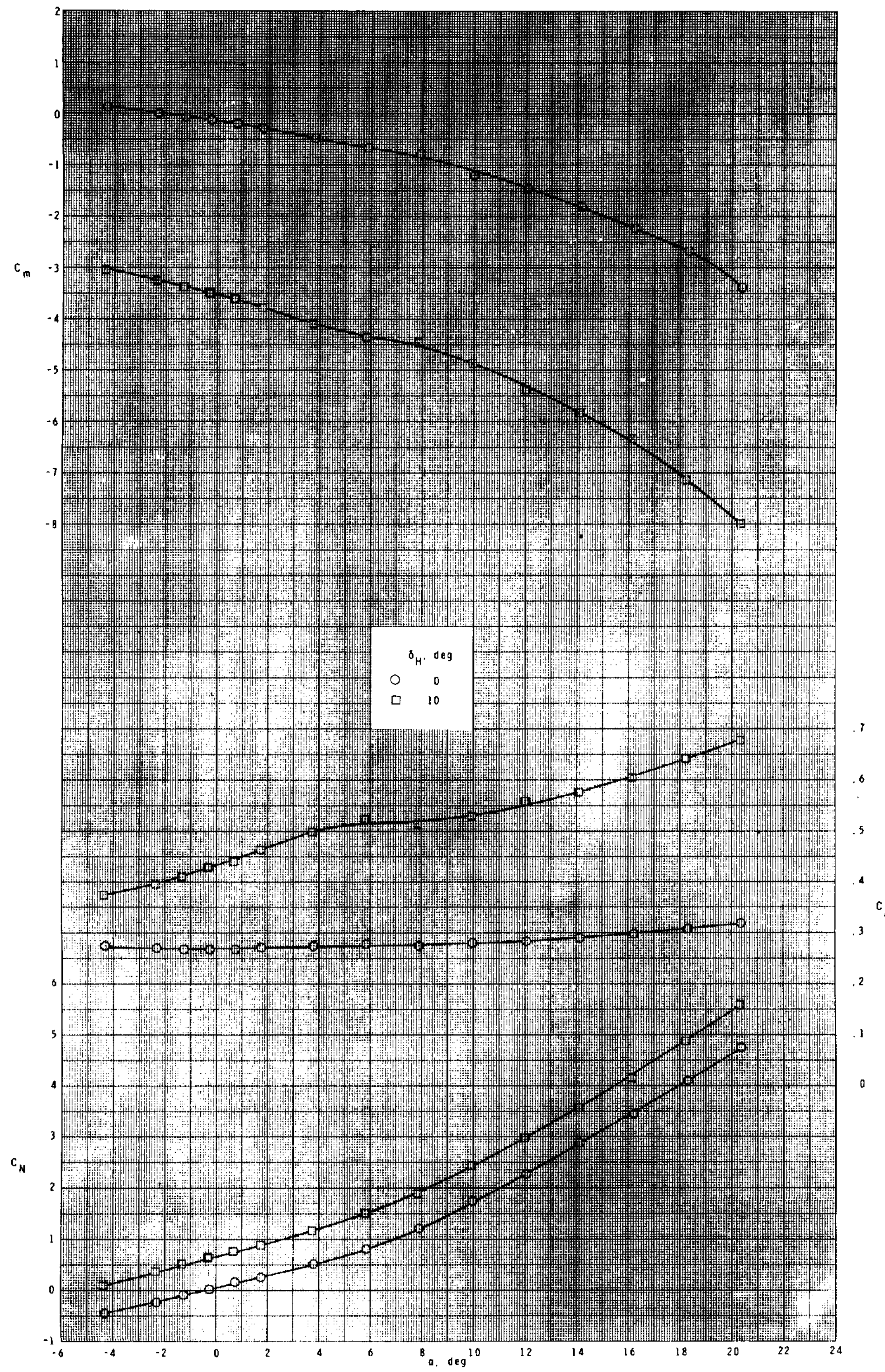

(c) Concluded.

Figure 8.- Concluded.

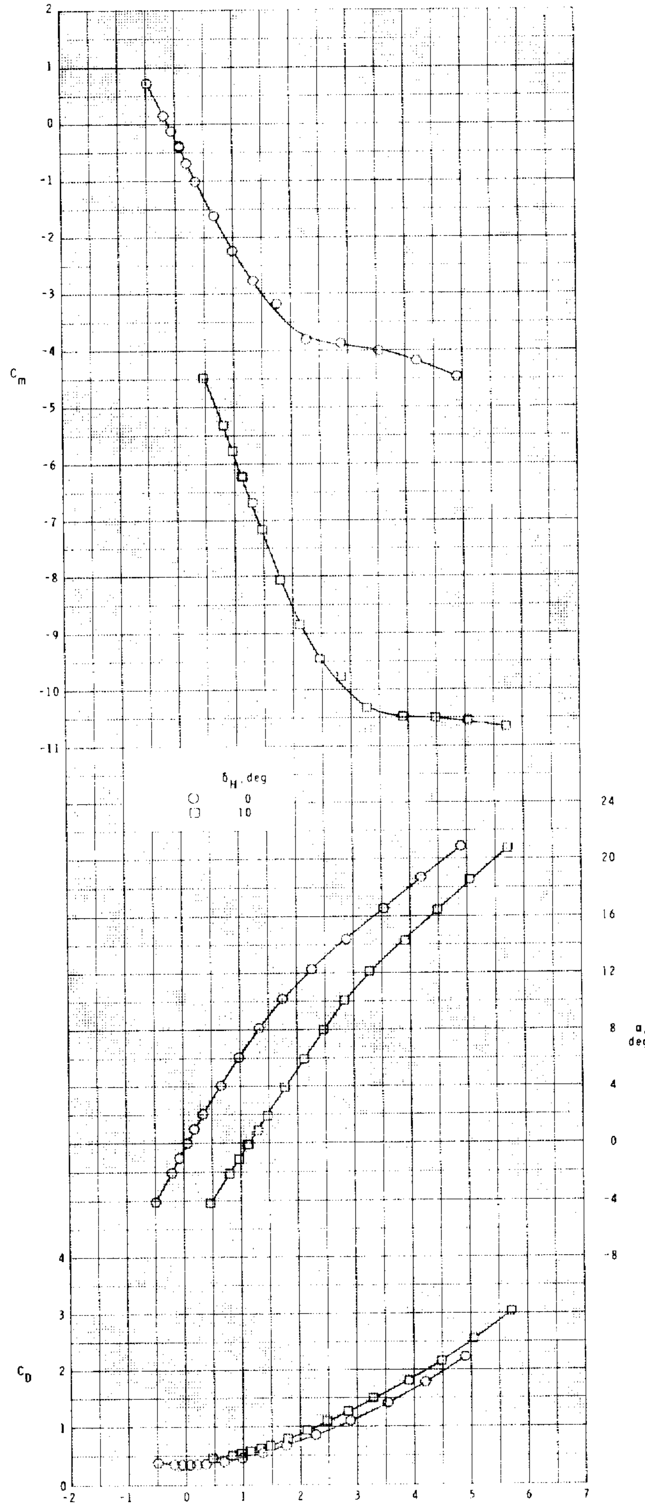

(a) M = 1.60.

Figure 9.- Longitudinal aerodynamic characteristics of the configuration with fin T_{11} at $\phi = 45^o$.

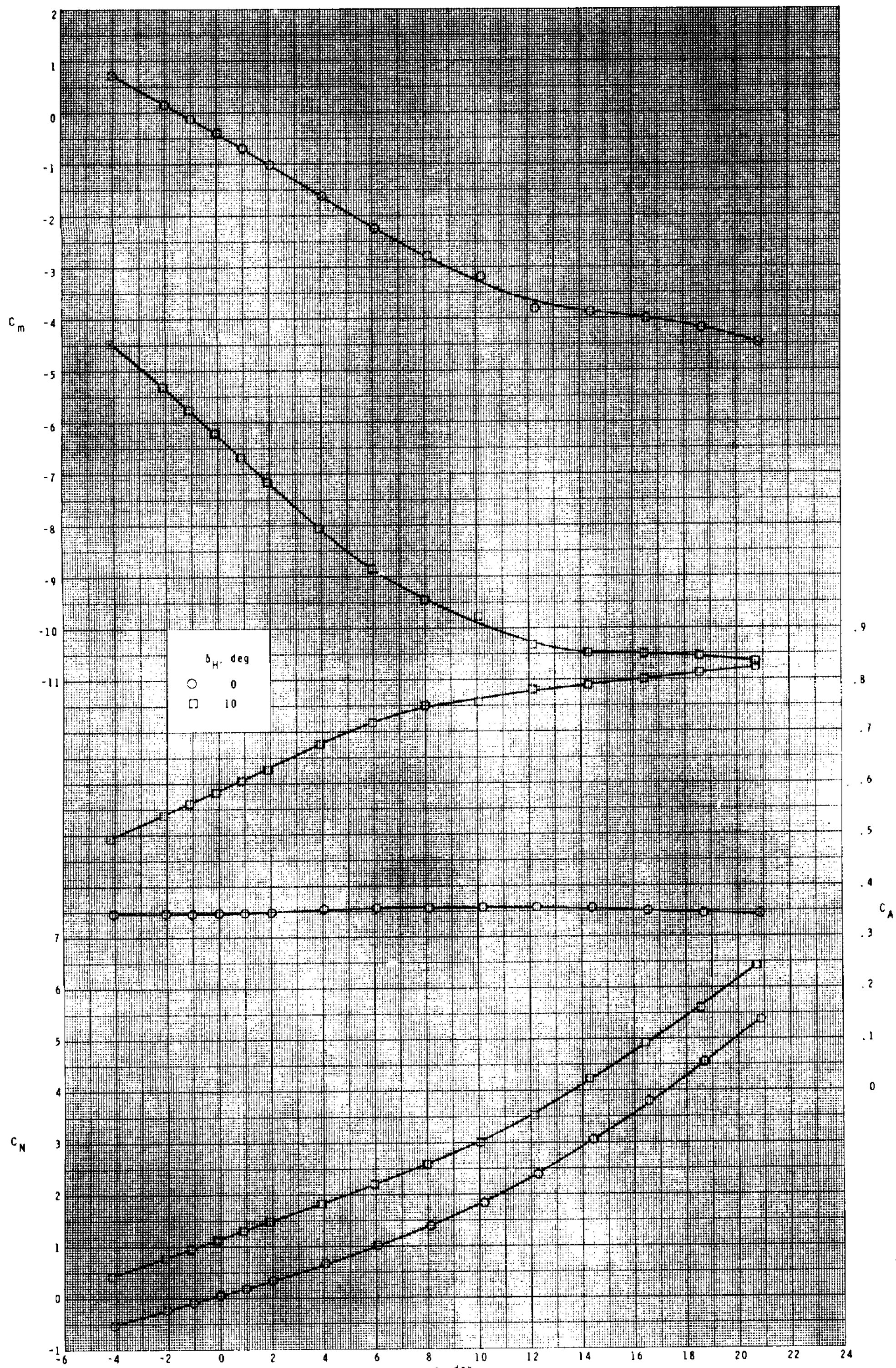

(a) Concluded.

Figure 9.- Continued.

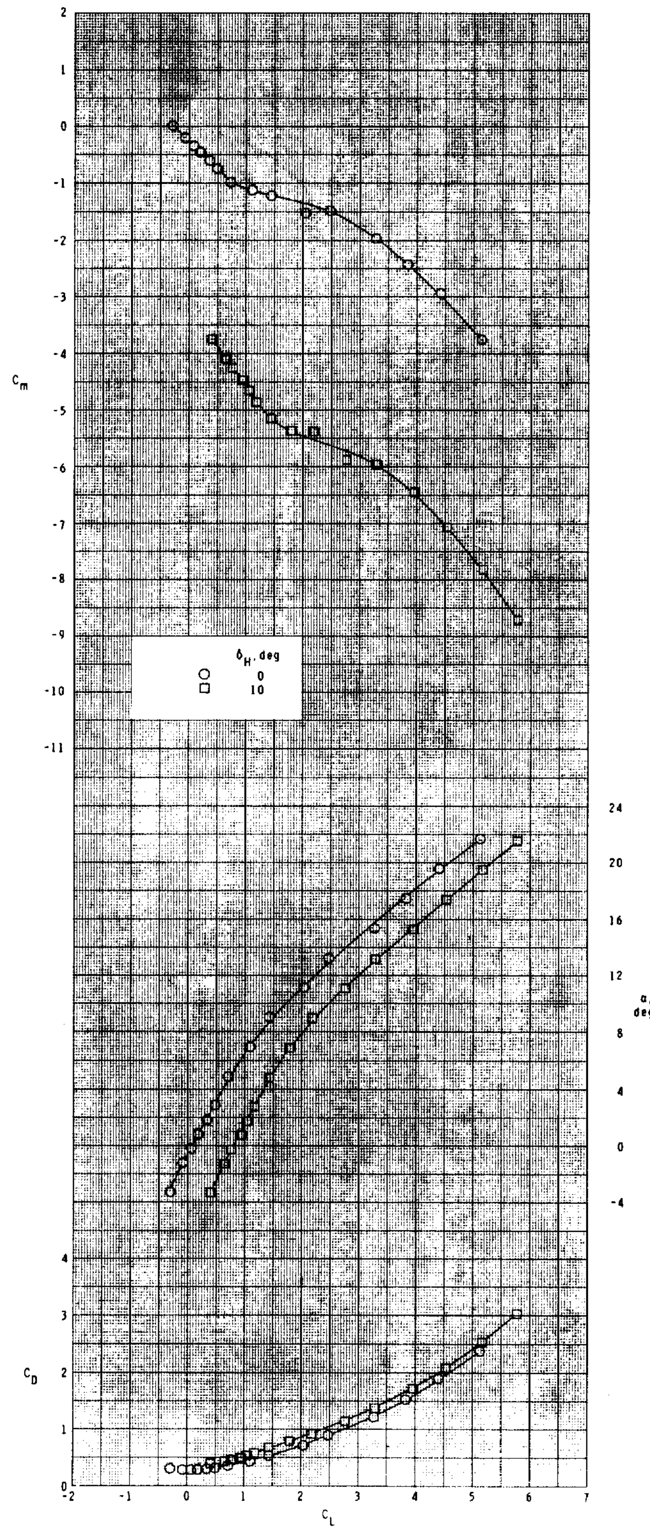

(b) M = 2.36.

Figure 9.- Continued.

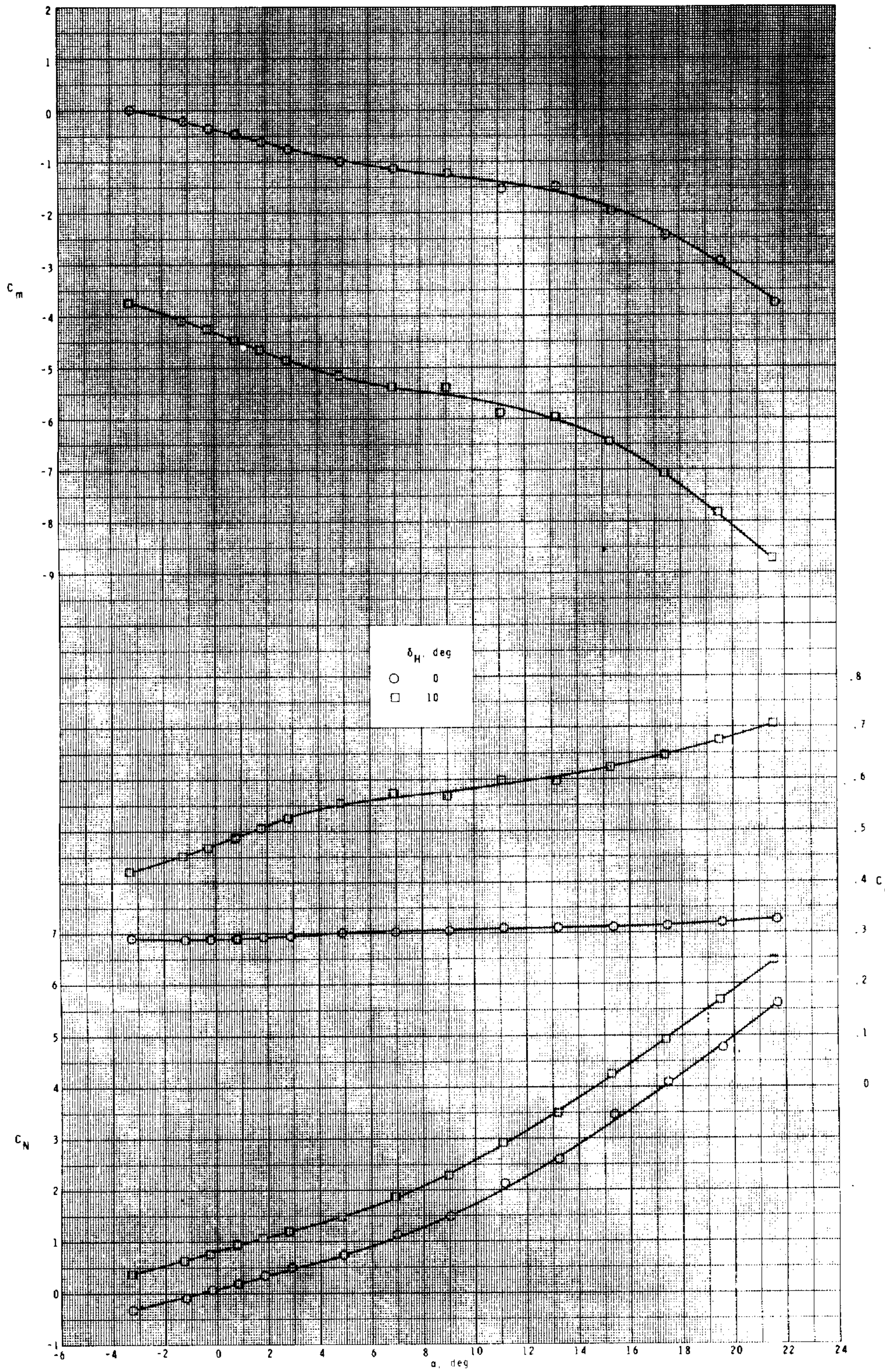

(b) Concluded.

Figure 9.- Continued.

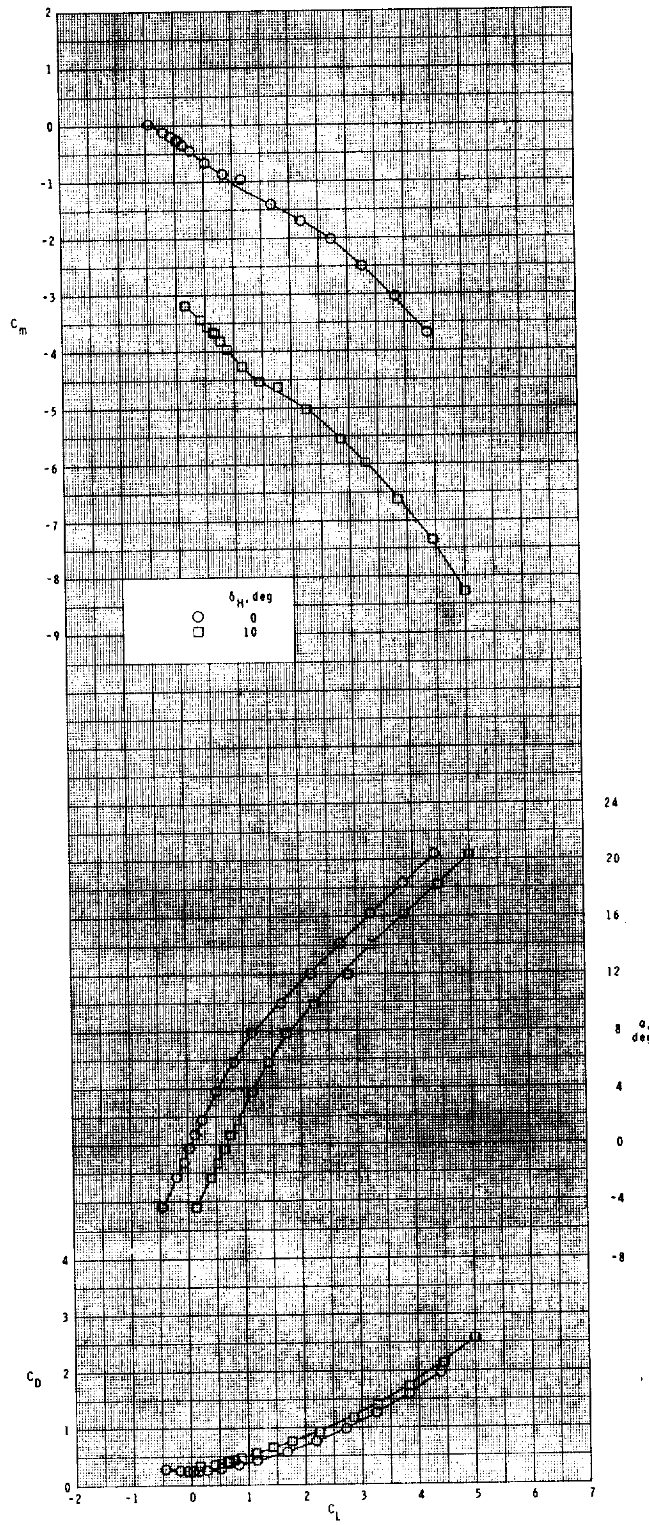

(c) M = 2.86.

Figure 9.- Continued.

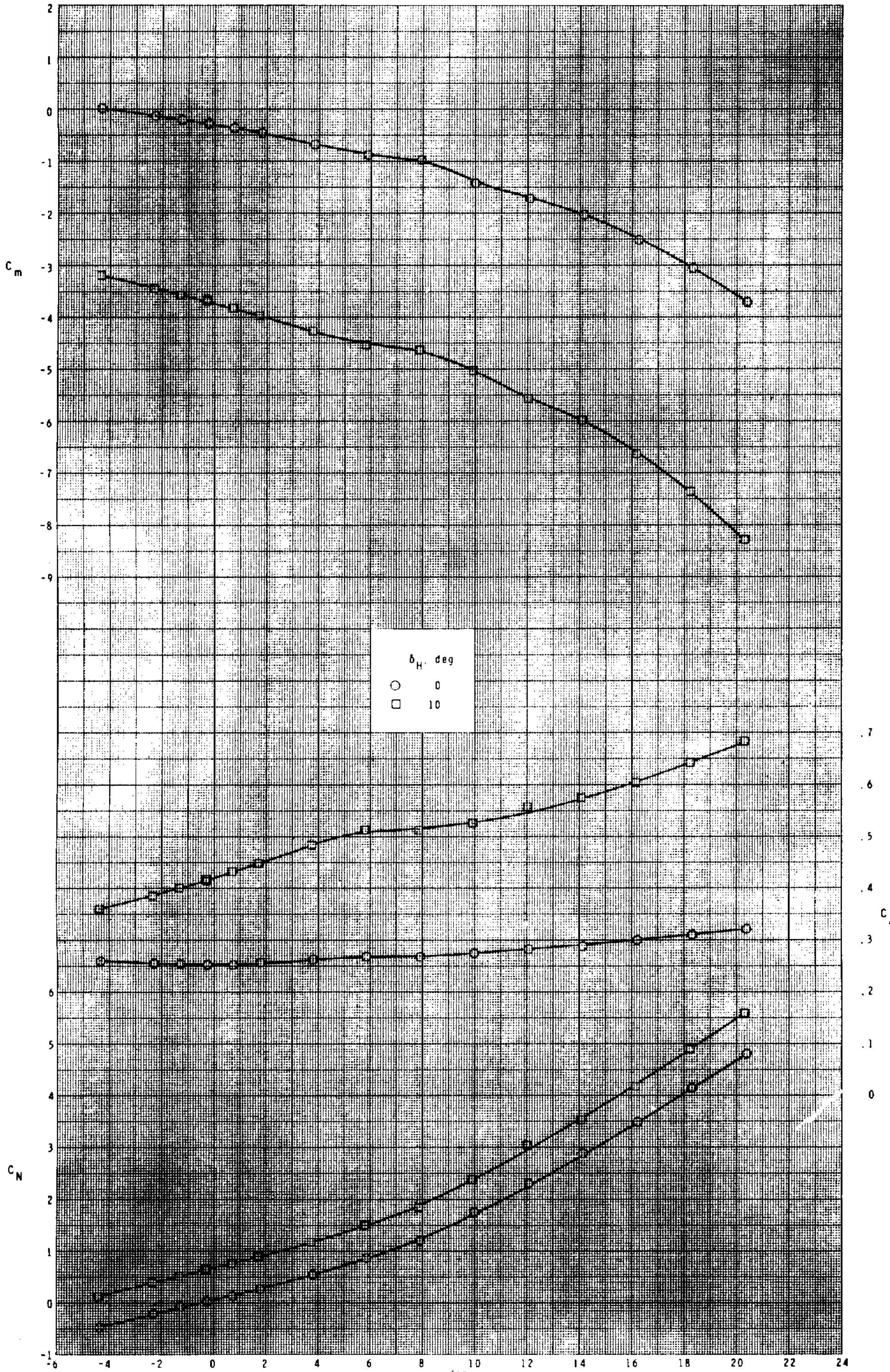

(c) Concluded.

Figure 9.- Concluded.

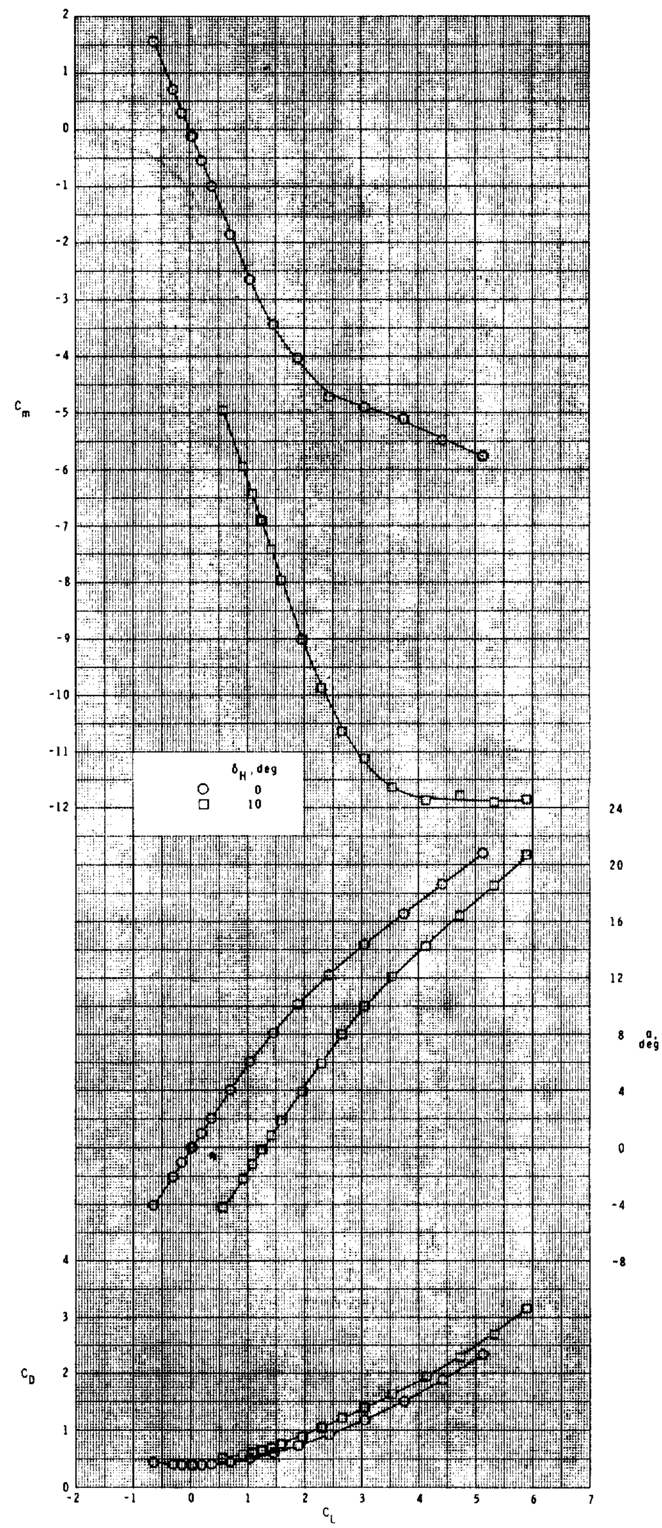

(a) M = 1.60.

Figure 10.- Longitudinal aerodynamic characteristics of the configuration with fin T_{12} at $\phi = 45^{\circ}$.

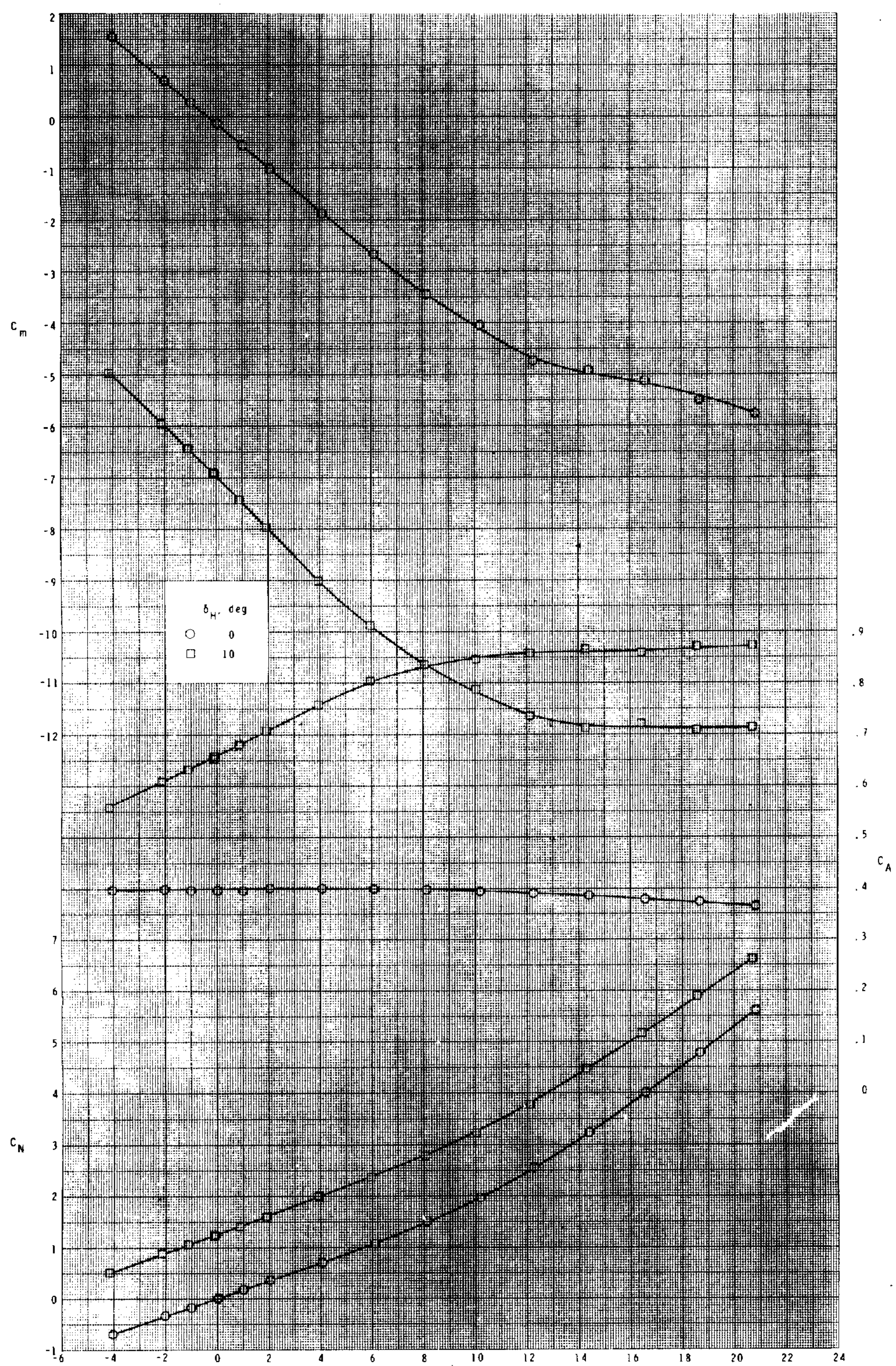

(a) Concluded.

Figure 10.- Continued.

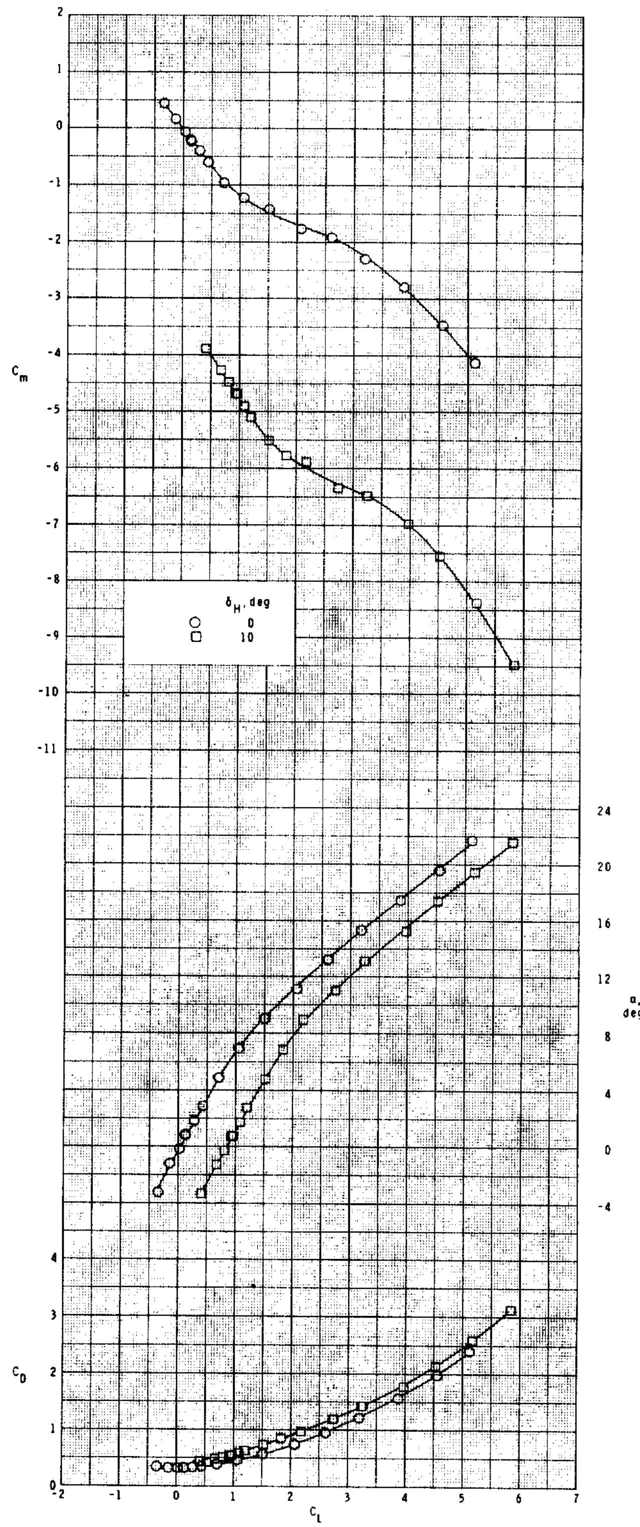

(b) M = 2.36.

Figure 10.- Continued.

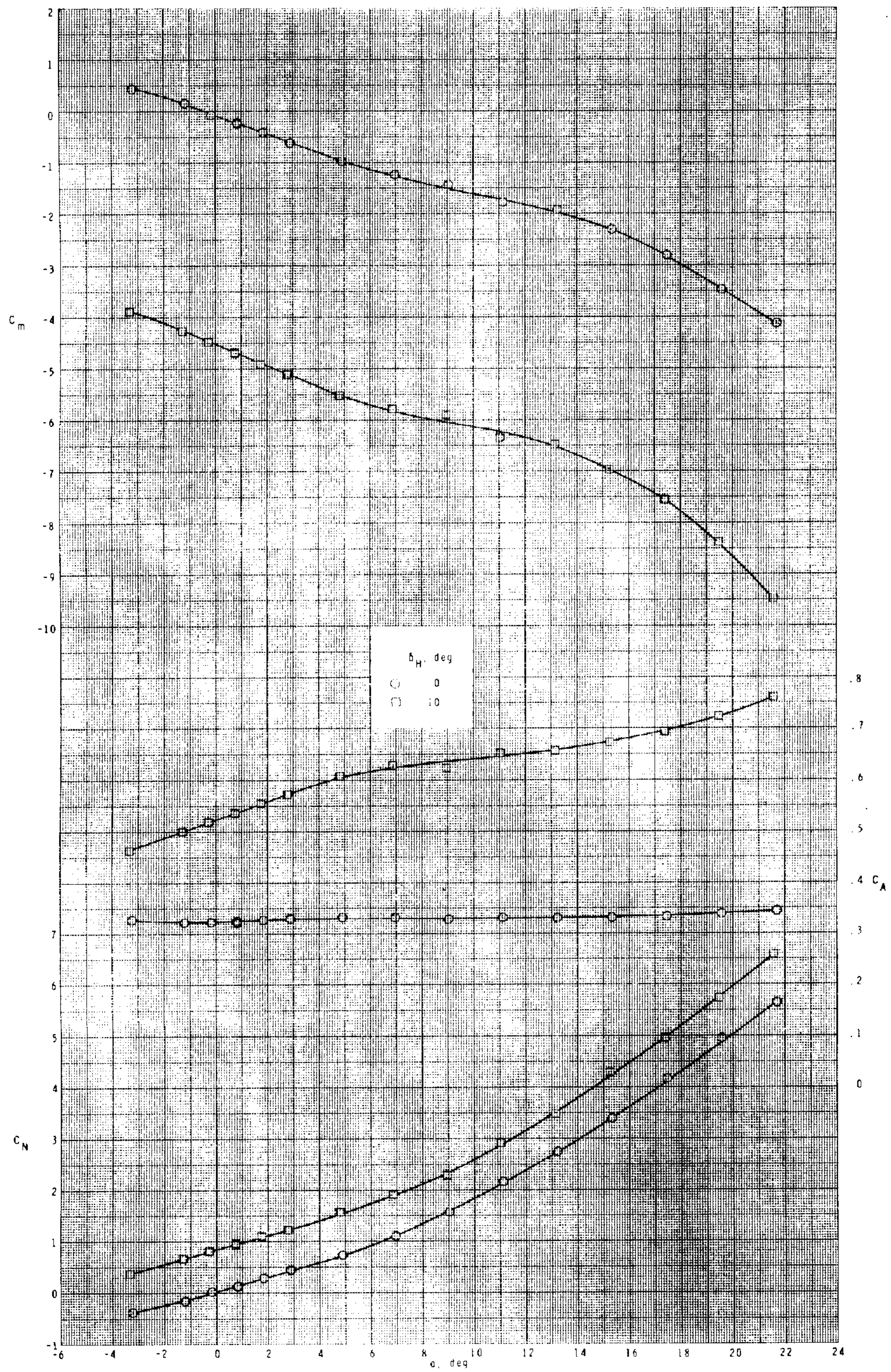

(b) Concluded.

Figure 10.- Continued.

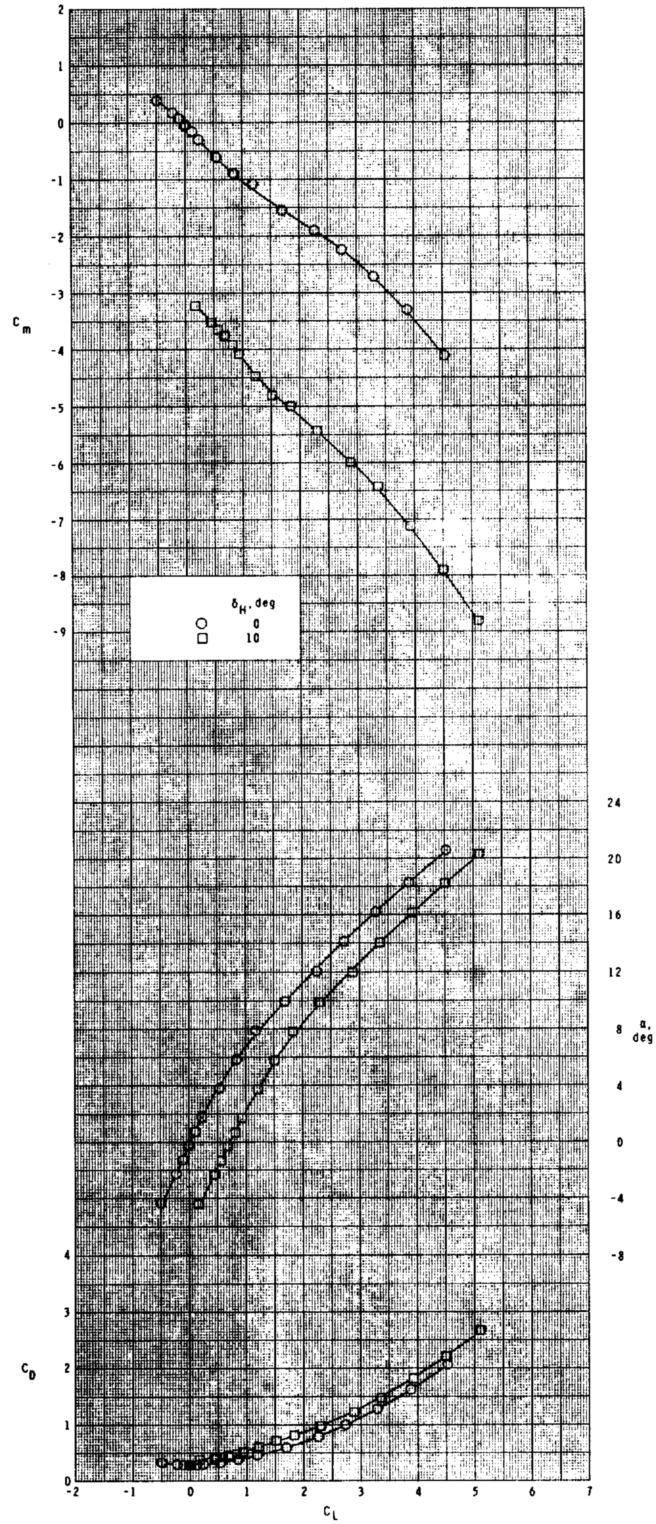

(c) M = 2.86.

Figure 10.- Continued.

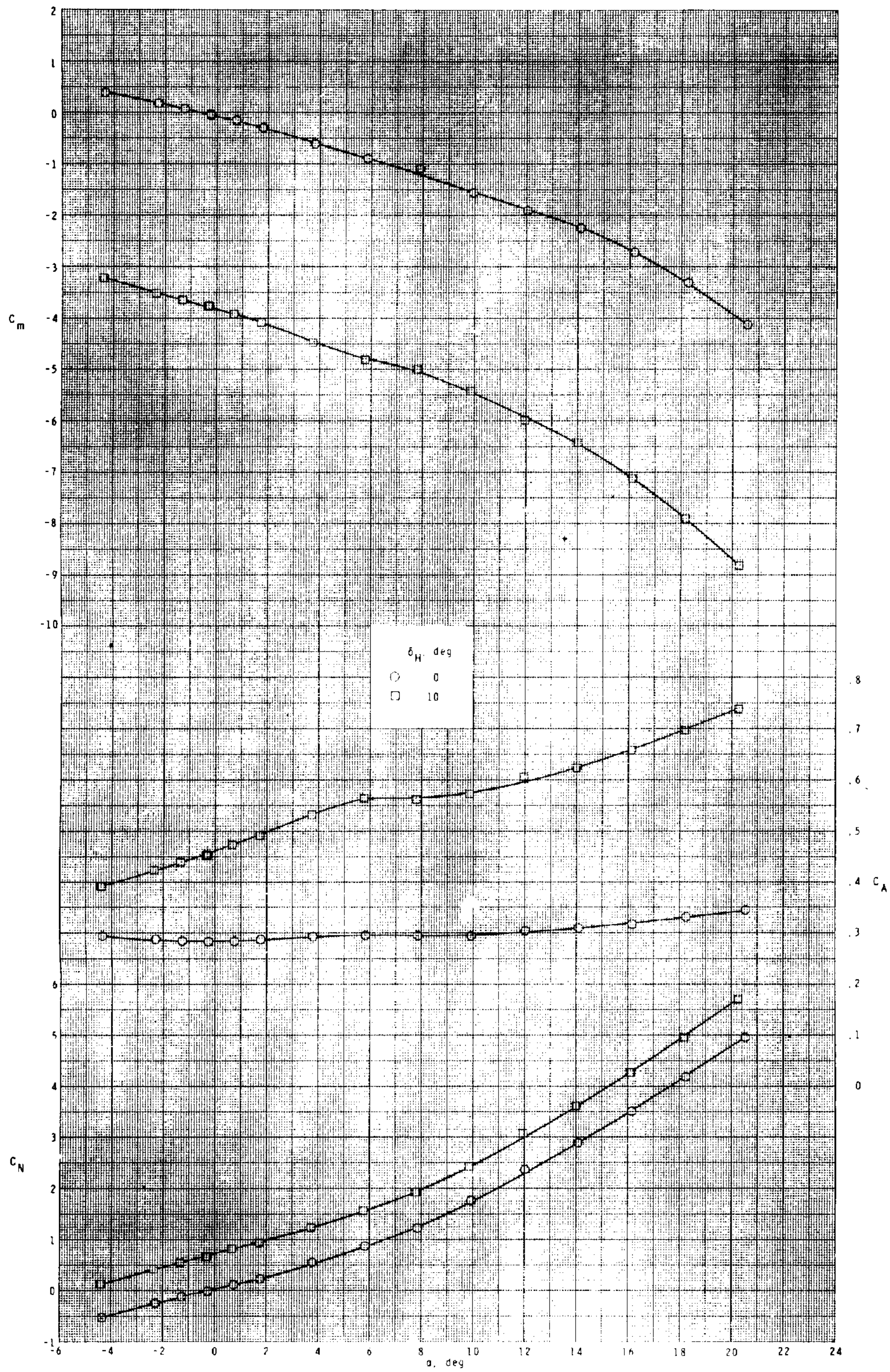

(c) Concluded.

Figure 10.- Concluded.

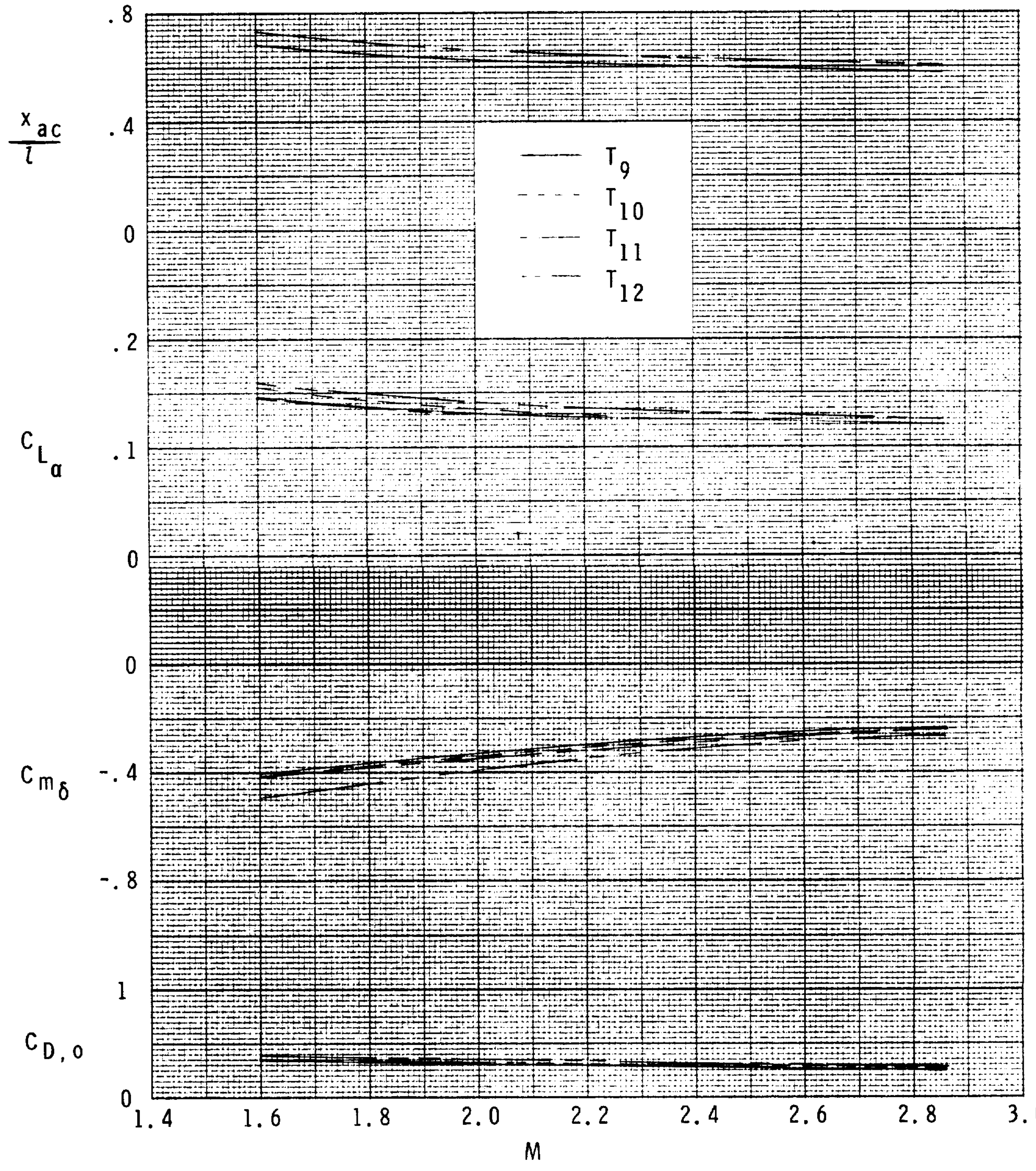

(a) $\phi = 0^o$.

Figure 11.- Summary of longitudinal characteristics.

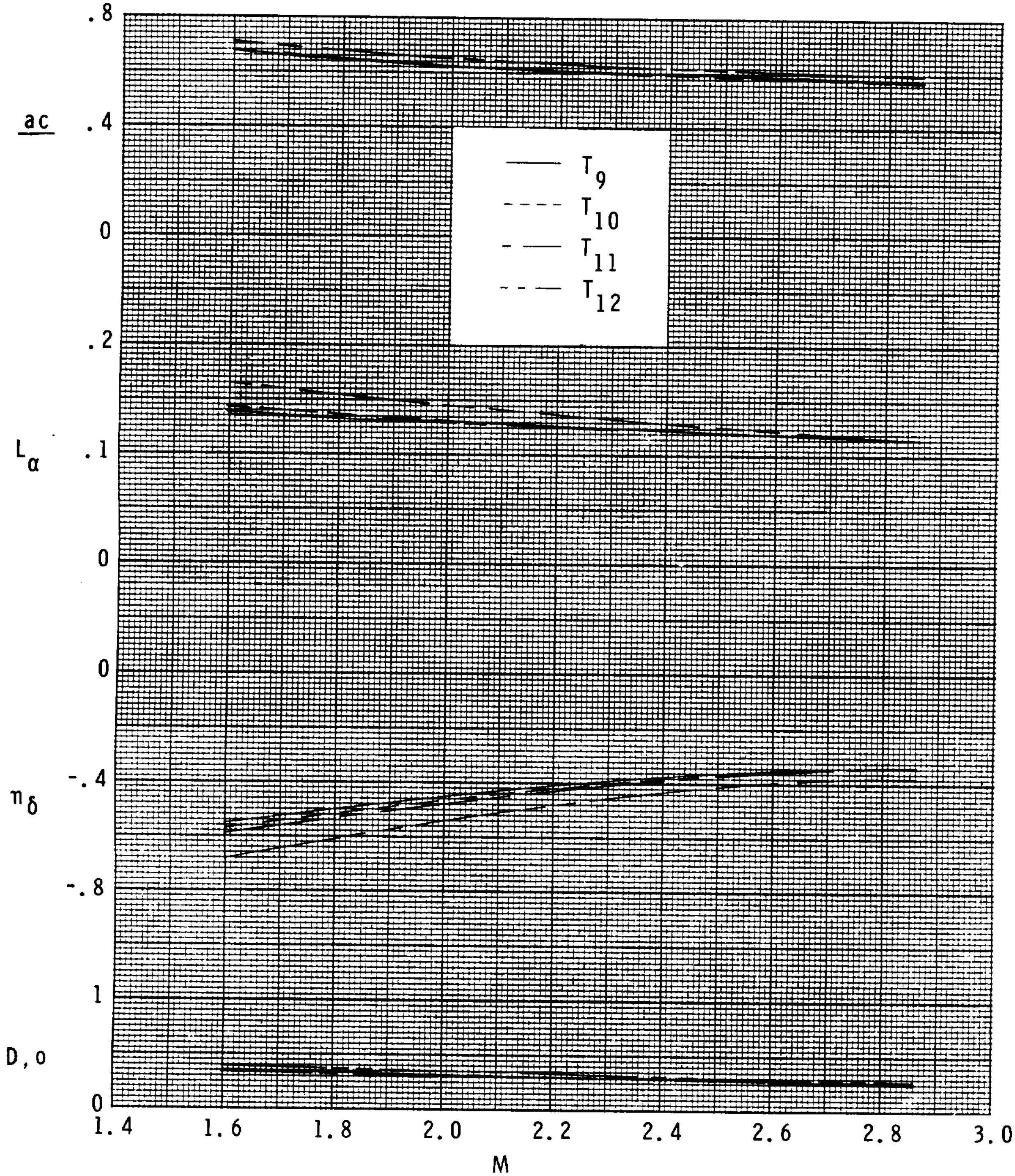

(b) $\phi = 45^{\circ}$.

Figure 11.- Concluded.

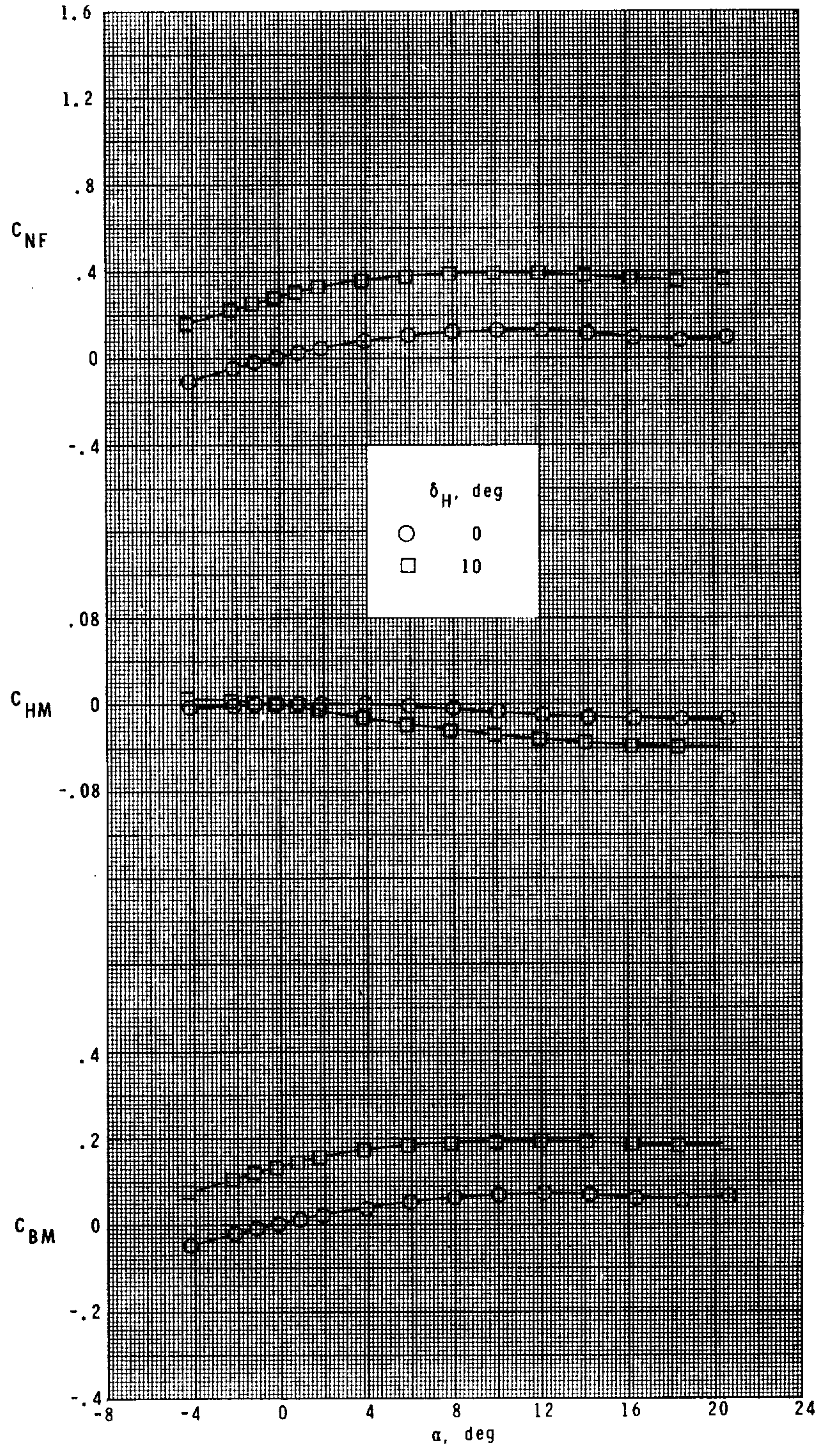

(a) M = 1.60.

Figure 12.- Variation of fin load coefficients with angle of attack for fin panel T_9 at $\phi_f = 45^0$.

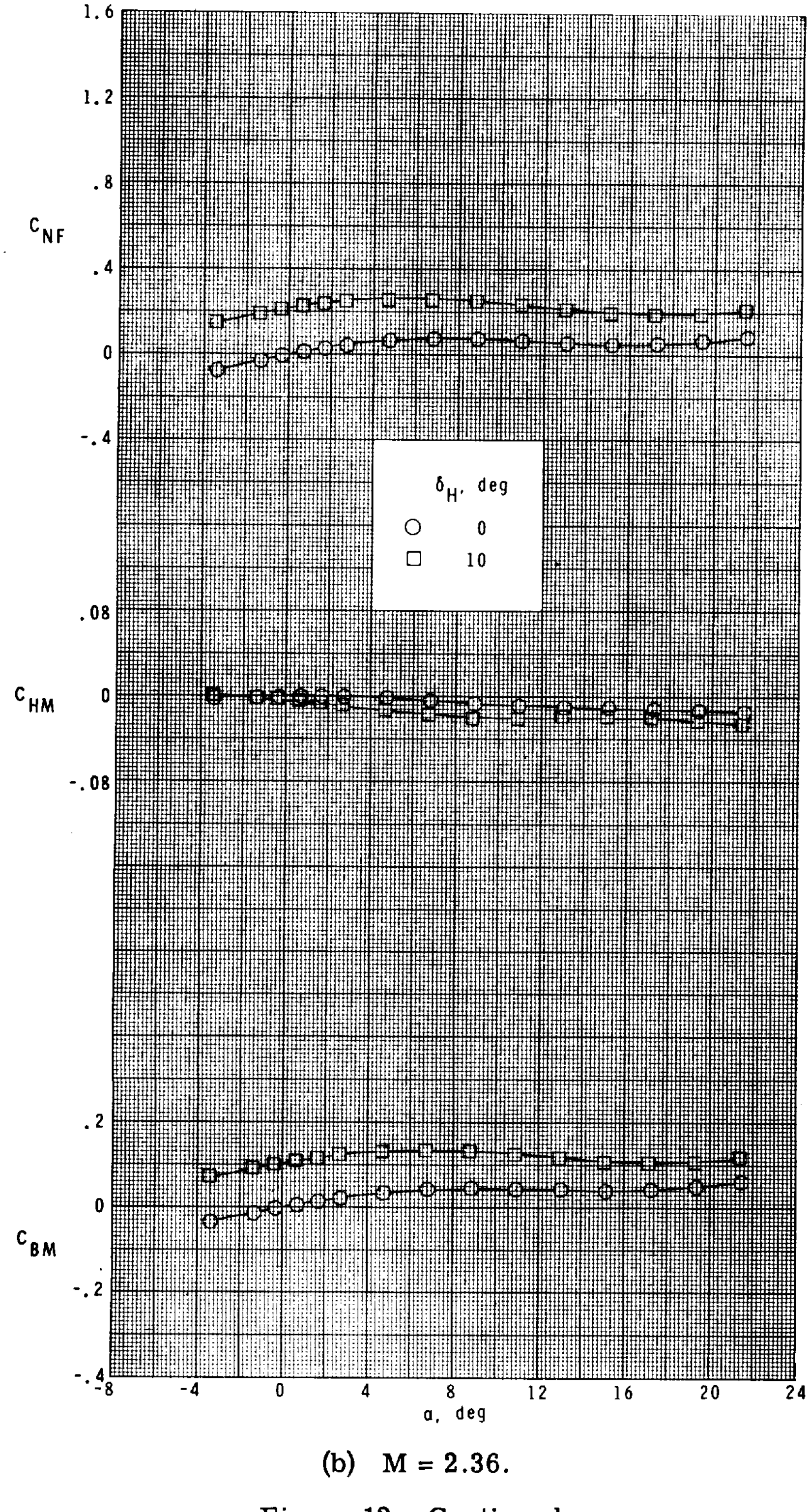

(b) M = 2.36.

Figure 12.- Continued.

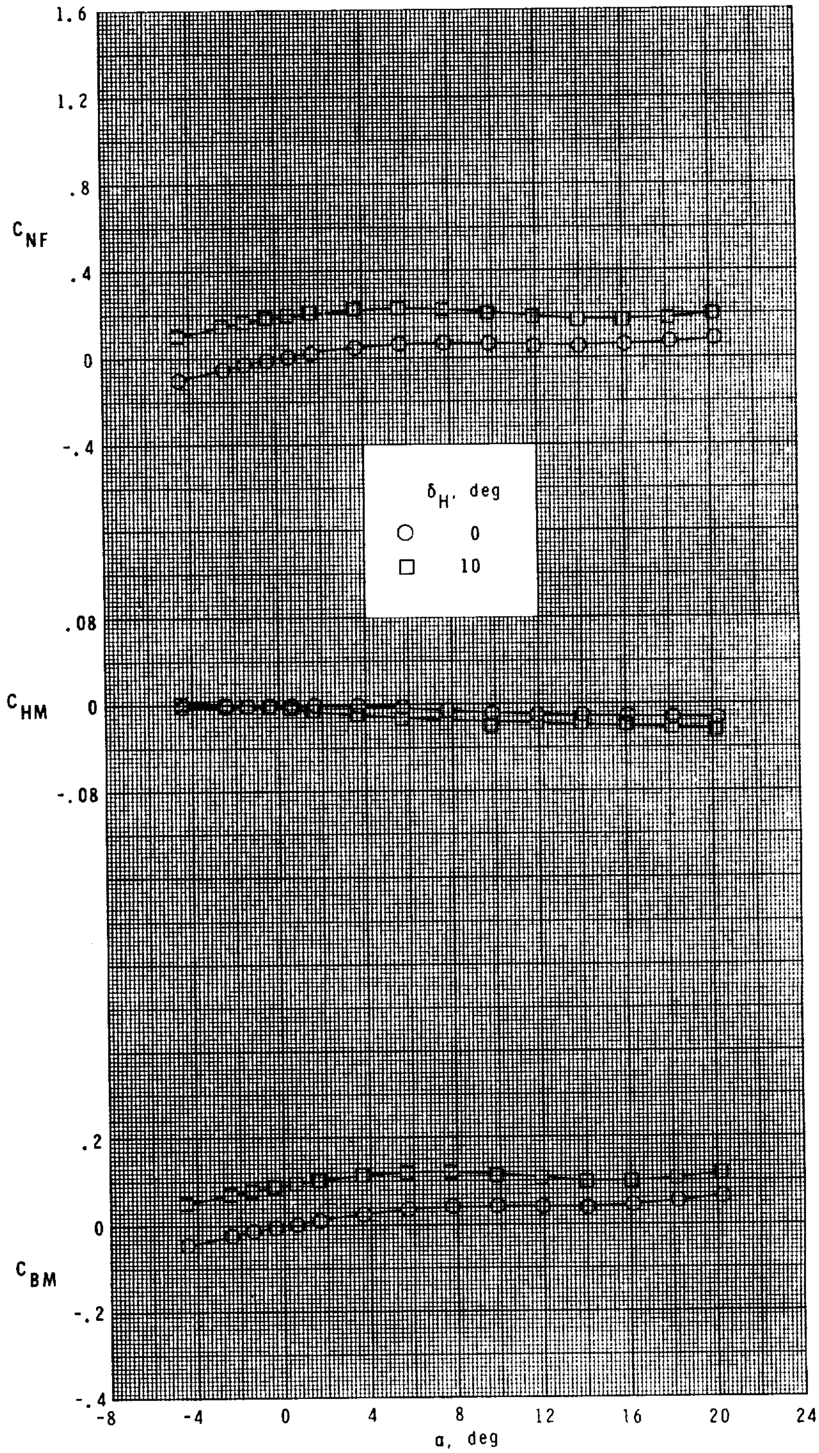

(c) M = 2.86.

Figure 12.- Concluded.

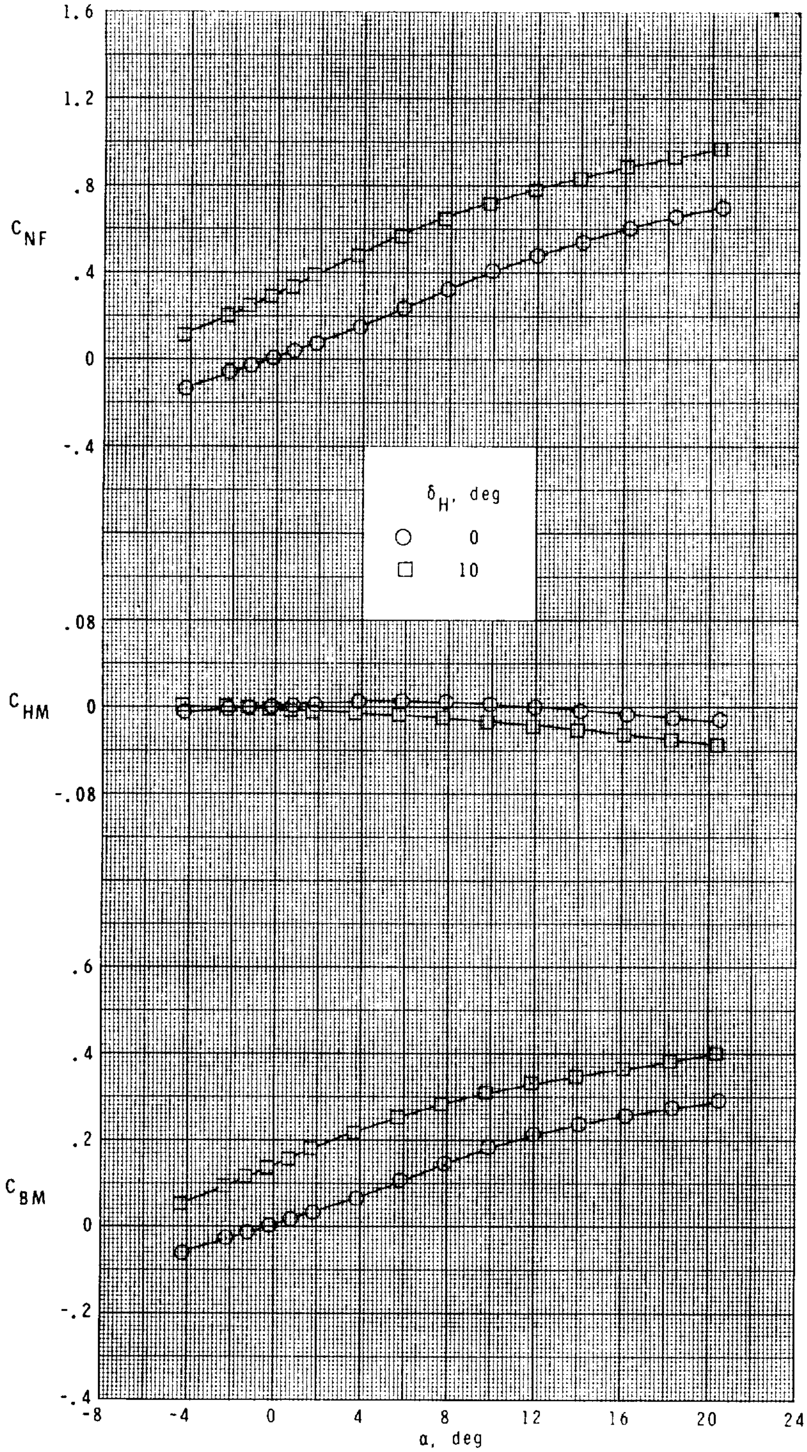

(a) M = 1.60.

Figure 13.- Variation of fin load coefficients with angle of attack for fin panel T_9 at $\phi_f = 90^o$.

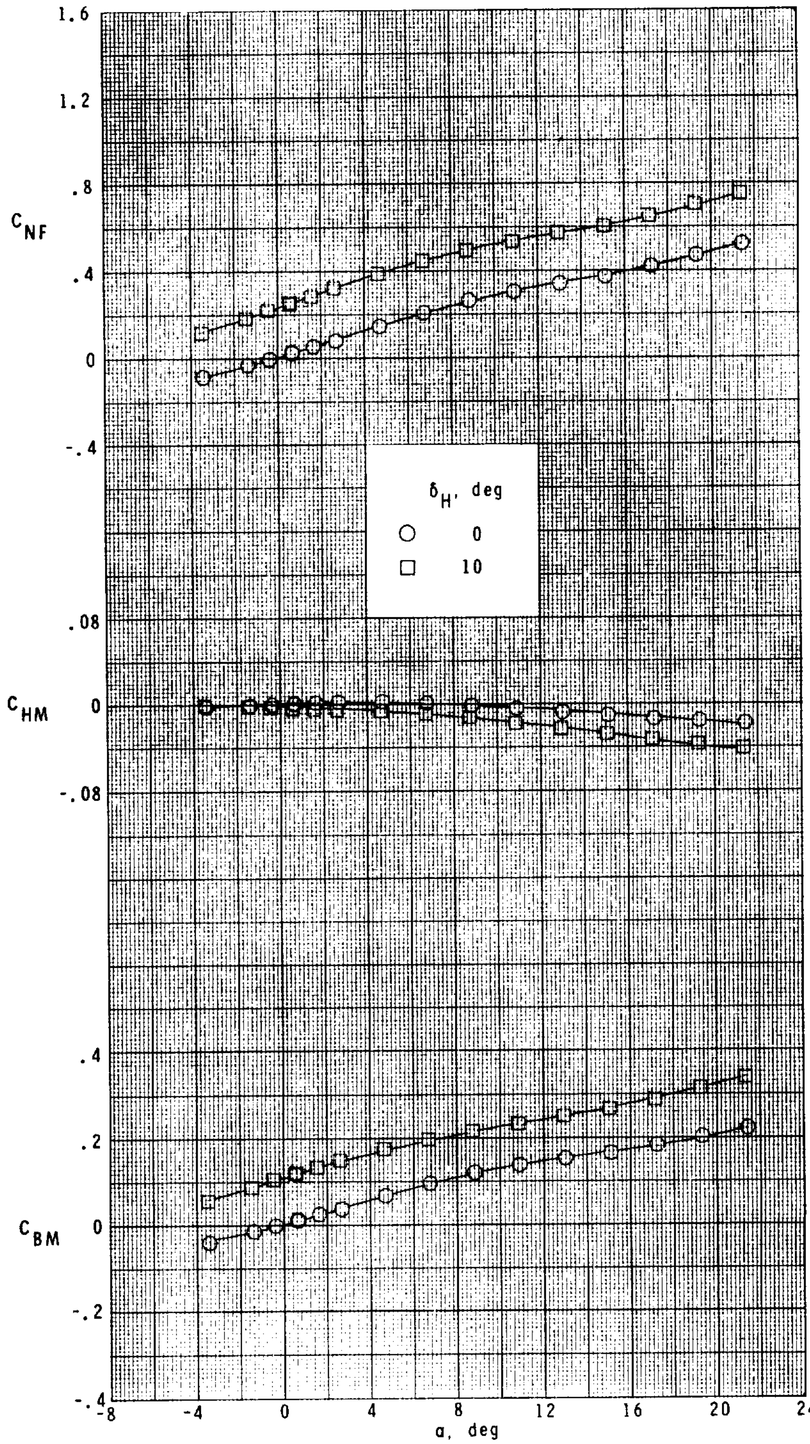

(b) M = 2.36.

Figure 13.- Continued.

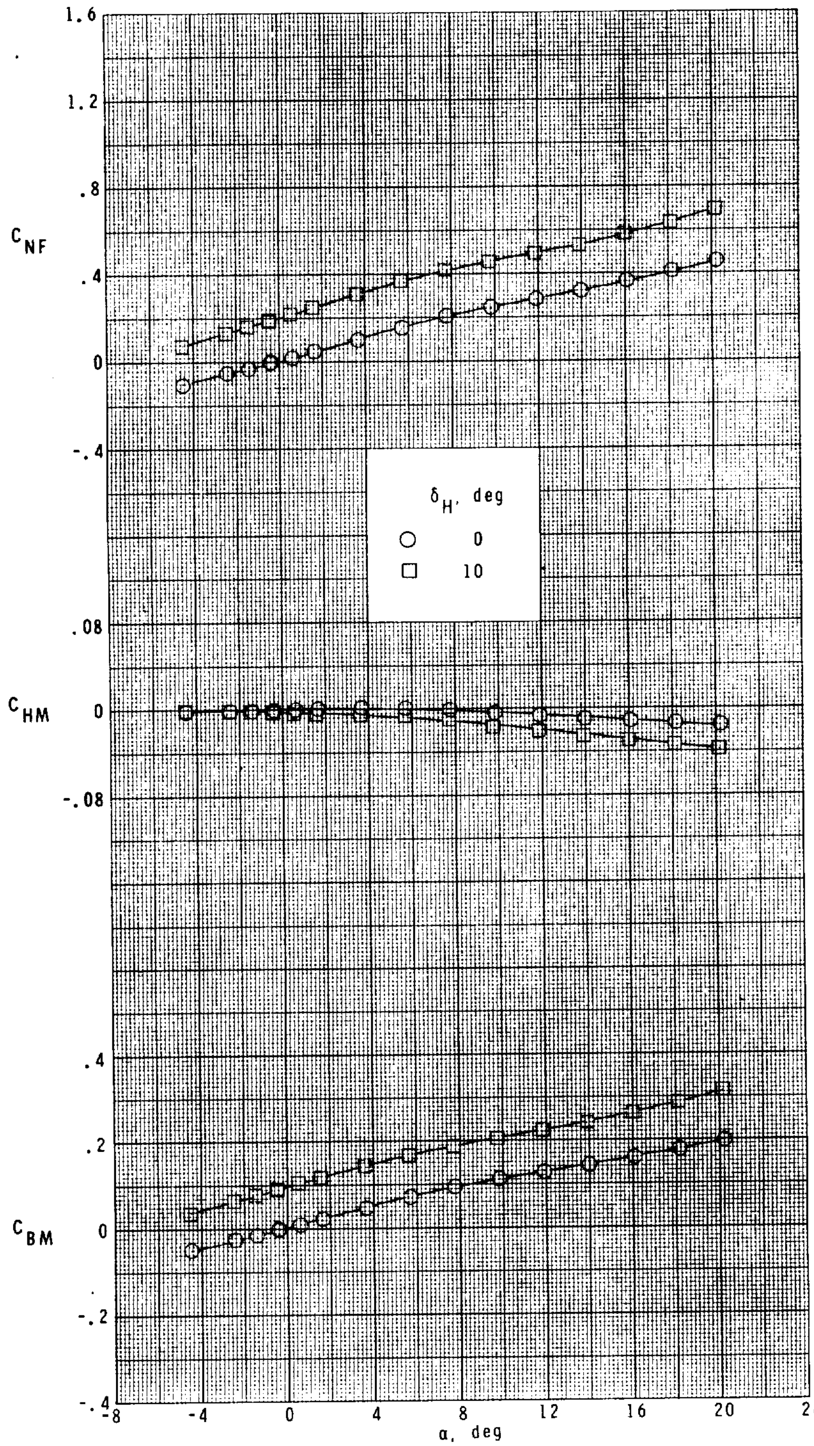

(c) M = 2.86.

Figure 13.- Concluded.

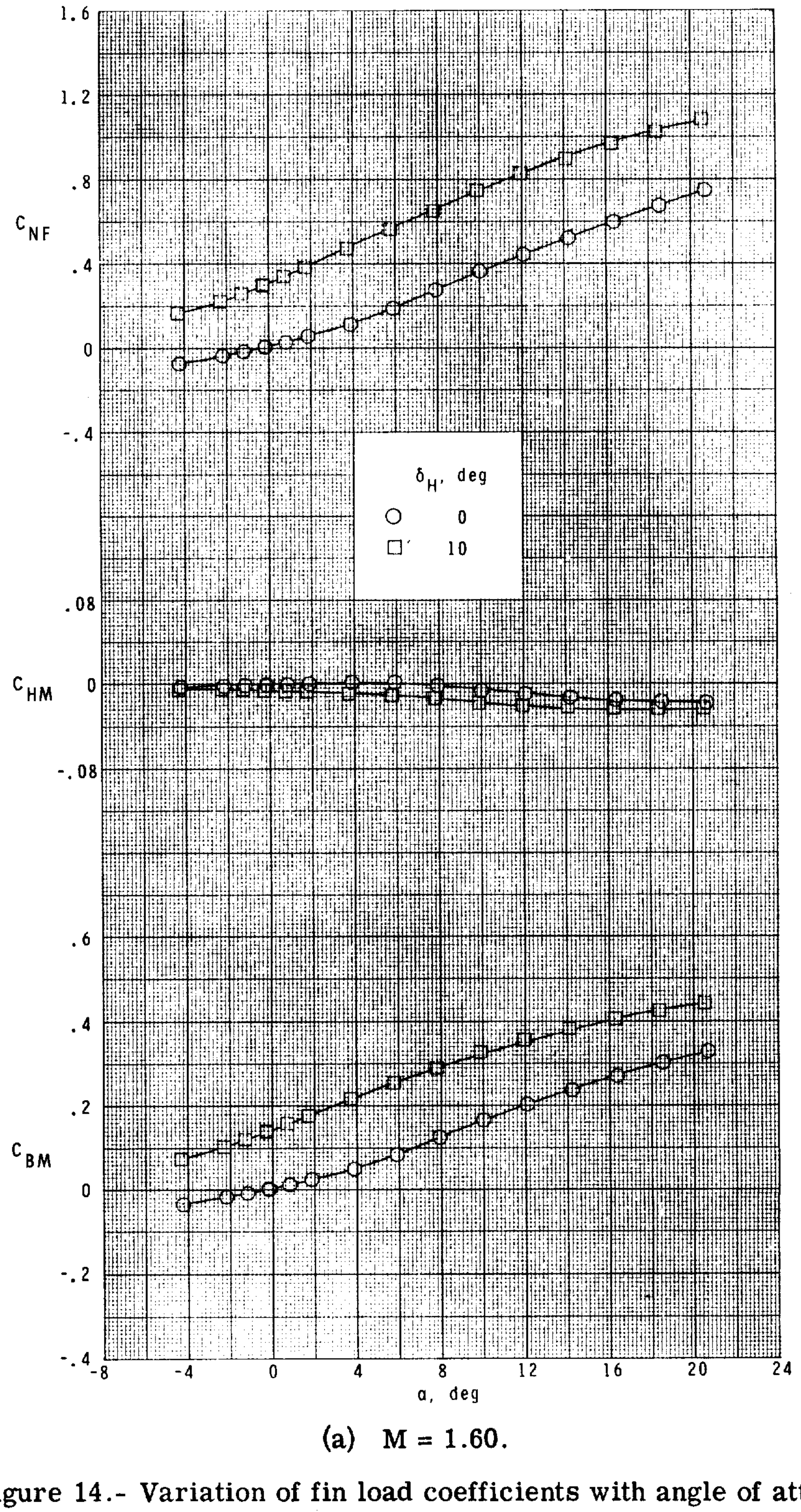

(a) M = 1.60.

Figure 14.- Variation of fin load coefficients with angle of attack for fin panel T_9 at $\phi_f = 135^0$.

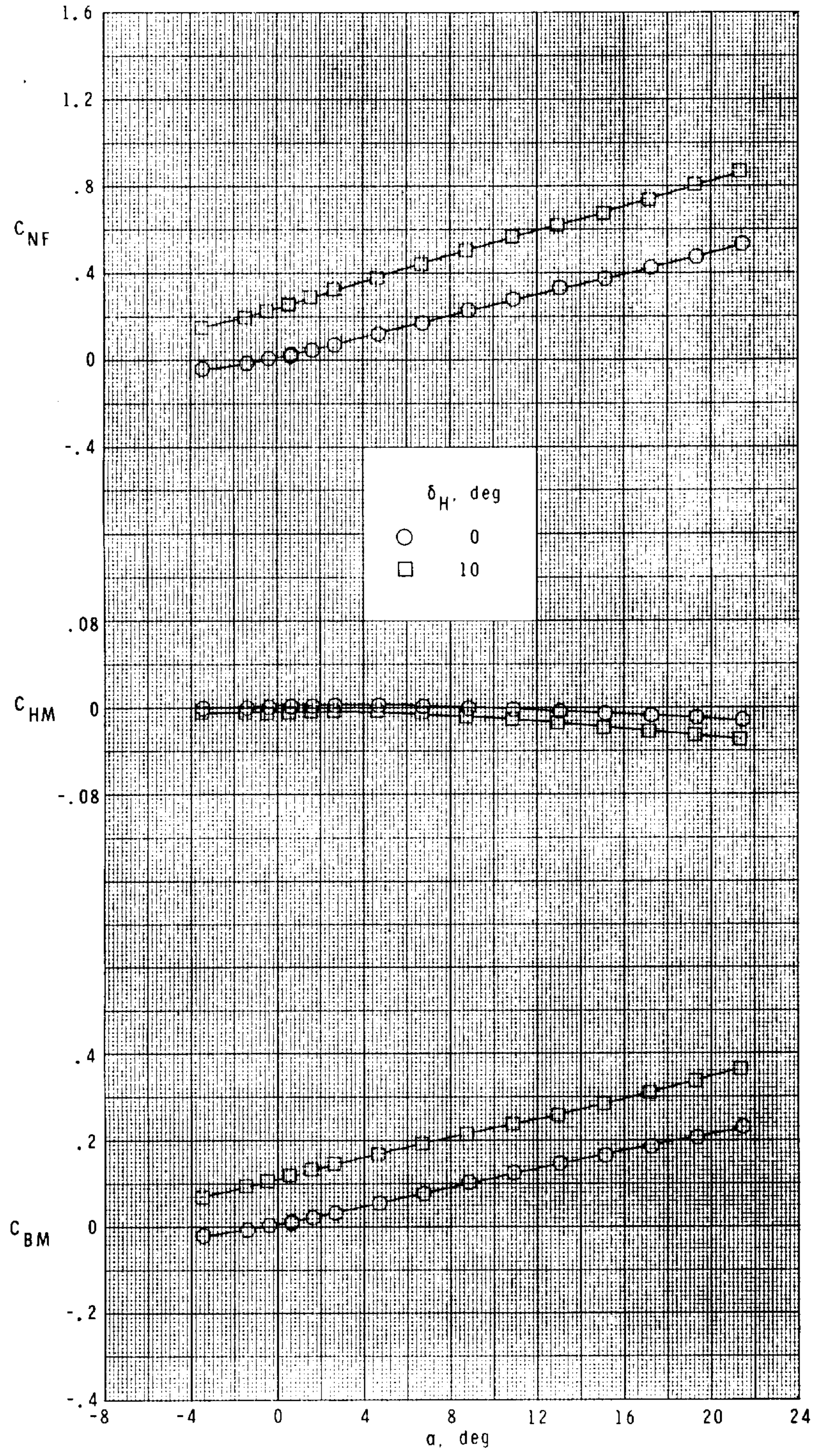

(b) M = 2.36.

Figure 14.- Continued.

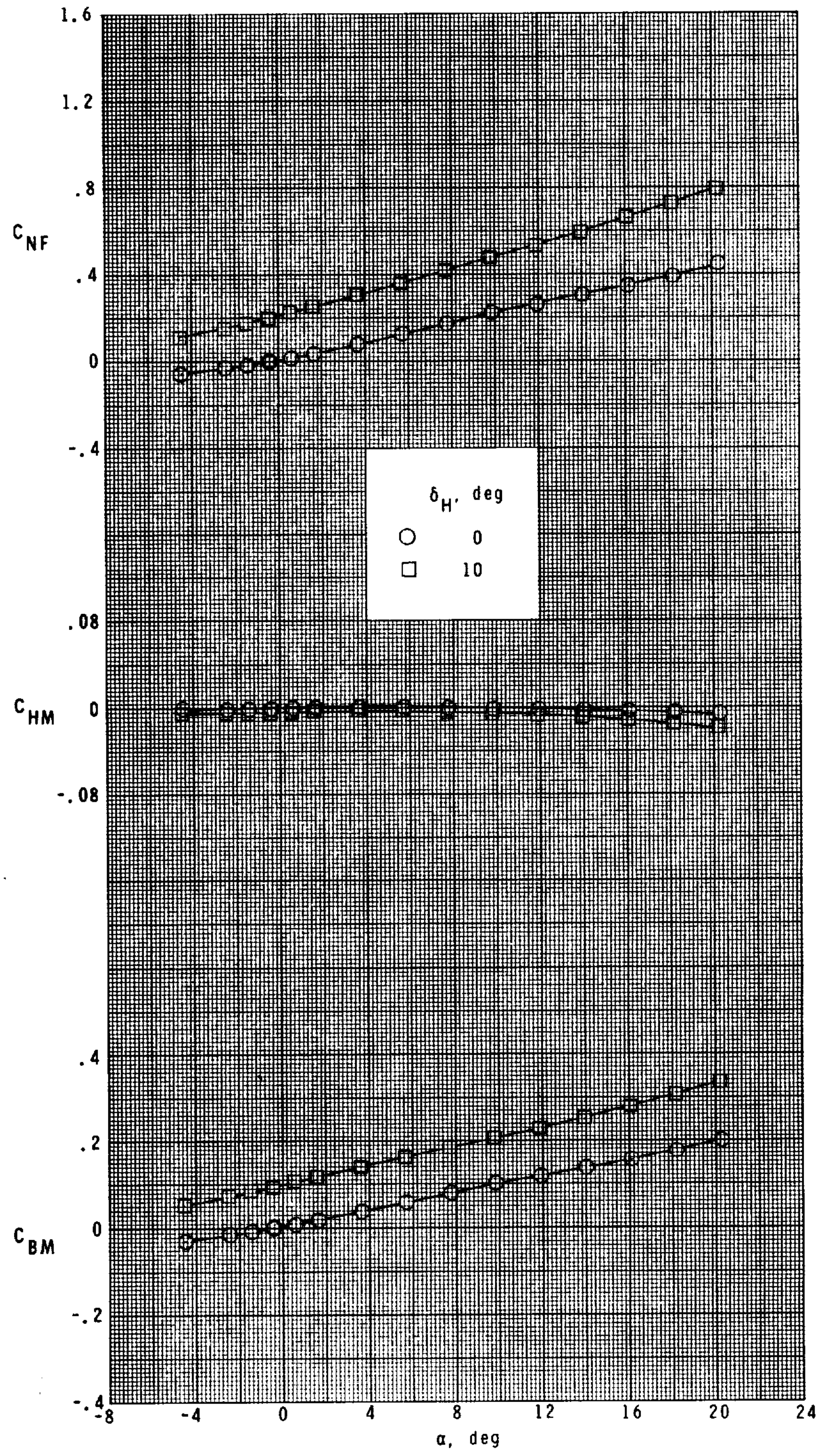

(c) M = 2.86.

Figure 14.- Concluded.

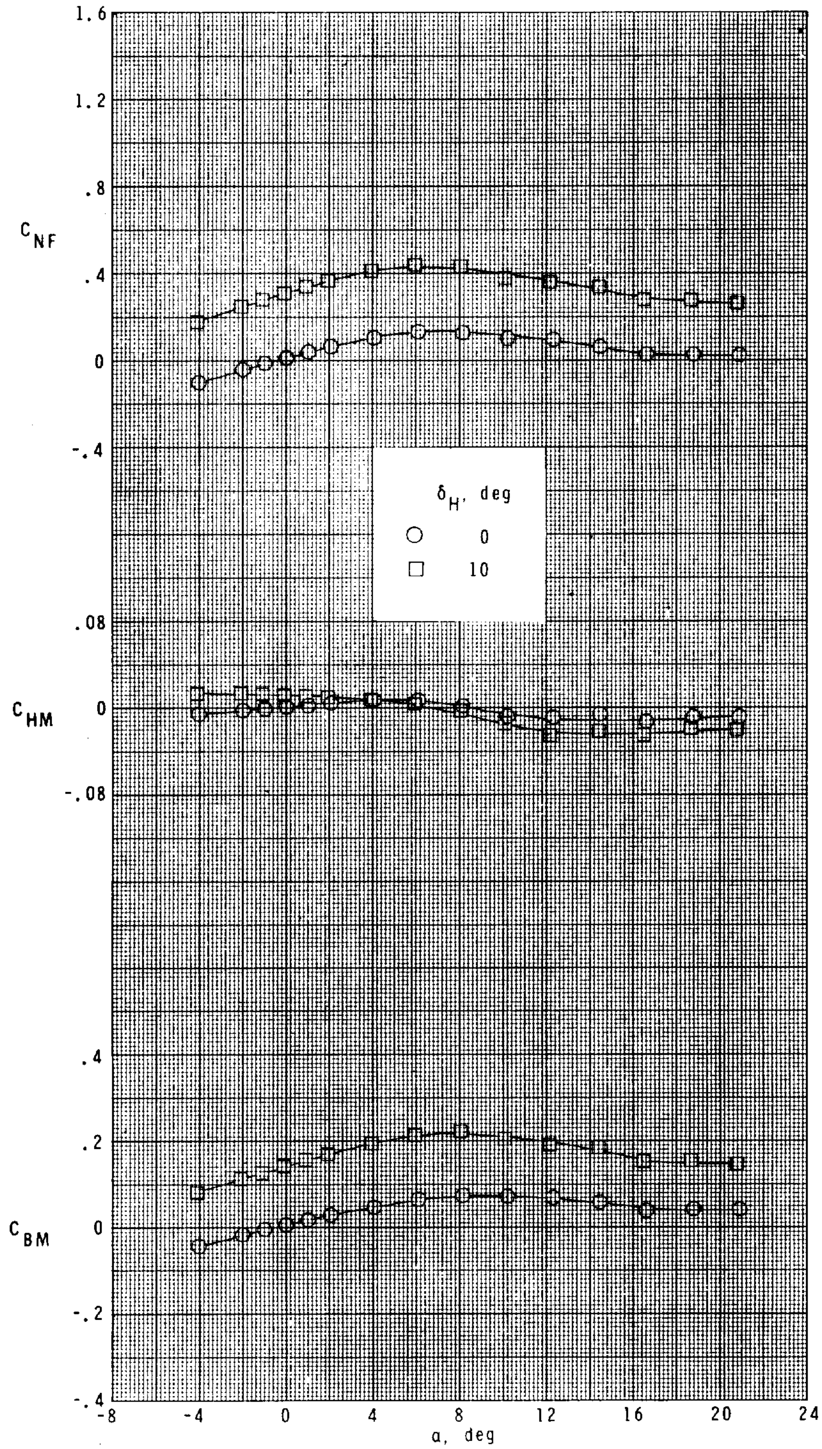

(a) M = 1.60.

Figure 15.- Variation of fin load coefficients with angle of attack for fin panel T_{10} at $\phi_f = 45^o$.

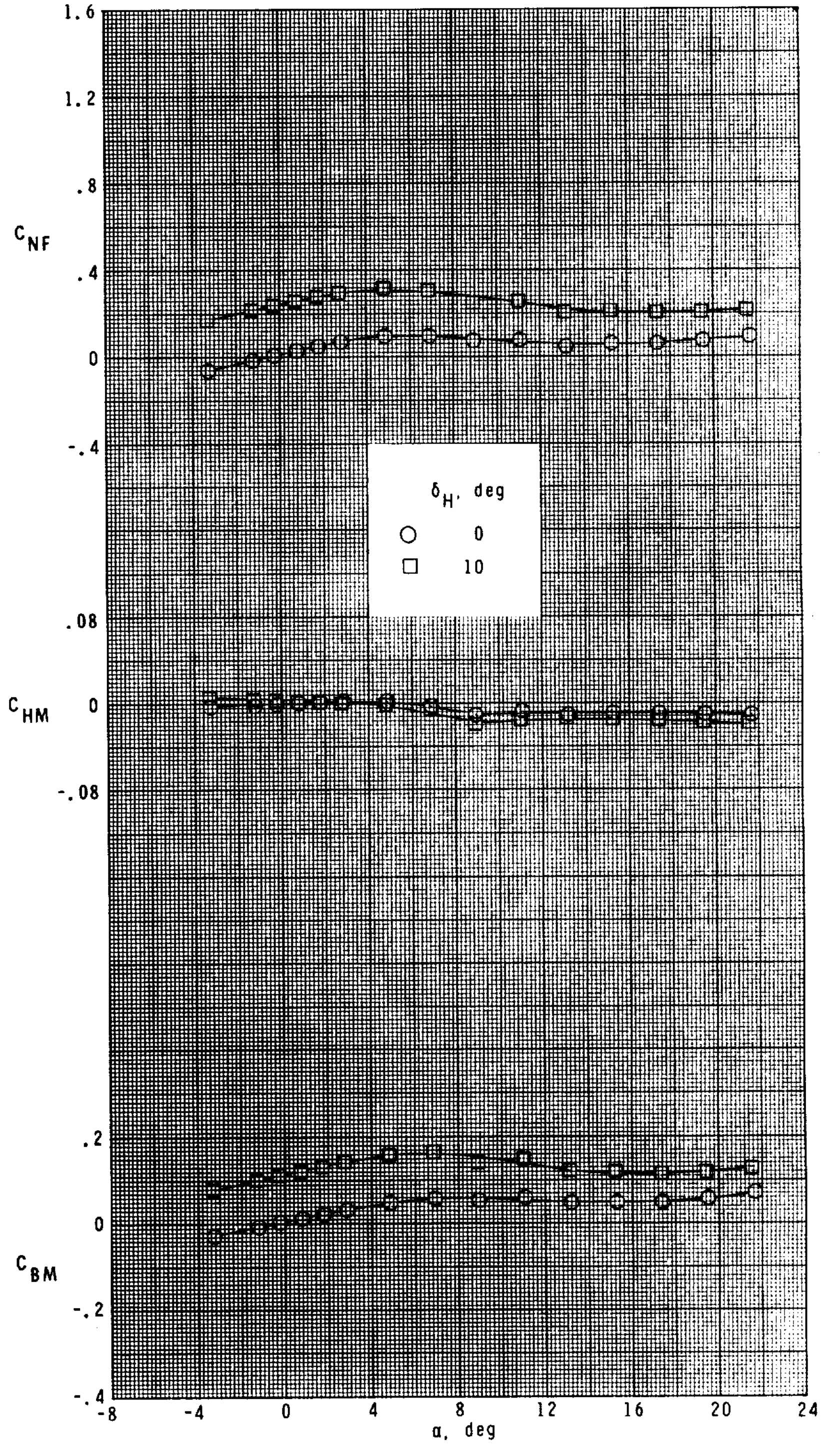

(b) M = 2.36.

Figure 15.- Continued.

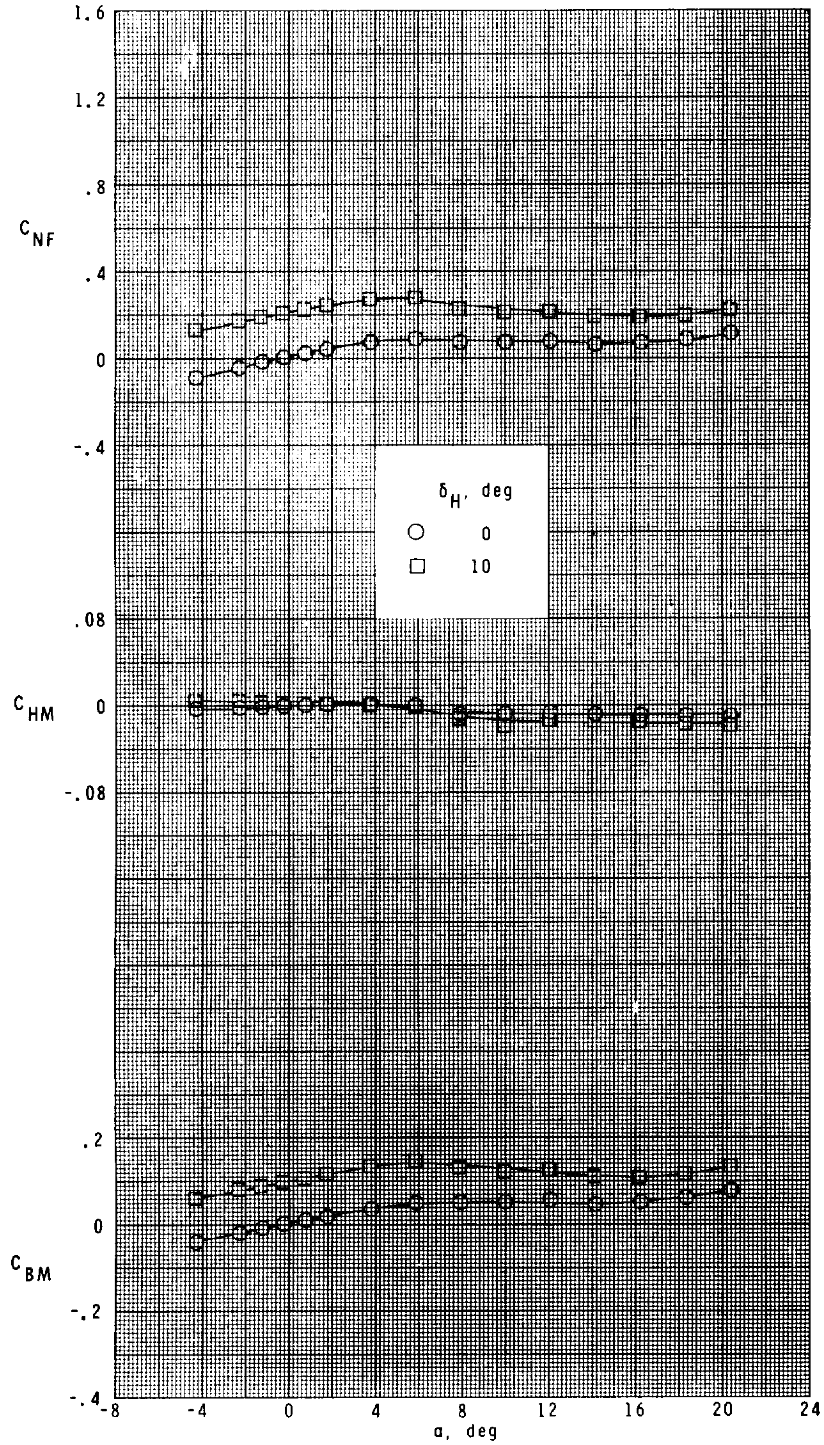

(c) M = 2.86.

Figure 15.- Concluded.

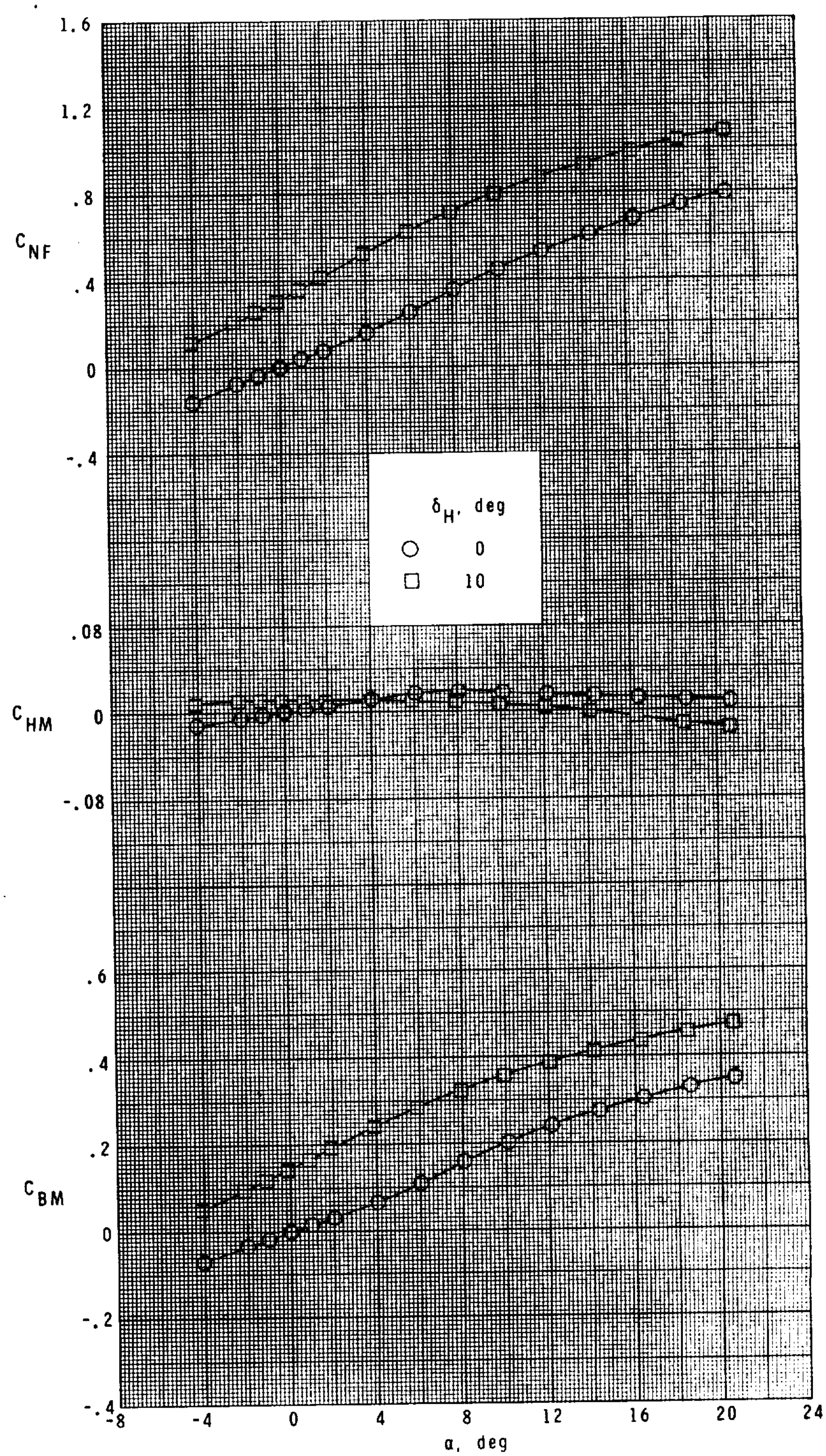

(a) M = 1.60.

Figure 16.- Variation of fin load coefficients with angle of attack for fin panel T_{10} at $\phi_f = 90^o$.

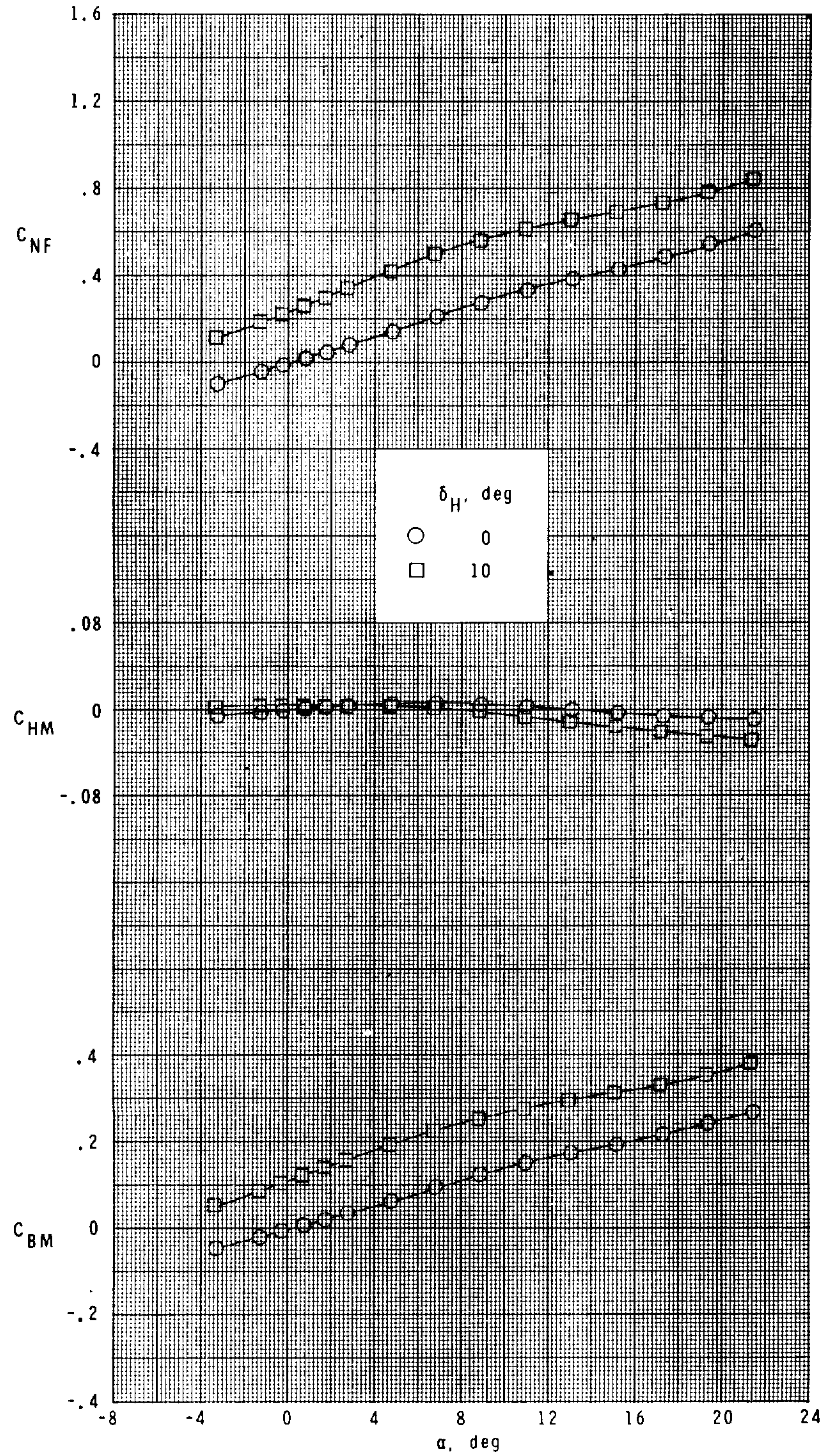

(b) M = 2.36.

Figure 16.- Continued.

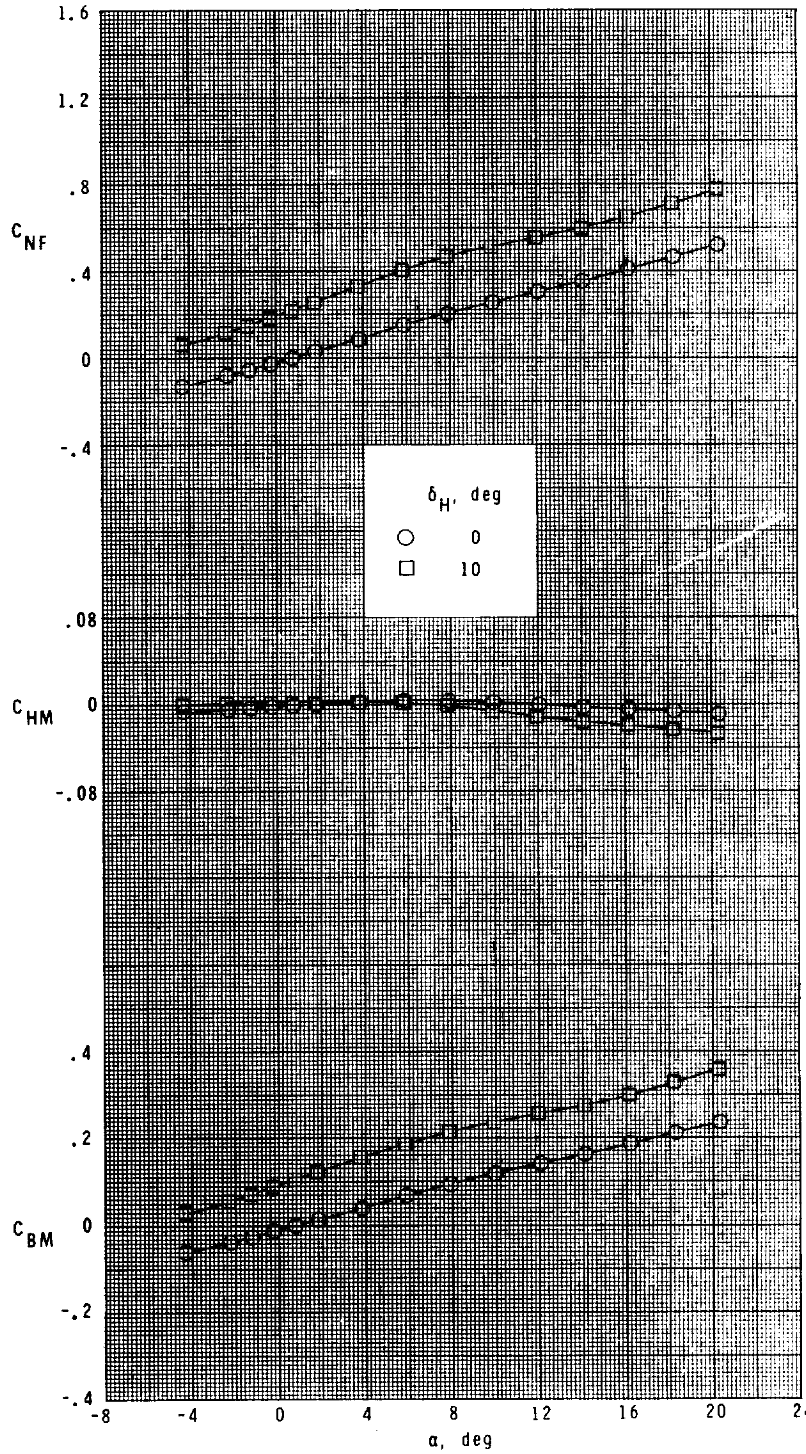

(c) M = 2.86.

Figure 16.- Concluded.

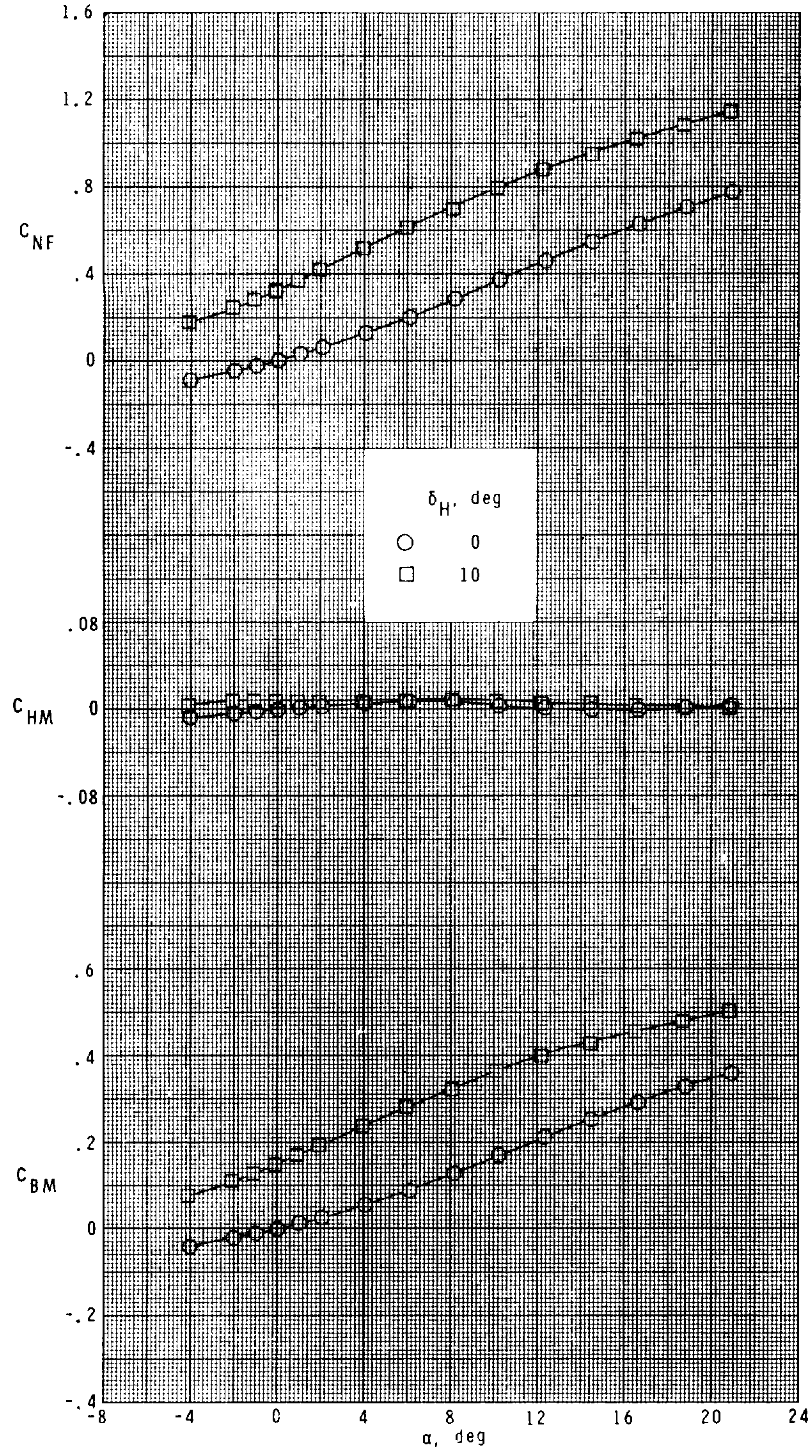

(a) M = 1.60.

Figure 17.- Variation of fin load coefficients with angle of attack for fin panel T_{10} at $\phi_f = 135^{\circ}$.

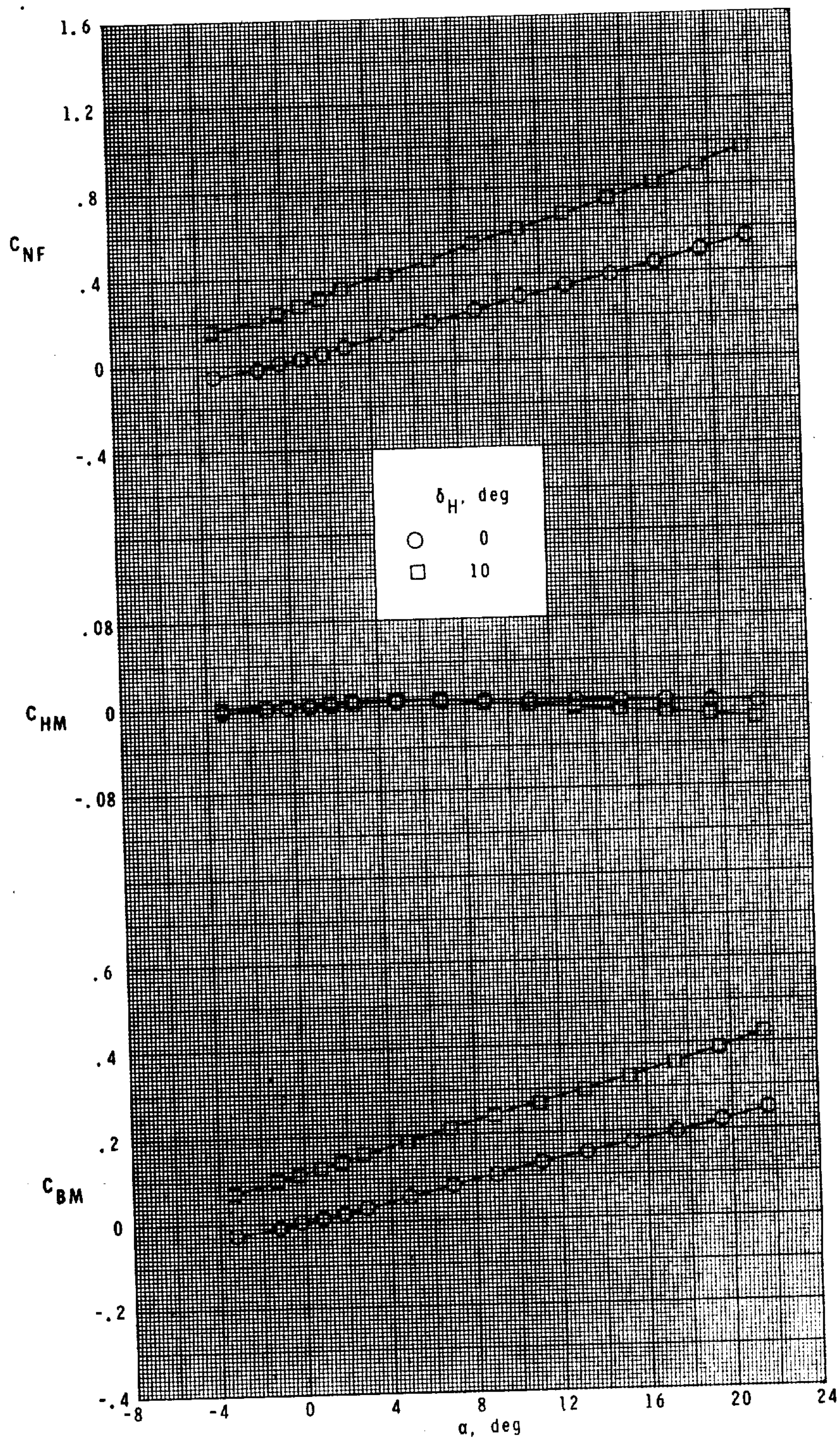

(b) M = 2.36.

Figure 17.- Continued.

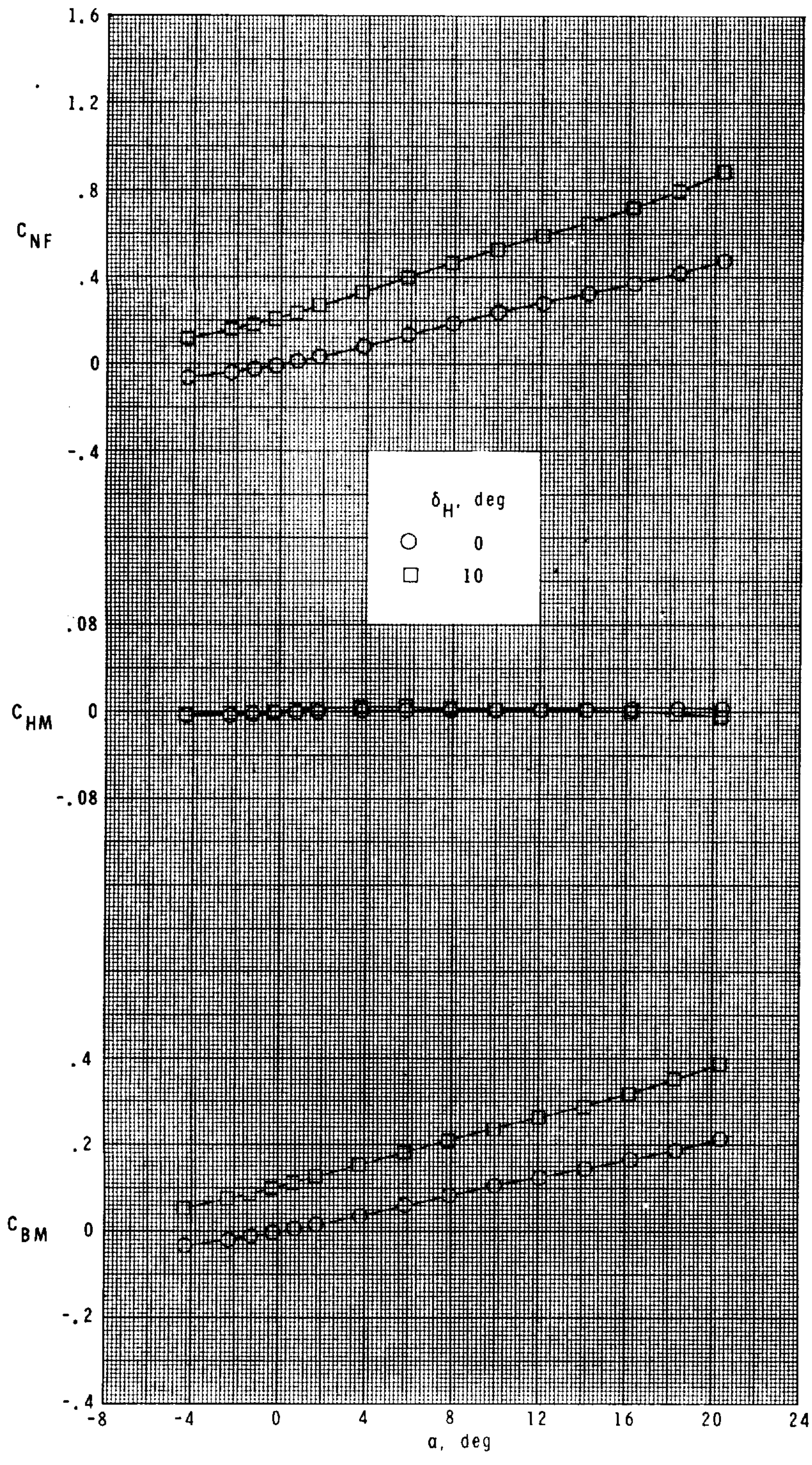

(c) M = 2.86.

Figure 17.- Concluded.

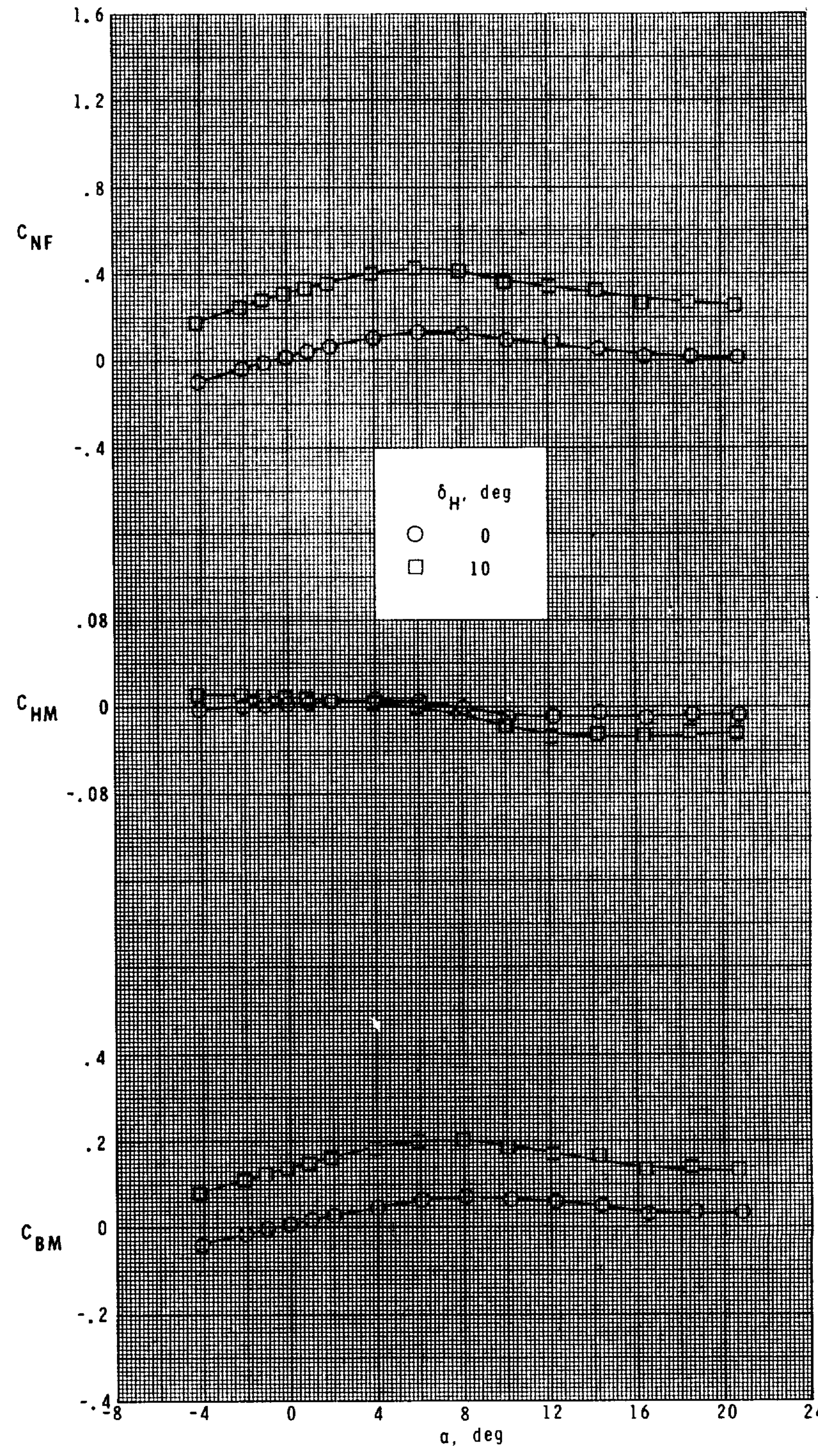

(a) M = 1.60.

Figure 18.- Variation of fin load coefficients with angle of attack for fin panel T_{11} at $\phi_f = 45^o$.

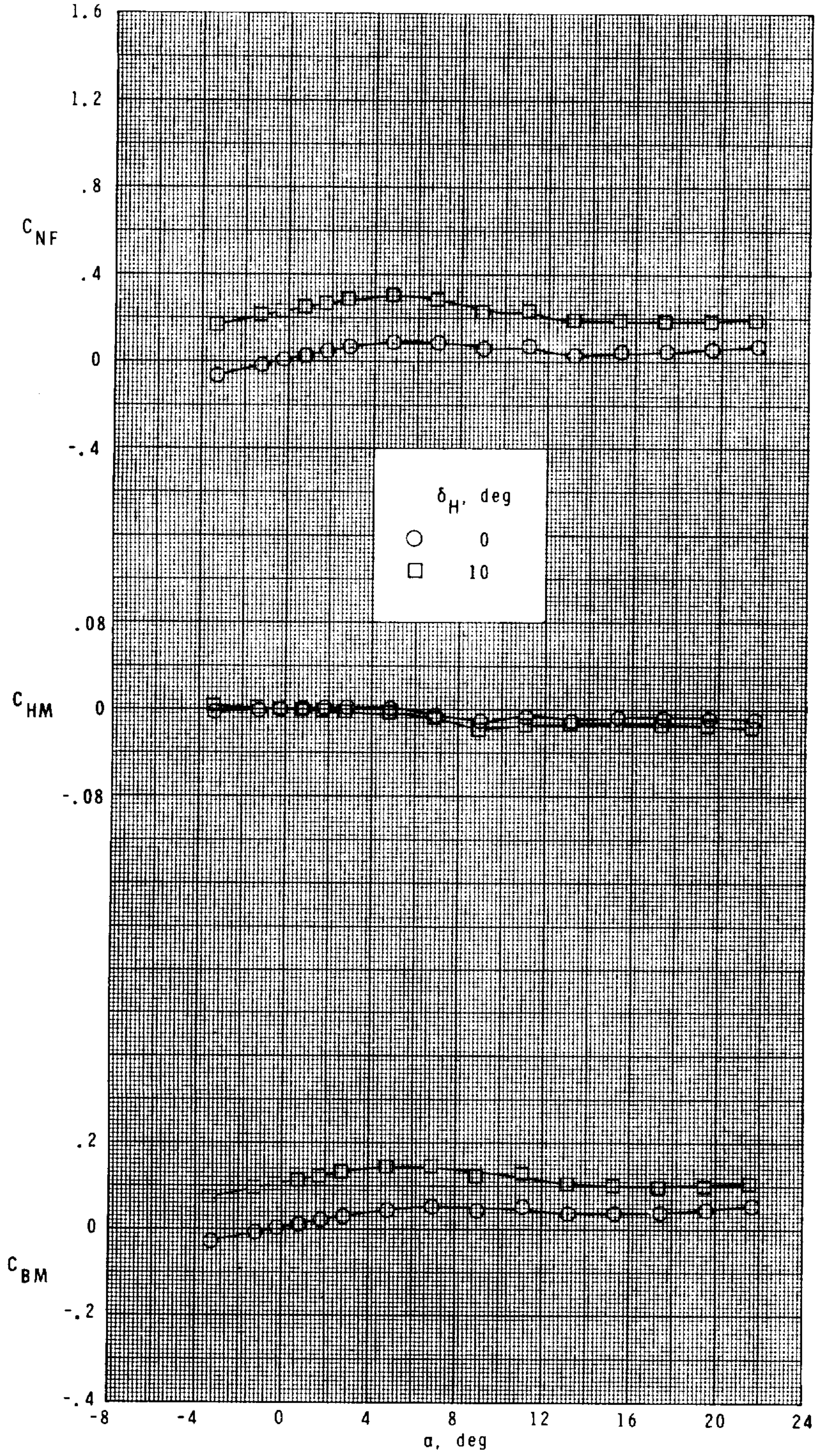

(b) M = 2.36.

Figure 18.- Continued.

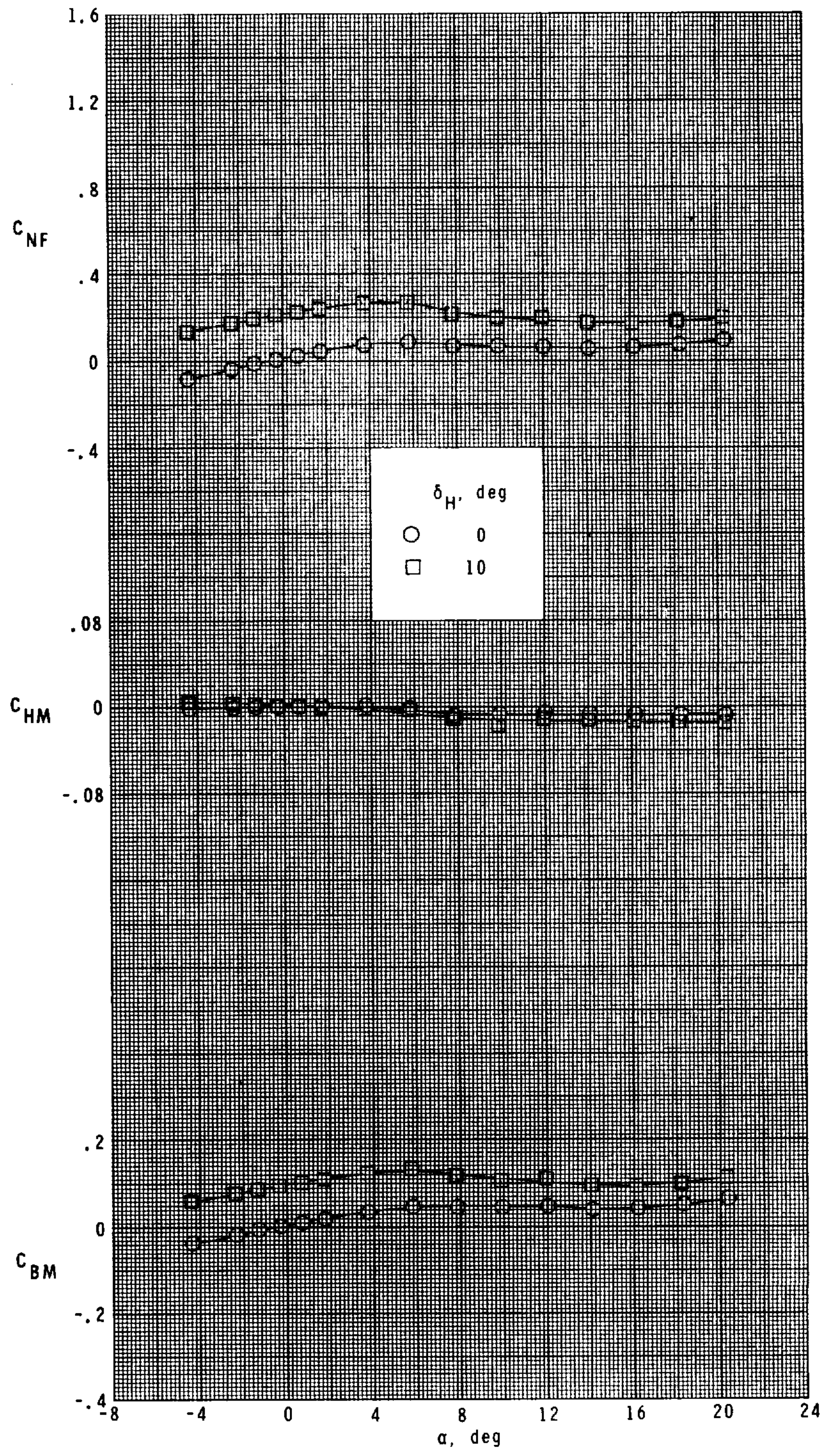

(c) M = 2.86.

Figure 18.- Concluded.

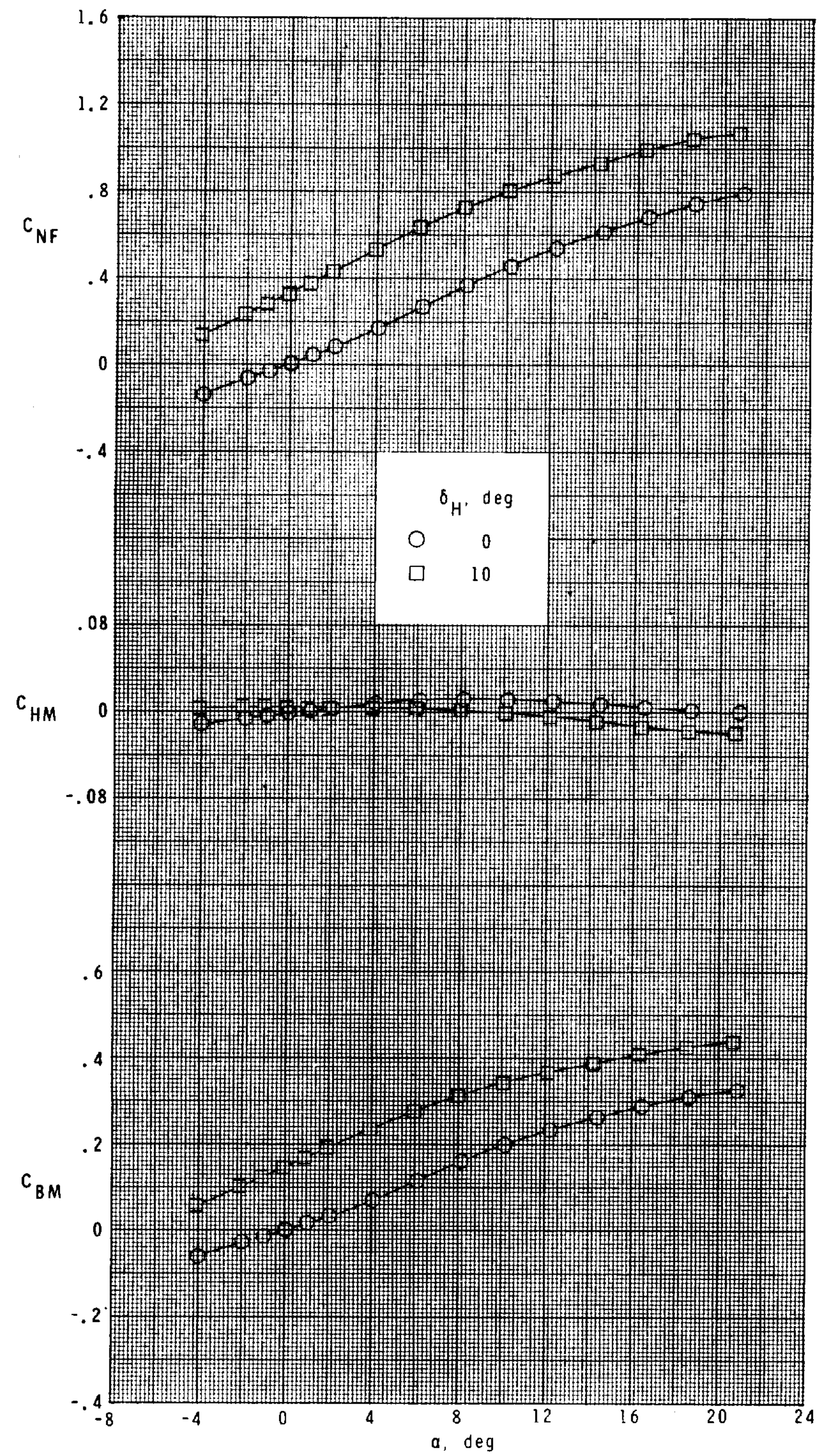

(a) M = 1.60.

Figure 19.- Variation of fin load coefficients with angle of attack for fin panel T_{11} at $\phi_f = 90^o$.

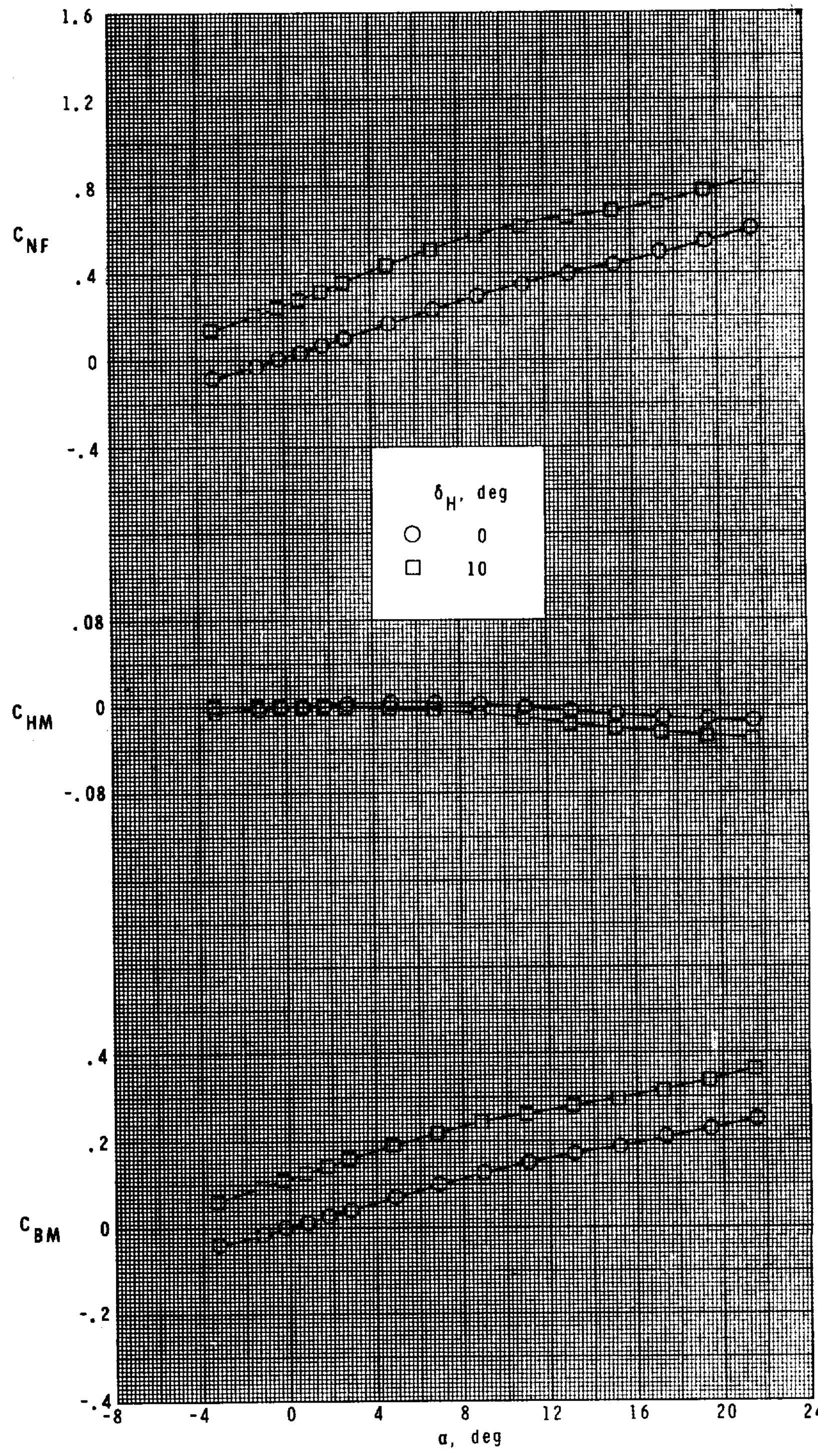

(b) M = 2.36.

Figure 19.- Continued.

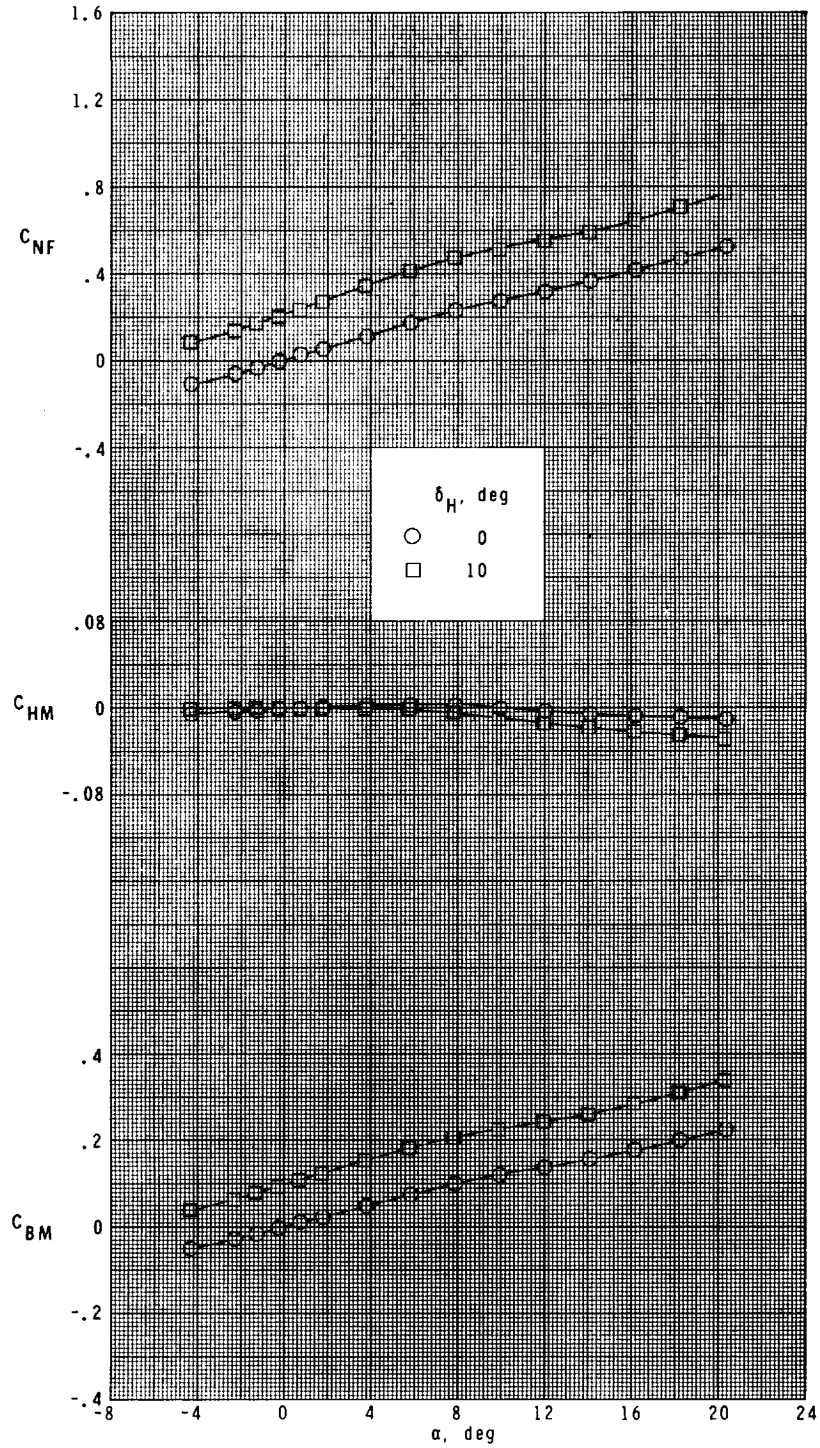

(c) M = 2.86.

Figure 19.- Concluded.

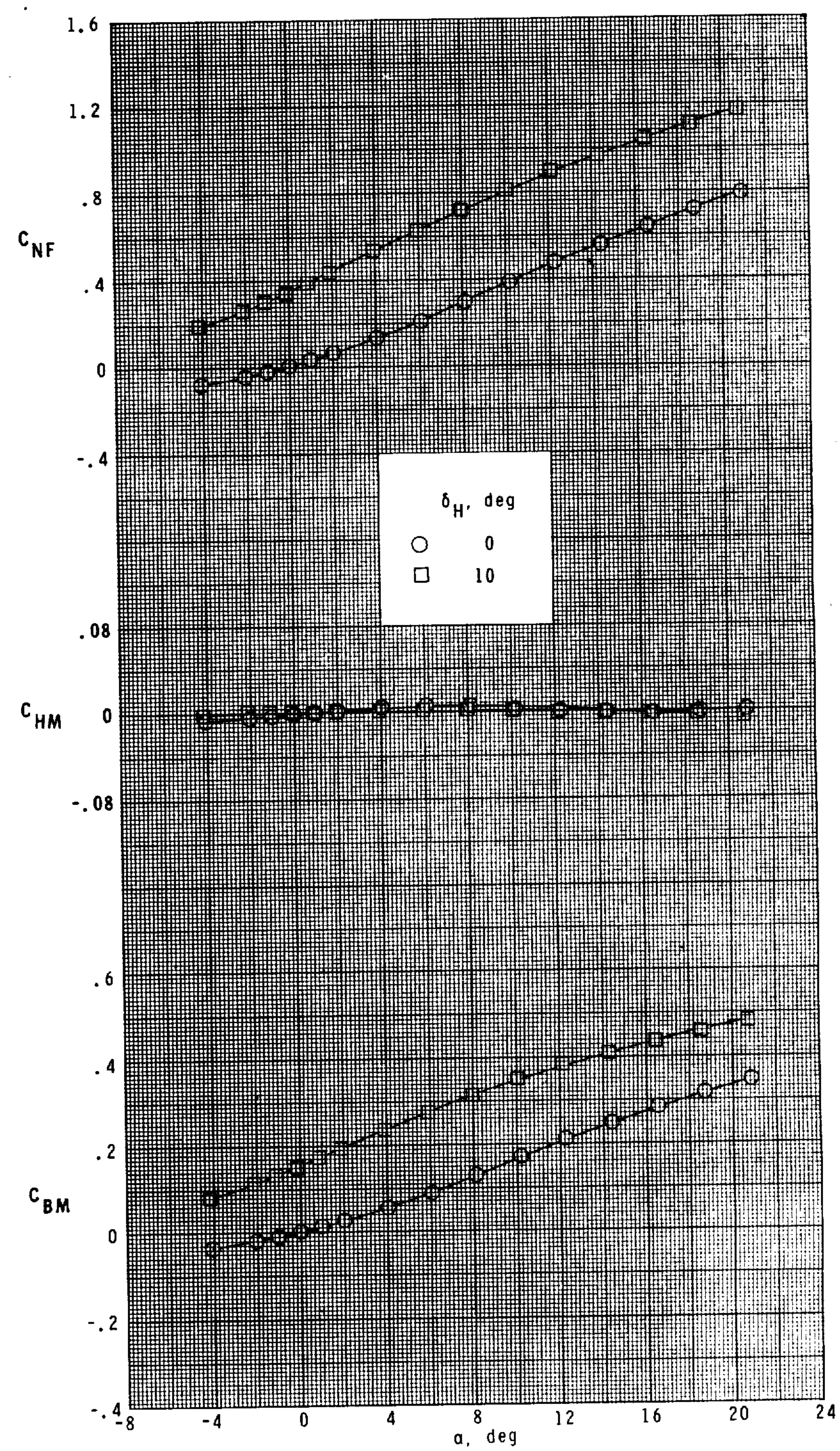

(a) M = 1.60.

Figure 20.- Variation of fin load coefficients with angle of attack for fin panel T_{11} at $\phi_f = 135^{\circ}$.

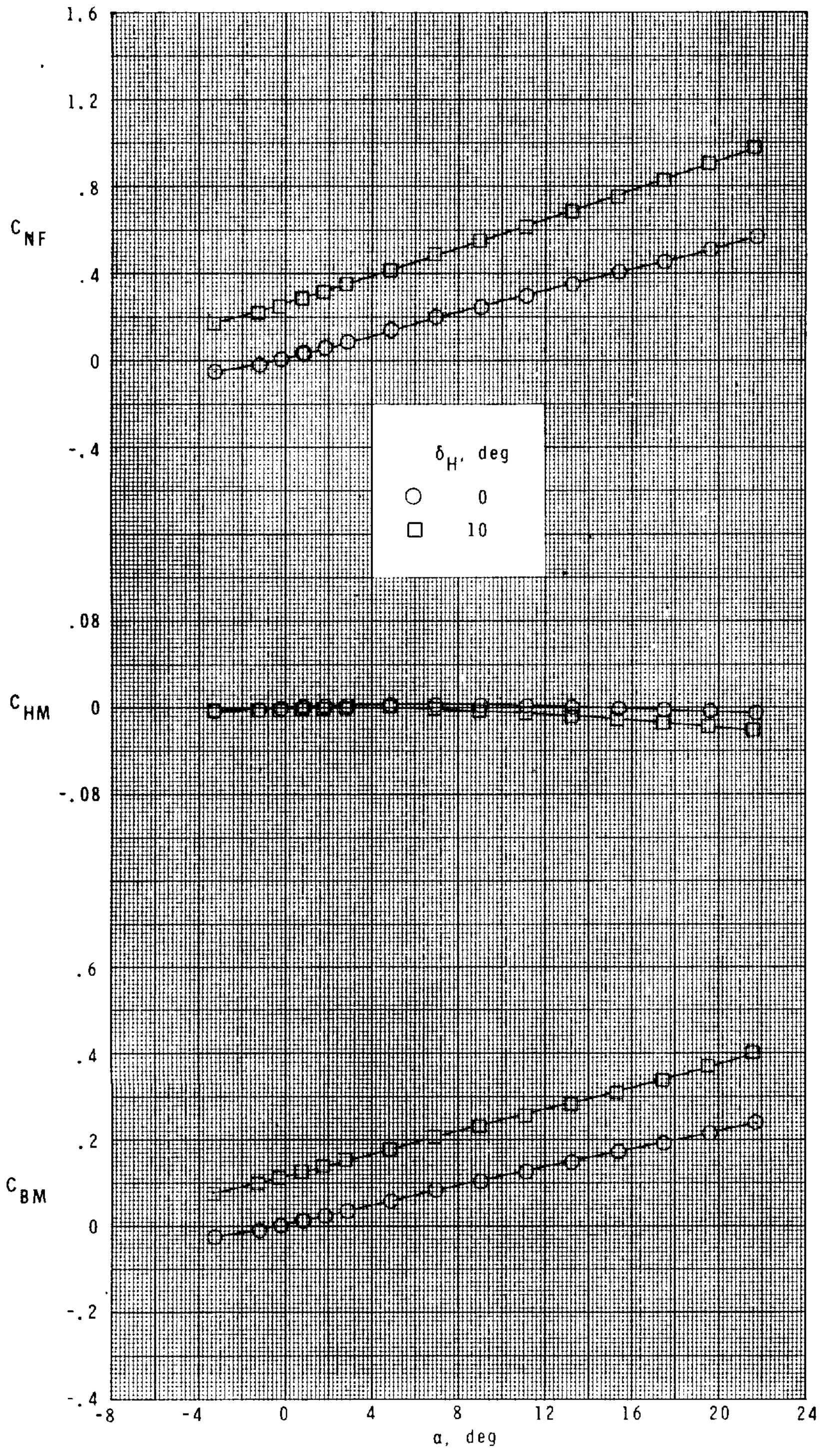

(b) M = 2.36.

Figure 20.- Continued.

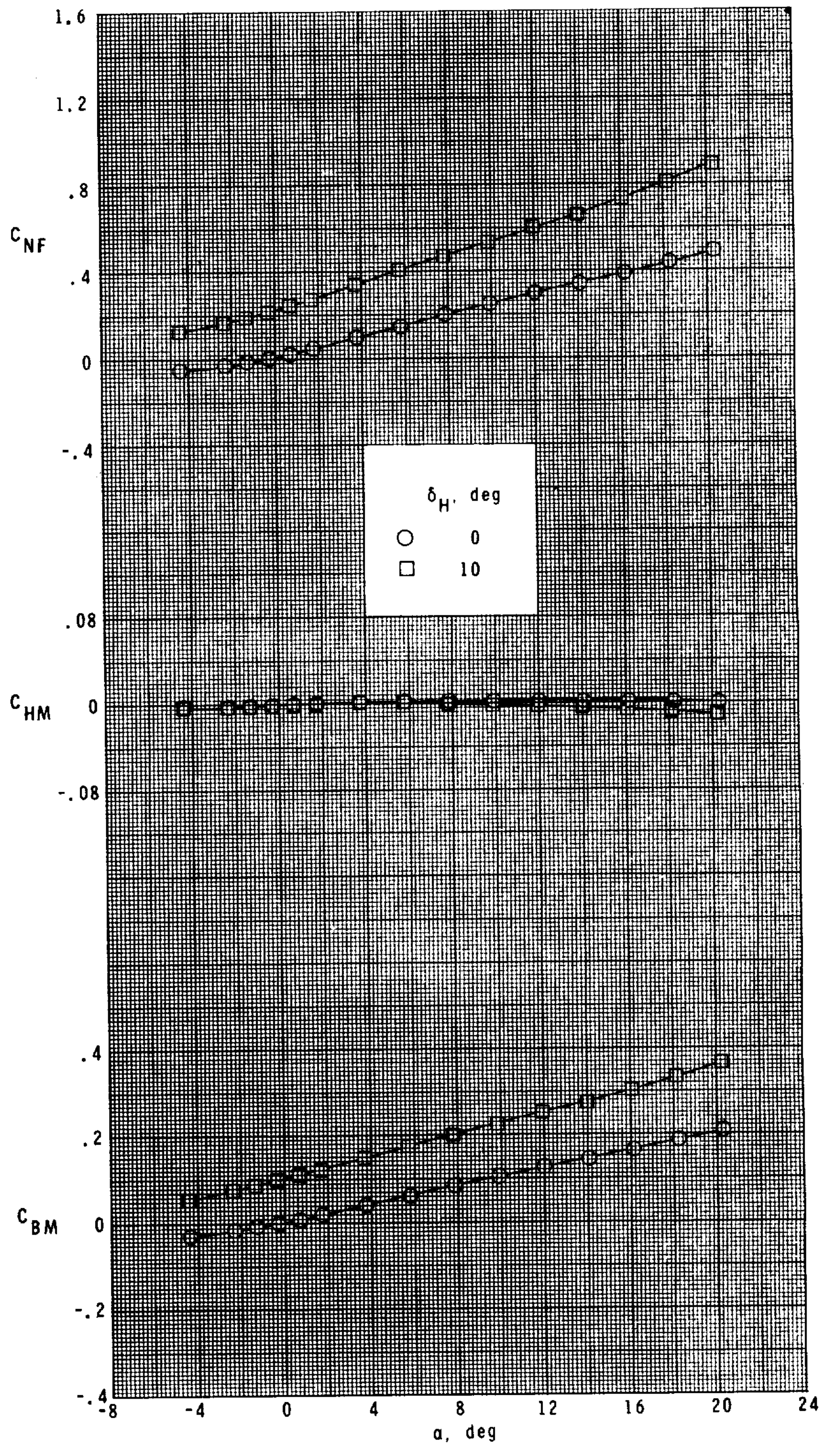

(c) M = 2.86.

Figure 20.- Concluded.

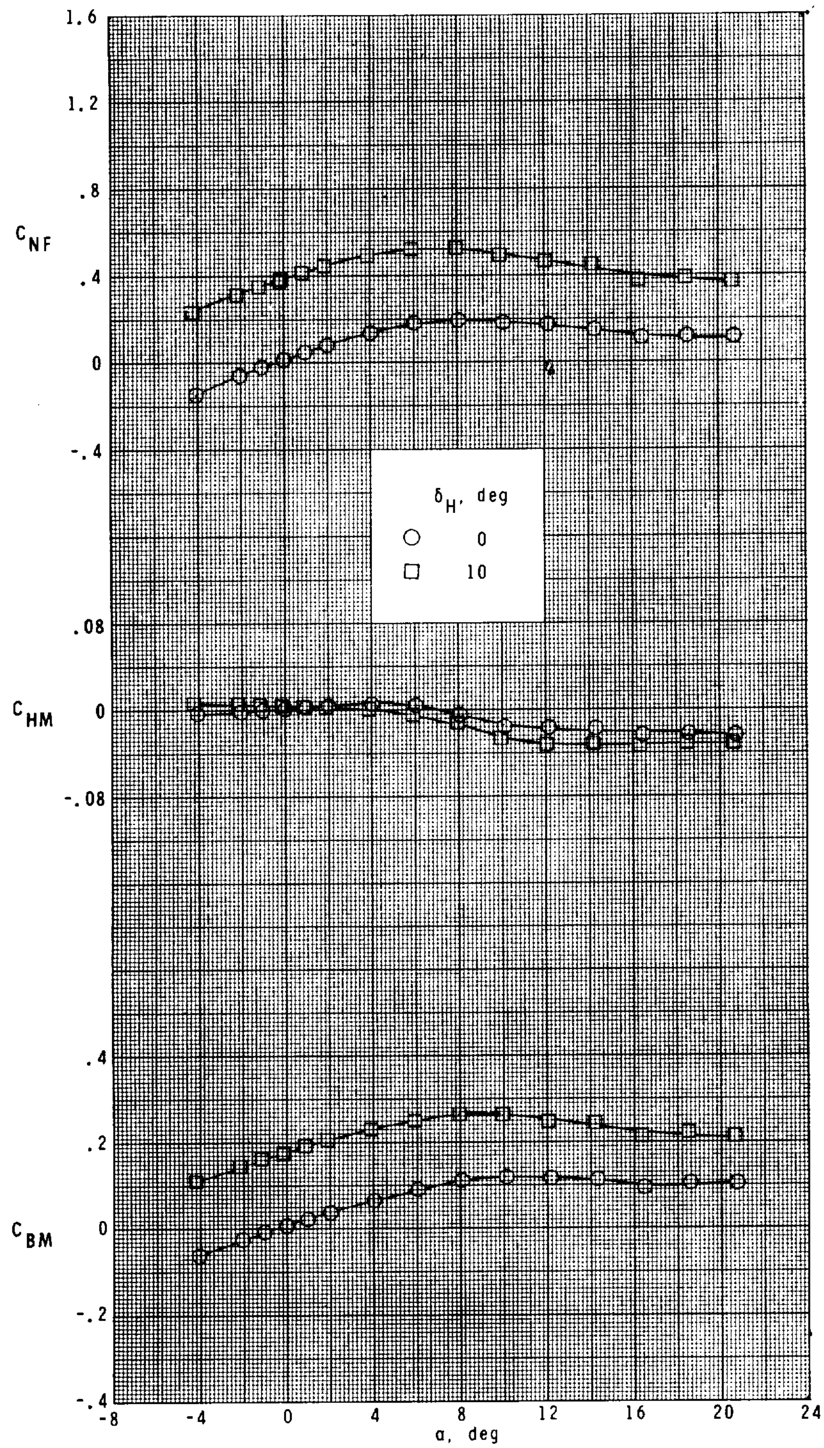

(a) M = 1.60.

Figure 21.- Variation of fin load coefficients with angle of attack for fin panel T_{12} at $\phi_f = 45^{\circ}$.

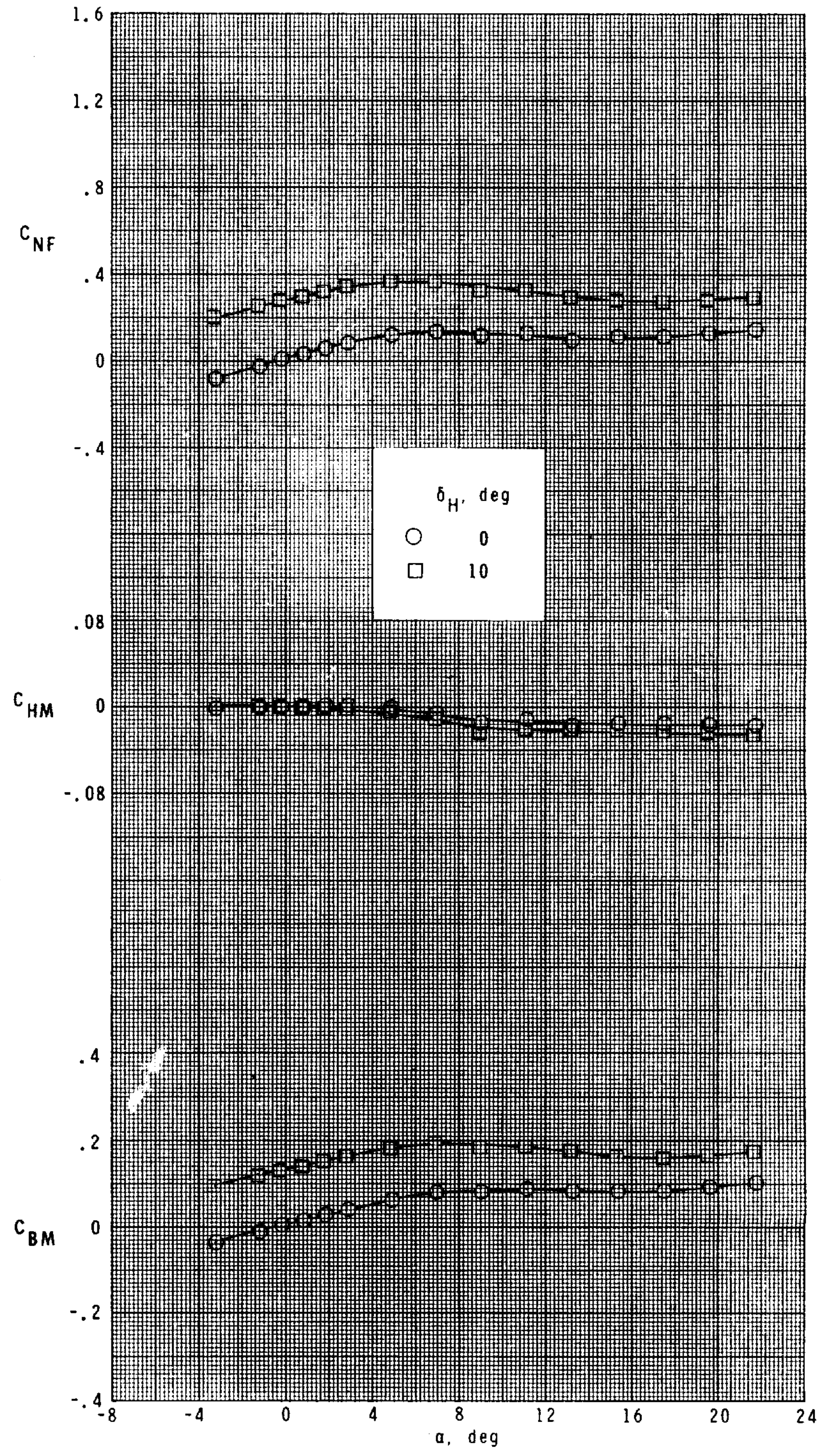

(b) M = 2.36.

Figure 21.- Continued.

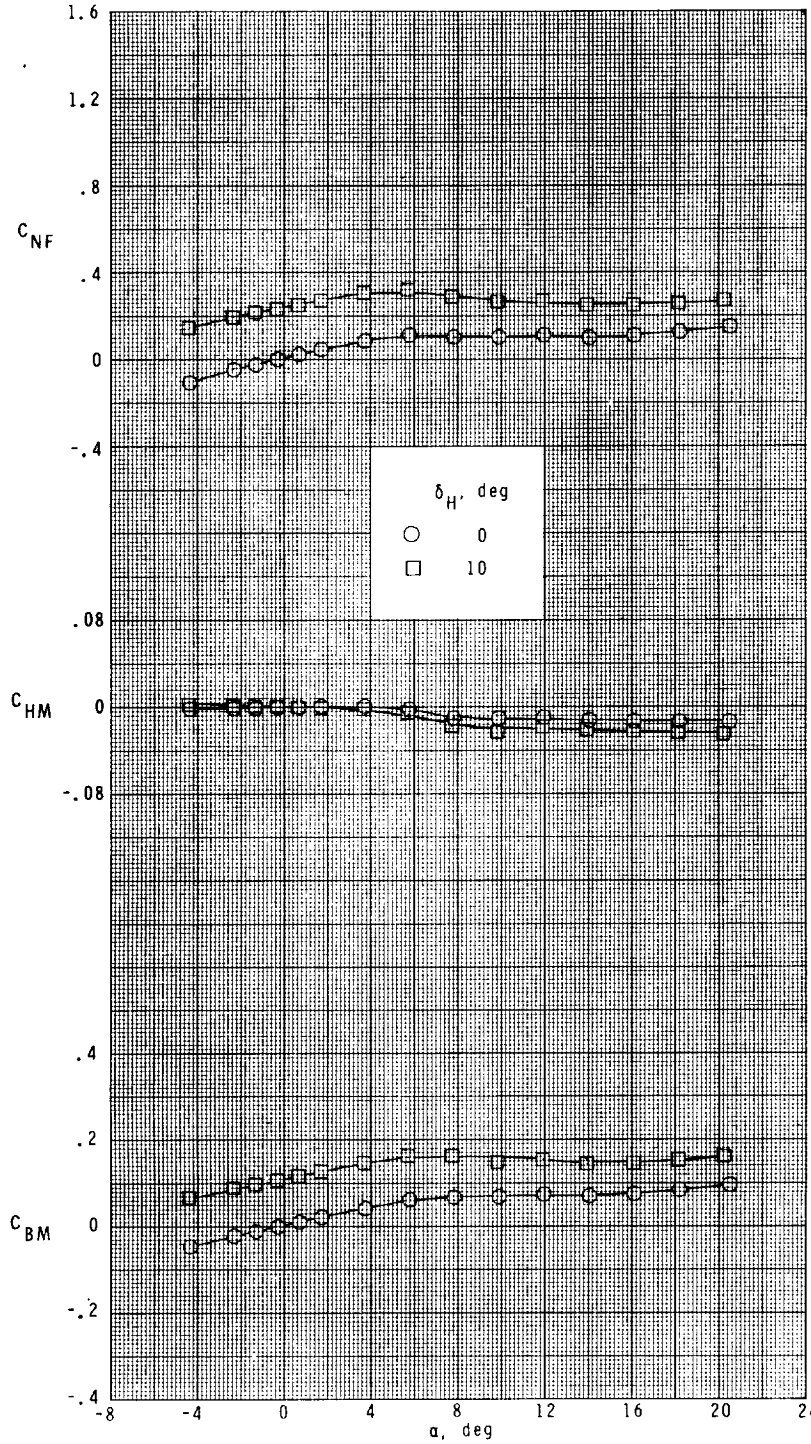

(c) M = 2.86.

Figure 21.- Concluded.

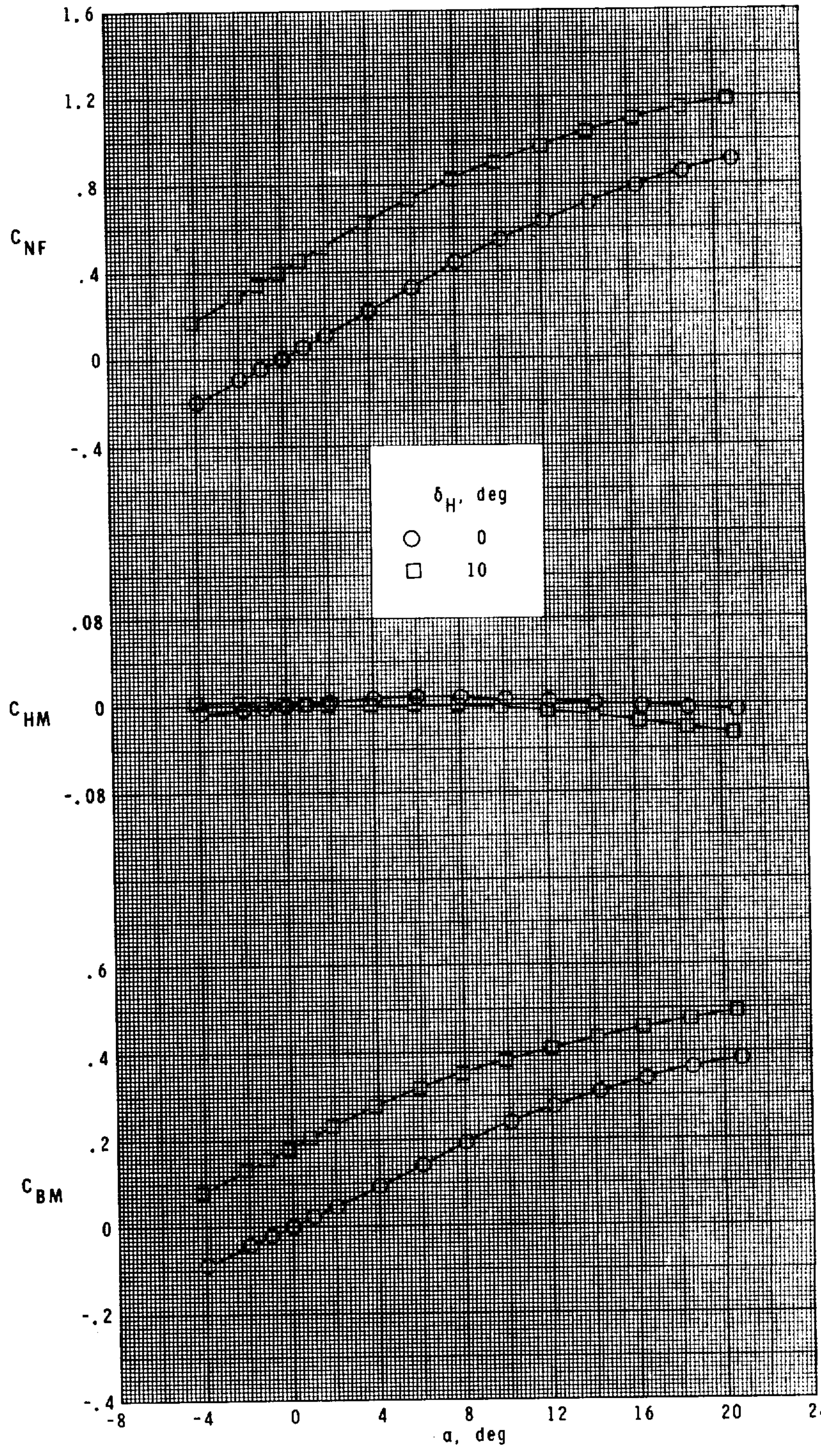

(a) M = 1.60.

Figure 22.- Variation of fin load coefficients with angle of attack for fin panel T_{12} at $\phi_f = 90^o$.

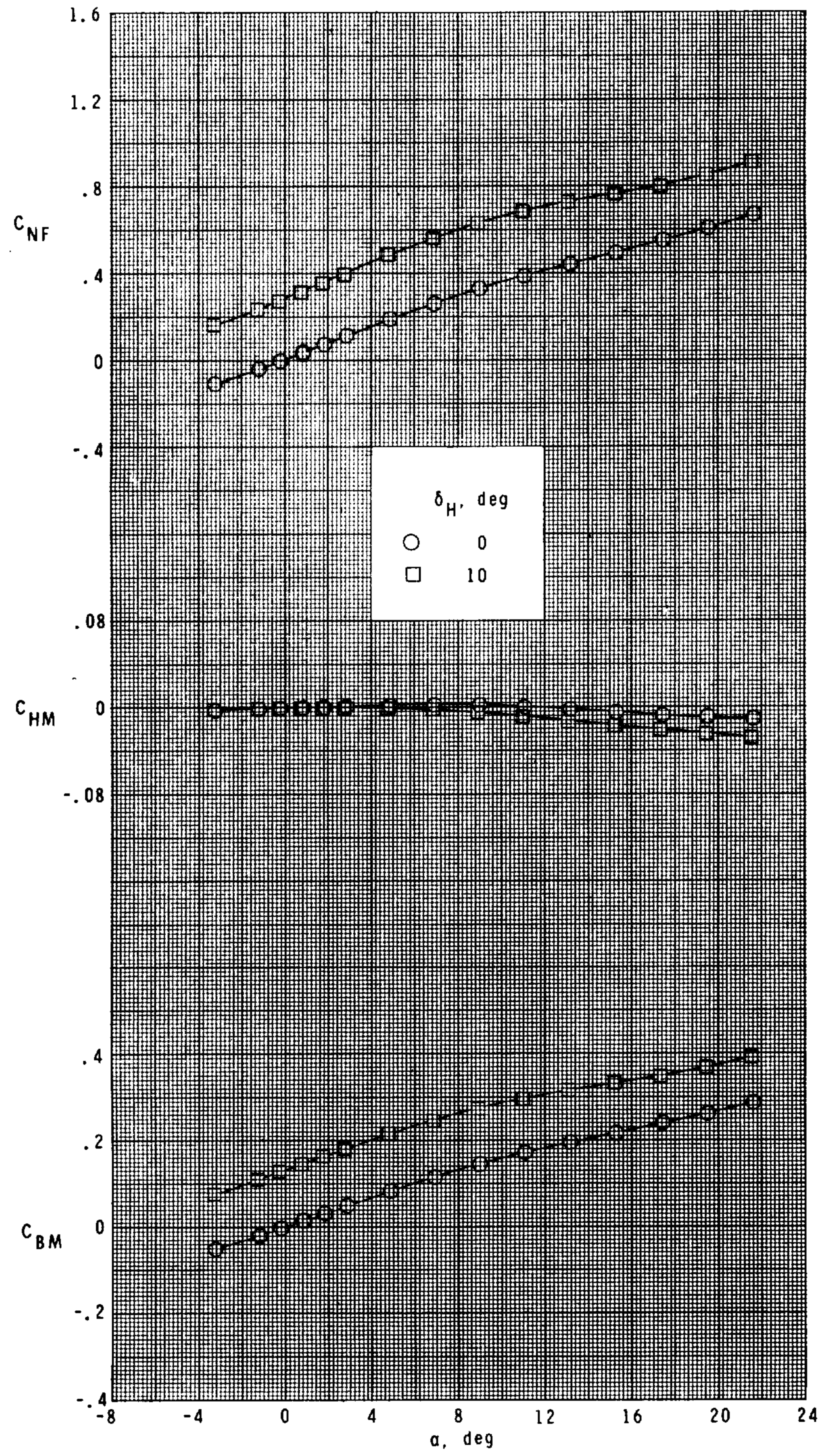

(b) M = 2.36.

Figure 22.- Continued.

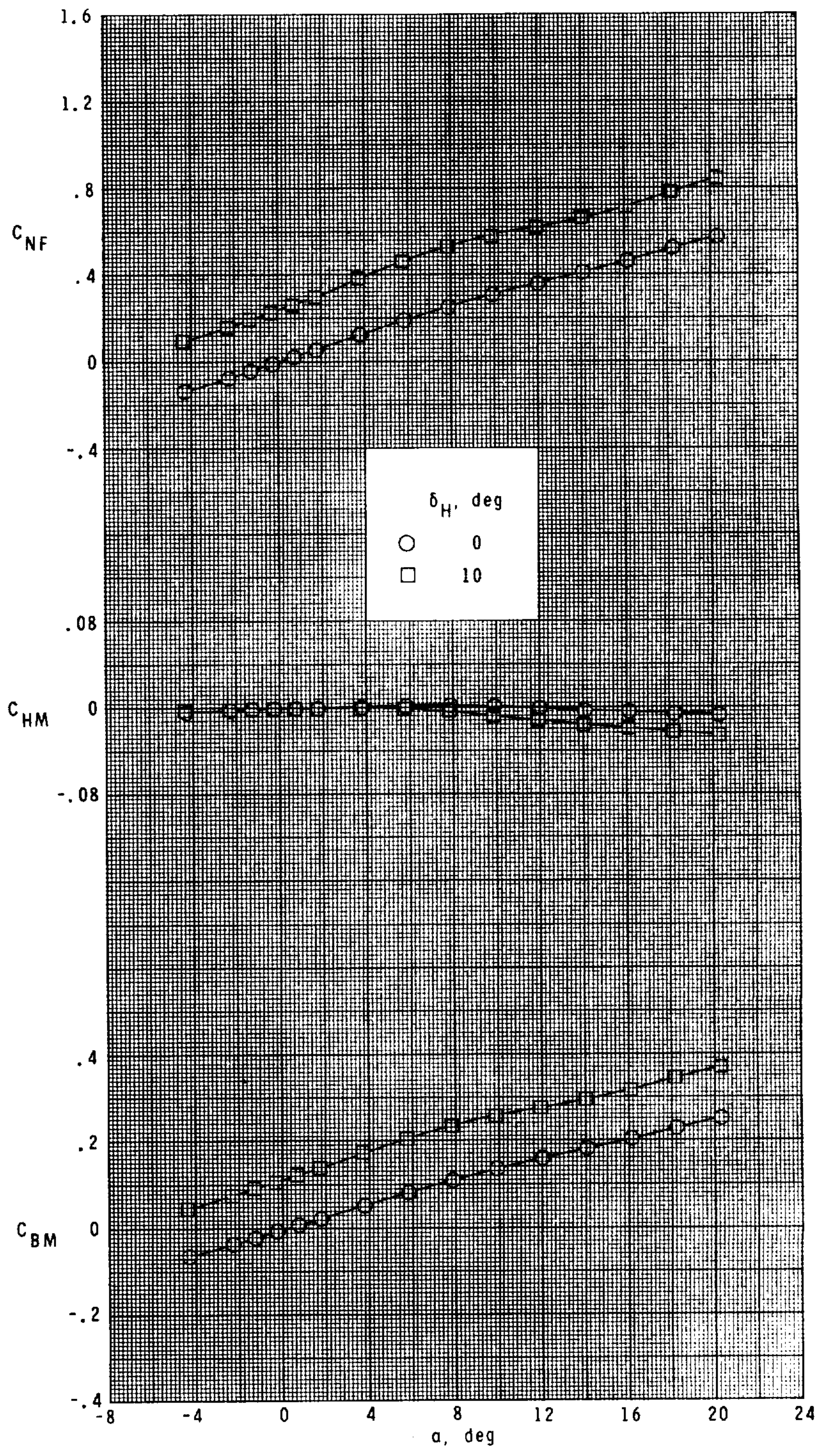

(c) M = 2.86.

Figure 22.- Concluded.

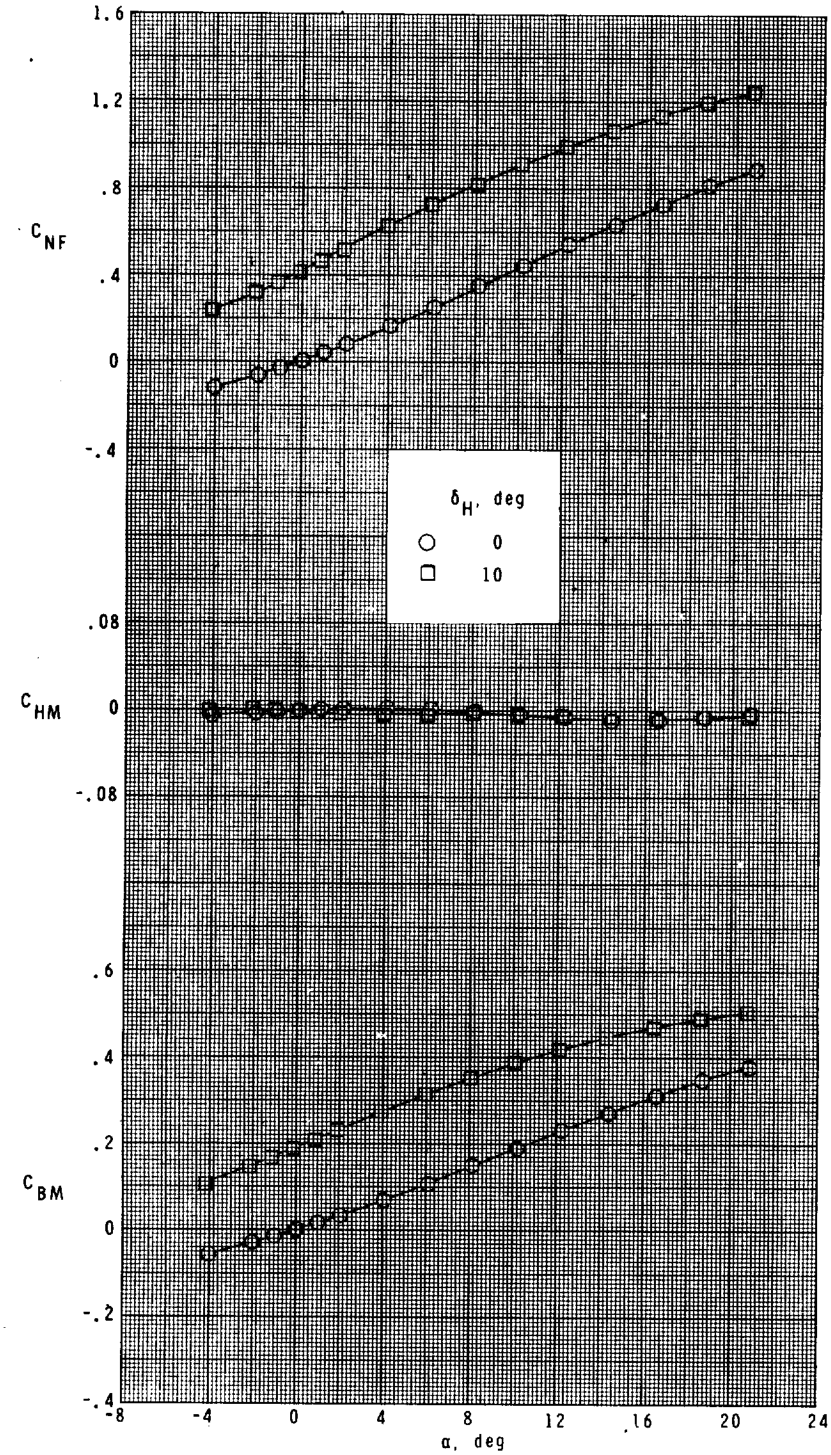

(a) M = 1.60.

Figure 23.- Variation of fin load coefficients with angle of attack for fin panel T_{12} at $\phi_f = 135^{\circ}$.

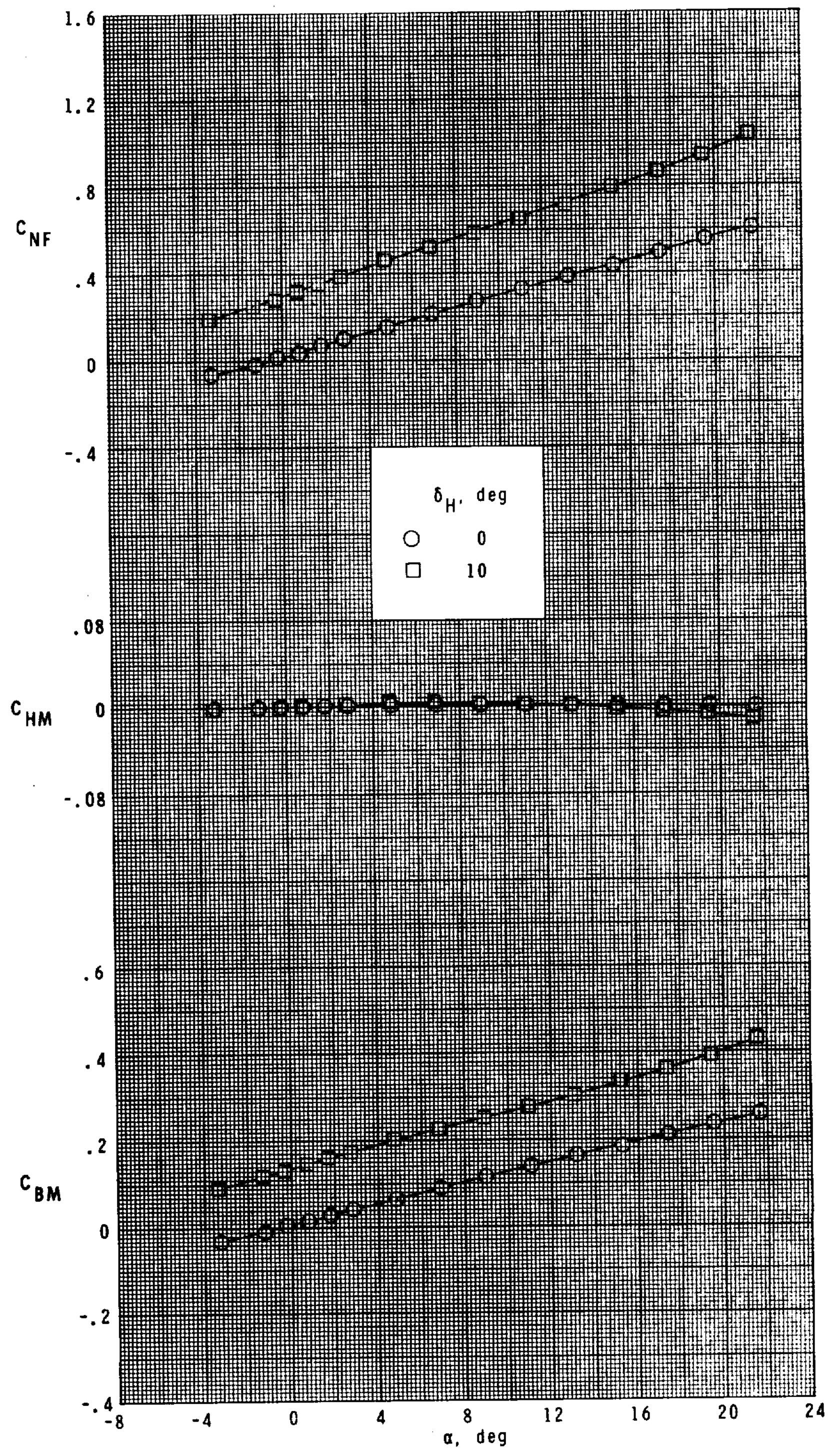

(b) M = 2.36.

Figure 23.- Continued.

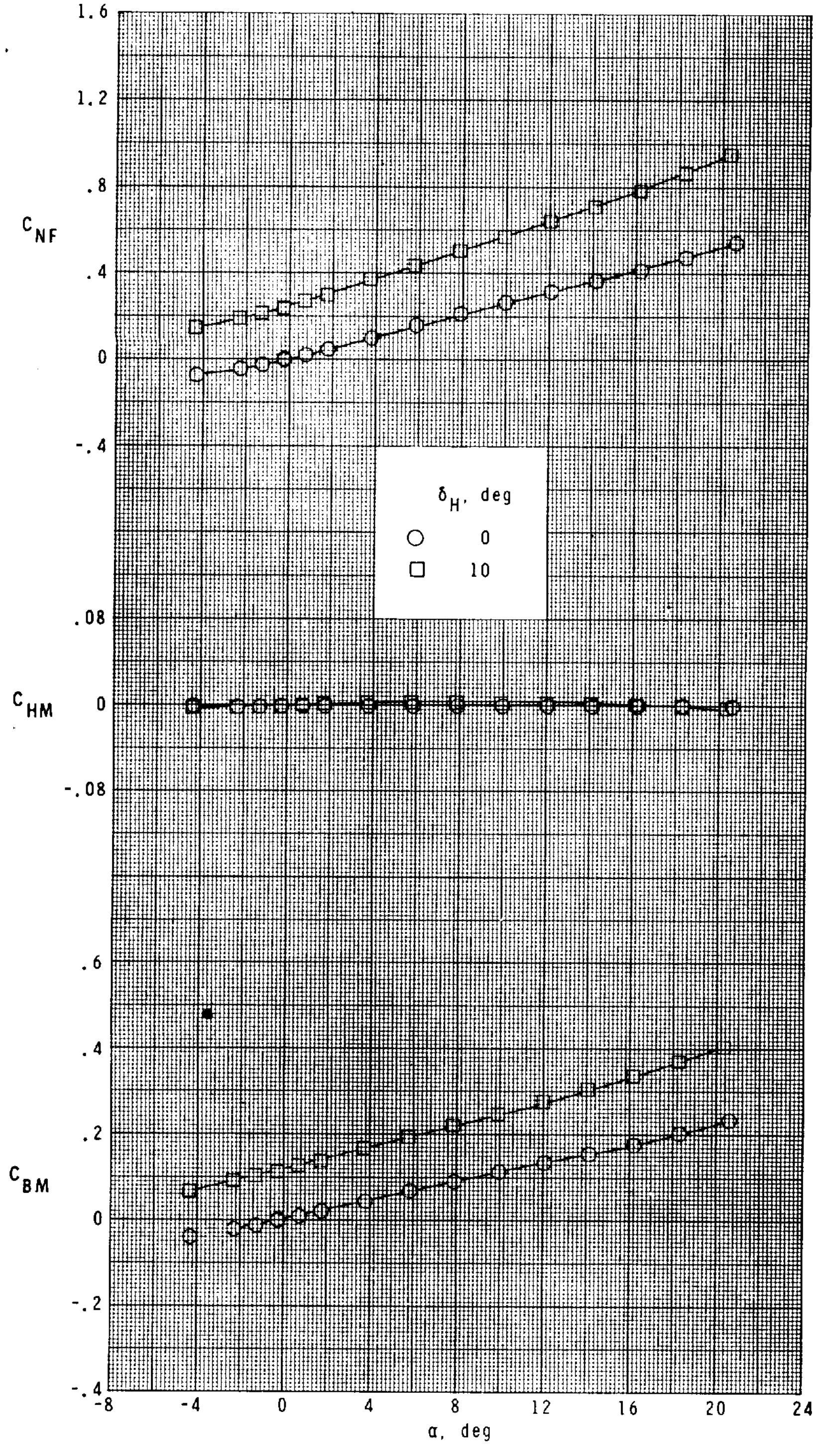

(c) M = 2.86.

Figure 23.- Concluded.